FACULTY OF MECHATRONICS,
INFORMATICS AND INTERDISCIPLINARY
STUDIES TUL

Dissertation

Diffusion-controlled release of substances from nanofibrous structures

Study programme: P3942 – Nanotechnology
Study branch: 3942V001 – Nanotechnology
Author: **Ing. Nikifor Asatiani**
Supervisor: doc. Ing. Petr Mikeš, Ph.D.

Liberec 2023

Declaration

I hereby certify, I, myself, have written my dissertation as an original and primary work using the literature listed below and consulting it with my thesis supervisor and my thesis counsellor.

I acknowledge that my dissertation is fully governed by Act No. 121/2000 Coll., the Copyright Act, in particular Article 60 – School Work.

I acknowledge that the Technical University of Liberec does not infringe my copyrights by using my dissertation for internal purposes of the Technical University of Liberec.

I am aware of my obligation to inform the Technical University of Liberec on having used or granted license to use the results of my dissertation; in such a case the Technical University of Liberec may require reimbursement of the costs incurred for creating the result up to their actual amount.

At the same time, I honestly declare that the text of the printed version of my dissertation is identical with the text of the electronic version uploaded into the IS STAG.

I acknowledge that the Technical University of Liberec will make my dissertation public in accordance with paragraph 47b of Act No. 111/1998 Coll., on Higher Education Institutions and on Amendment to Other Acts (the Higher Education Act), as amended.

I am aware of the consequences which may under the Higher Education Act result from a breach of this declaration.

20. 10. 2023   Ing. Nikifor Asatiani

Difuzně řízené uvolňování látek z nanovlákenných struktur

Abstrakt

Výzkum a vývoj nanovlákenných nosičů léčiv jsou stále aktuálním tématem v oboru řízené dopravy léčiv. Nicméně, nanovlákenné systémy mají řadu unikátních vlastností, které nutí hledat nové přístupy pro popis a předpověď uvolňování bioaktivních látek z nanovláken. Cílem této disertační práce byl výzkum a vývoj polymerních nanovlákenných systémů zejména pro využití v kožní medicíně. V této studii byly různé molekuly inkorporovány do nanovláken metodou elektrostatického zvlákňování a výrobené materiály byly charakterizovány z hlediska relevantních parametrů, klíčových pro výsledné aplikace. Matematický model vyvinutý v rámci této studie umožňuje přesnější stanovení difuzních koeficientů léčiv a také predikci kinetiky jejich uvolňování na základě morfologie vláken. Výsledkem práce je také metoda umožňující efektivní enkapsulaci citlivých biomolekul do struktury polymerních nanovláken. Výsledky této studie mohou sloužit jako dobrá platforma pro další studie v oblasti výroby a také charakterizace elektrostaticky zvlákněných krytů ran. Kromě toho tato práce poskytuje poznatky o dosud neprozkoumaných mechanismech uvolňování léčiv z nanovláken.

Klíčová slova: difúze, řízená doprava léčiv, kožní kryty, matematický model, morfologie

Diffusion-controlled release of substances from nanofibrous structures

Abstract

The research and development of nanofibrous drug carriers is a hot topic in the field of controlled drug delivery. However, nanofibrous systems have many unique properties that force the search for new approaches to describe and predict the release of bioactive compounds from nanofibers. This dissertation aimed to research and develop polymeric nanofiber systems mainly for use in skin medicine. In this study, various molecules were incorporated into nanofibers by electrospinning, and the fabricated materials were characterized in terms of key parameters relevant to the resulting applications. The mathematical model developed in this study enables a more accurate determination of drug diffusion coefficients and prediction of drug release kinetics based on fiber morphology. The work also resulted in a method to efficiently encapsulate sensitive biomolecules into polymer nanofibers' structure. The results of this study can serve as a good platform for further studies in the manufacturing and characterization of electrospun wound dressings. In addition, this work provides insights into previously unexplored mechanisms of drug release from nanofibers.

Keywords: diffusion, drug delivery, wound dressing, mathematical modeling, morphology

Acknowledgements

First of all, I would like to thank my supervisor doc. Ing. Petr Mikeš, Ph.D. for his supervision, invaluable professional assistance provided to me while writing this thesis, his helpful advice, and his patience.

I am grateful to my beloved family for supporting me throughout my postgraduate journey and inspiring me to overcome all the difficulties on this challenging path. I could not have done it without you.

I am also very grateful to my colleagues at the Technical University of Liberec and Mae Fah Luang University for their moral support and for not letting me give up.

Thank you to anyone who takes the time to read this thesis.

Contents

List of abbreviations

AC	Alternating Current
ACN	Acetonitrile
API	Active Pharmaceutical Ingredient
CNS	Central Nervous System
CV	Coefficient of Variation
DC	Direct Current
DH	Degree of Hydrolysis
DLS	Dynamic Light Scattering
DMSO	Dimethyl Sulfoxide
DSC	Differential Scanning Calorimetry
ECM	Extracellular matrix
FDA	Food and Drug Administration
FTIR	Fourier-transform Infrared Spectroscopy
GFP	Green Fluorescent Protein
GPC	Gel Permeating Chromatography
HBDI	(4-(p-hydroxybenzylidene) imidazolidin-5-one
HPLC	High Performance Liquid Chromatography
HPMC	Hydroxypropyl methylcellulose
IGF-I	Insulin-like growth factor 1
IPA	Isopropyl Alcohol
IQR	Interquartile Range
KDE	Kernel Density Estimation
LPPO	Lipophosphonoxin
MIF	Melanocyte-stimulating hormone
ODF	Oral Dissolving films
PBS	Phosphate-buffered saline
PCL	Polycaprolactone
PEO	Poly(ethylene oxide)
PVA	Polyvinyl Alcohol
PVP	Polyvinylpyrrolidone
SD	Standard Deviation
SEM	Scanning Electron Microscopy
SLS	Sodium Lauryl Sulphate
SURS	Systematic Uniform Random Sampling
SNV	Standard Normal Variate
TUL	Technical University of Liberec

Notation

Symbol	Meaning	Usual Dimensions (values)	Section References*
Roman Symbols			
C_n	concentration of a substance within an aliquot	$mg \cdot L^{-1}$	7.8.1
D	diffusion coefficient	$cm^2 \cdot s^{-1}$	3.3.1
e	Euler's number,	2.718281	3.3.3
E	1) Young's modulus	MPa	1.3
	2) strength of an electric field	$V \cdot m^{-1}$	1.4
f	1) frequency	Hz	1.4
	2) sampling fraction	none	7.4.1
h	mass transfer coefficient	$cm \cdot s^{-1}$	3.3.2
ΔH_{cc}	cold crystallization enthalpy	$J \cdot g^{-1}$	7.6
ΔH_m	melting enthalpy	$J \cdot g^{-1}$	7.6
j_R	diffusive flux	$kg \cdot m^2 \, s^{-1}$	3.3.4
J_0, J_1	Bessel functions of the first kind of orders zero and one	none	3.3.3
k	pre-exponential factor (Korsmeyer-Peppas model)	none	3.2
k_B	Boltzmann constant	$1.380649 \cdot 10^{-23} \, J \cdot K^{-1}$	6.2
k_H	Higuchi dissolution constant	none	3.2
l	length of a fiber	cm	3.3.4
M	amount of diffusing substance	mg	3.3.4
M_t	absolute cumulative amount of substance release at time t	mg	3.2
M_∞	absolute cumulative amount of substance release at infinite time	mg	3.2
n	1) number of measurements	none	2.3
	2) Korsmeyer-Peppas model exponent	none	3.2
	3) density of the individual particles	cm^{-3}	6.2
N	number of fibers	none	3.3.4
p	1) sampling periodicity	none	7.4.1
	2) p - value (statistics)	none	2.3.2
P	probability	none	3.3.6
Q	drug loading	$mg \cdot g^{-1}$	2.5.1
Q_1	first quartile (0.25)	none	7.9
Q_3	third quartile (0.75)	none	7.9
r	1) fiber radius (at the center)	nm	3.3
	2) particle radius	cm	6.2
R	1) fiber radius (at the surface)	nm	3.3
	2) droplet radius	mm	1.4
R^2	coefficient of determination	none	3.2
t	time	h	2.5
T_c	crystallization temperature	°C	7.6
T_m	melting temperature	°C	7.6
u	concentration of a diffusive substance	$mg \cdot cm^{-3}$	3.3
U_0	concentration of the drug in the fiber	$mg \cdot cm^{-3}$	3.3
U_∞	concentration of the substance trapped inside the polymeric matrix by means of intermolecular interactions at infinite time	$mg \cdot cm^{-3}$	3.3
V_R	total volume of the release medium	mL	7.8.1
V_S	volume of an aliquot	mL	7.8.1

*Reference to the section where a particular symbol is used for the first time and/or where its definition is given

Symbol	Meaning	Usual Dimensions (values)	Section References
Greek Symbols			
α	collision efficiency factor	none	1.4
β_{ij}	collision frequency function	$cm^{-3} \cdot s^{-1}$	6.2
β_n	eigenvalues (roots of equation 3.8)	none	3.3.3
ε	vacuum permittivity	$8.854187 \cdot 10^{-12} \ F \cdot m^{-1}$	1.4
η	dynamic viscosity	$N \cdot s \cdot m^{-2}$	6.2
ρ	density of the liquid	$kg \cdot m^{-3}$	1.4
σ	solution's surface tension	$N \cdot m^{-1}$	1.4
τ	characteristic relaxation time	s	1.4
ω	angular frequency of the external electric field	s^{-1}	1.4

Publications by the author

Articles

1. **Asatiani, N.**, Novotný, V., Lukáš, D., & Mikeš, P. (2021). A novel approach to studying the kinetics of release of alaptide from poly- -caprolactone nanofibers. *Journal of Drug Delivery Science and Technology*, 63 doi:10.1016/j.jddst.2021.102492

2. **Asatiani, N.**, Filipová, B., Pechočiaková, M., Kluk, A., Kunc, Š., & Mikeš, P. (2023). Electrospun HPMC/PEO-blend orodispersible films: How slight batch differences affect the crucial mechanical properties. *Cellulose*, 30(7) doi:10.1007/s10570-023-05137-4

3. Mikeš, P., Brož, A., Sinica, A., **Asatiani, N.**, & Bačáková, L. (2020). *In vitro* and *in vivo* testing of nanofibrous membranes doped with alaptide and L-arginine for wound treatment. *Biomedical Materials* (Bristol), 15(6) doi:10.1088/1748-605X/ab950f

4. Vrchovecká, S., **Asatiani, N.**, Antoš, V., Wacławek, S., & Hrabák, P. (2023). Study of adsorption efficiency of lignite, biochar, and polymeric nanofibers for veterinary drugs in WWTP effluent water. *Water, Air, and Soil Pollution*, 234(4) doi:10.1007/s11270-023-06281-0

5. Do Pham, D. D., Jenčová, V., Kaňuchová, M., Bayram, J., Grossová, I., Šuca, H., ... , **Asatiani, N.**, ..., Gál, P. (2021). Novel lipophosphonoxin-loaded polycaprolactone electrospun nanofiber dressing reduces staphylococcus aureus induced wound infection in mice. *Scientific Reports*, 11(1) doi:10.1038/s41598-021-96980-7

6. Mikeš, P., Baker, D. A., Uhlin, A., Lukáš, D., Kuželová-Košťáková, E., Vidrich, A., ... , **Asatiani, N.**, ..., Tomani, P. (2021). The mass production of lignin fibres by means of needleless electrospinning. *Journal of Polymers and the Environment*, 29(7), 2164-2173. doi:10.1007/s10924-020-02029-7

Textbooks

1. Lukáš, D., **Asatiani, N.,** Jenčová, V., Košťáková, E., & Mikeš, P. (2018). Fyzika polymerů. Technická univerzita.

Conferences

1. **Asatiani, N.**, Valtera, J., Lisnenko, M., Havlickova, K., Kovacicin, J., Lukas, D., …Moláček, J. (2021). Evaluation of fiber orientation of AC and DC electrospun PLCL nanofibrous layer. Paper presented at the *NANOCON Conference Proceedings - International Conference on Nanomaterials*, 240-245. doi:10.37904/nanocon.2021.4353

2. **Asatiani, N.**, Mikeš P. (2019). Analysis of drug release kinetics from electrospun-based nanofibrous wound dressings. Paper presented at *the 7th International Conference on Advances in Skin, Wound Care and Tissue Science*, Copenhagen, Denmark (*Journal of Tissue Science & Engineering*, 10 (2019)).

Patents

1. Zajicek, R., Gal, P., Rejman, D., Pham, D. D., Mojr, V., Havlickova, K., Jencova, V., Lukas, D., **Asatiani, N.**, Mikes, P., & Kuzelova Kostakova, E. (2021). Nanofibrous material particularly for topical use in therapies. (Patent No. WO2021244684A1). WIPO (PCT). https://patents.google.com/patent/WO2021244684A1

Introduction

The problem of effective delivery of drugs and finding the most effective treatment method has been known to humans since the beginning of time. Gradually, people have found new ways of treatment, either by discovering new drugs or modifying existing solutions. One of the successfully utilized approaches toward modification was introducing drugs into a structure of polymeric carriers. The rapid evolution of technologies allowed us to go from a macroscopic scale to a microscopic scale. Particularly, polymeric matrices in the form of nanofibers have several key advantages over any other types of conventional dosage forms. On the other hand, nanofibrous materials represent a highly complex system with many parameters affecting the efficiency of drug incorporation into the fiber structure and the physio-chemical properties of the resulting material. Although research in this field has been conducted extensively during the last two decades, many methodological and theoretical questions remain unanswered.

Nowadays, one of the main gaps in the field is understanding what mechanisms are responsible for drug release of substances from polymeric nanofibers. It is still not sufficiently clear whether using conventional mathematical models to describe drug release from nanofibers is appropriate, as the microscopic structure might not be comparable to traditional devices. There is also a great demand for new strategies to incorporate sensitive substances into polymeric nanofibers, mainly produced from harsh organic solvents, while preserving the native bioactivity of the incorporated substance.

This Ph.D. study considers different aspects of the problem within the design and development of nanofibrous drug delivery systems. The thesis aims to contribute to filling gaps in understanding the release mechanisms of drugs from nanofibers. Additionally, a significant effort is aimed toward the quantitative prediction of drug release by developing a novel mechanistic model based on the diffusion equation, taking into account the unique complexity of a nanofibrous structure. Finally, the thesis contributes to the field by proposing a novel approach to incorporating sensitive drugs into polymers through a combination of direct-current electrospinning and alternate-current electrospraying techniques. The impact of the raw starting polymer's properties on the final material is also considered.

The primary significance of this Ph.D. research lies in using a mathematical model, which is neither empirical nor numerical but developed based on natural physicochemical phenomena. This phenomena-driven approach might help significantly to understand the relationships between the variables involved in the substance release process. As there is still a lack of mechanistic mathematical models

developed explicitly for nanofibers, elaboration on how the complex structure of fibers affects the release will contribute to gaining insights into the substance release process mechanisms. Examining various model drugs in conjunction with the obtained results could accelerate the design and development of a novel active wound dressing utilizing electrospun nanofibers.

This thesis consists of seven chapters which are connected by the overall introduction and overall conclusion. The first chapter, *Fundamentals and State-of-the-art*, provides the reader with fundamental information about the problems within the field and a brief literature survey on the topics concerned in the thesis. The second chapter, *Fabrication of nanofibrous wound dressings*, covers the case study of the development process of active nanofibrous wound healing materials with incorporated bioactive substances and their subsequent characterization. The process of the development of a mathematical model to describe the release of the incorporated bioactive substances from the nanofibers is then described in the third chapter, *Development of the mathematical model of drug release*, and the evaluation of the developed model is covered in the fourth chapter, *Application of a mathematical model of release kinetics*. The fifth chapter, *Effect of polymer parameters on electrospun matrix*, investigates the importance of homogeneity of the starting polymer material to produce nanofibers with reproducible physicochemical properties. The sixth chapter, *New approach on the incorporation of sensitive bioactive substances to nanofibrous structures*, explores the ways of combining different advanced techniques to establish a novel approach to incorporating sensitive bioactive substances into the nanofibers. Finally, the seventh chapter, *Materials and Methods*, is dedicated to the detailed description of the materials, experimental procedures, and analyses utilized throughout the thesis.

The scope of the thesis is focused on polymeric electrospun-based drug delivery systems. For the most part, the delivery systems studied in this work can be characterized as "diffusion-controlled", although diffusion is not always the only driving release mechanism present. Also, it is important to mention that according to a generally adopted convention, the author uses the term "*nanofiber*" to describe a fiber with a diameter below 1 μm. Throughout this thesis, the words 'microfiber', '*sub-micro fiber*' and "*nanofibe*r" might be used interchangeably unless explicitly stated otherwise. Methodologically, this study covers mainly the direct-current electrospinning technique for the fabrication of the nanofibers, followed by characterization mainly by scanning electron microscopy, image analysis, and high-performance liquid chromatography. The theoretical approach toward developing a mathematical model is primarily defined by the solution of the diffusion equation in cylindrical coordinates and model verification employing non-linear regression.

This Ph.D. study intended to demonstrate that the unique structure and nature of nanofibers not only give us many advantages over more conventional drug dosage forms but, on the other hand, impose a particular portion of responsibility and nuances to consider associated with the development of a nanofiber-based drug delivery system.

Aims and objectives of the thesis

Building upon the aspects introduced in the introduction chapter, the overall aim of this dissertation was to design and develop nanofiber-based drug delivery platforms intended mainly for wound healing applications by incorporating bioactive substances into the nanofibrous structure. Additionally, this thesis aimed to gain insights into the release mechanism of incorporated substances from fabricated materials, taking into account the unique complexity of nanofibrous systems. Thus, the overall aim was divided into eight objectives:

1. Electrospinning of polymeric solutions (or suspensions) doped with selected bioactive substances.

2. Characterization of physicochemical properties of the fabricated electrospun materials.

3. Evaluation of the effectiveness of incorporating the substances into the nanofibers.

4. Investigation of drug release kinetics from the fabricated nanofibers.

5. Development of a mathematical model as a predictive tool for electrospun drug-delivery platforms.

6. To justify the appropriateness of the developed mathematical model on the real experimentally obtained data.

7. To estimate the diffusion coefficients of the selected substances within the nanofibers.

8. To formulate a more sophisticated electrospun drug delivery platform of sensitive bioactive molecules.

1 Chapter I - Fundamentals and state-of-the-art

This chapter is a literature review on the current state-of-the-art in the field of nanofibrous drug delivery systems. The chapter is aimed to familiarize the reader with the problems within the topic and provide necessary background information to enhance the general understanding of the thesis text. The structure of the chapter consists of four connected sections. The first section will briefly introduce the overall issues related to the wound healing process and wound dressing development. The second section will present the current approaches to characterizing the release kinetics of substances from nanofibrous structures. The following section will cover the issues related to developing relatively new dosage forms - nanofibrous orodispersible films. Finally, the last section discusses the approaches for incorporating sensitive biomolecules into nanofibers spun from harsh organic solvents.

1.1 Brief introduction to wound healing

Wound healing is a complex biological process consisting of several overlapping stages. Although there are different conceptions on distinguishing the individual steps, an ideal wound healing process is usually described by four essential phases; according to Figure 1.1, the wounding stage itself is considered rapid (George Broughton et al., 2006; Hassiba et al., 2016; Rieger et al., 2013).

Even though the skin can repair most wounds by itself, there are a number of adverse factors, including potential infection (sepsis) and contamination of the wound with foreign bodies. These factors may result in prolonged healing and possibly chronic wound formation. Such a wound requires the use of antibiotics, which can produce harmful negative side effects, e.g., sleep disorders, headaches, and diarrhea (Kataria et al., 2014) either through direct toxicity or by contributing to the appearance of resistant microorganisms (Robson, 1997; Brown et al., 2016). Additionally, many currently used topical antimicrobial agents exert cytotoxic effects on keratinocytes and fibroblasts, which may delay wound healing (Cartotto, 2017). Localized drug delivery to the wound is therefore being studied as an alternative to generalized drug application. It has been known for a very long time that using an appropriate wound dressing can significantly improve the wound healing process compared to a wound left open to the air (Dhivya et al., 2015). However, traditional wound dressings, e.g., lint, gauzes, and cotton wools, cannot prevent wound beds

from drying and bacterial infection and thus need to be periodically replaced. This replacement, in turn, often damages the wound integrity and the newly healed tissue.
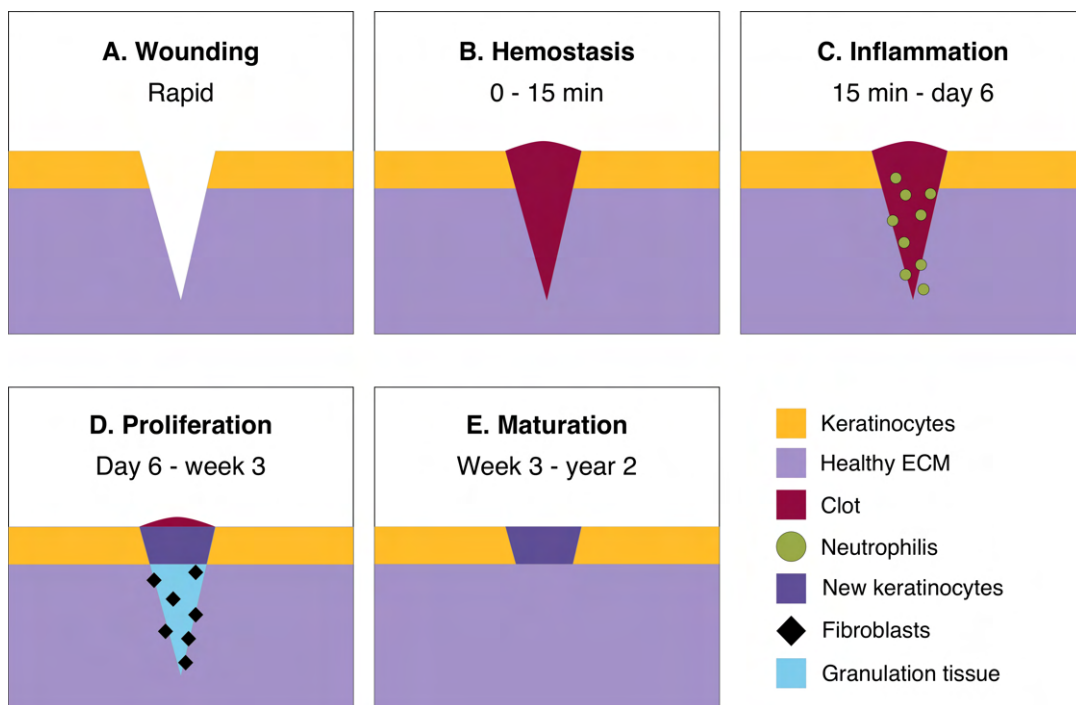

Figure 1.1: Schematic representation of the main phases of wound healing process: Wounding (A), Hemostasis (B), Inflammation (C), Proliferation (D), and Maturation (E). Adapted from (Rieger et al., 2013; Hassiba et al., 2016).

Taking into account all of the above factors, we can conclude that the development of an active biodegradable antibacterial and regeneration-promoting wound dressing can open new horizons for modern therapy of wounds in a fully controlled manner (Johnson et al., 2013; Xu et al., 2018; C. Wang et al., 2018).

Synthetic polymers are a prominent group among the wide range of clinically approved wound dressing materials. Synthetic polymers-based wound dressings can effectively adjust wound moisture by absorbing the excess exudate and can provide sufficient oxygen permeability (Boateng et al., 2008; Kataria et al., 2014). The polycaprolactone (PCL)-based nanofibrous scaffold wound dressing produced by electrospinning can undoubtedly be considered one of the most promising materials. PCL is biodegradable and degrades naturally occurring metabolite 6-hydroxyhexanoic acid. The electrospun PCL nanofibers can mimic the original structure of the native extracellular matrix (ECM), which may positively affect cell proliferation, e.g., fibroblasts. Considering the omplexity of bureaucratic components when developing a drug delivery system, it is important to mention that PCL scaffold has been approved by the American Food and Drug Administration (FDA) for biomedical applications (Zibiao Li et al., 2014).

In addition, electrospun polymeric wound dressings can be conveniently functionalized with a wide range of biomolecules and drugs (Hassiba et al., 2016; Preem

et al., 2017). Particularly, a promising group of such biomolecules are short peptides, which are getting more and more interest in medical applications due to their positive effects on wound healing in terms of their antibacterial properties and acceleration of the healing process (Gomes et al., 2017). Indeed, a predictable release regime is required to achieve the desired therapeutic effect adequately. In the present Ph.D. study, this group was represented by the dipeptide Alaptide and the amino acid L-Arginine. The second-generation lipophosphonoxins (LPPO), synthesized by Dominik Rejman's group (Institute of Organic Chemistry and Biochemistry, Czech Academy of Sciences, Prague), were utilized as an antimicrobial agent. These three selected biomolecules have great potential in the wound-healing process. The rationale behind choosing these particular biomolecules is covered in the following section. The biomolecules were incorporated into electrospun nanofibrous PCL membranes to fabricate an active wound healing/antimicrobial dressing. The studies were conducted in collaboration with the Institute of Organic Chemistry and Biochemistry, Czech Academy of Sciences (Prague), Institute of Physiology of the Czech Academy of Sciences, (Prague), First Faculty of Medicine, Charles University, (Prague), Prague Burn Centre, Third Faculty of Medicine, University Hospital Královské Vinohrady (Prague) and others. Besides publications in impacted journals, the studies of LPPO-loaded nanofibers resulted in a published international patent (Zajicek et al., 2021) of nanofibrous wound dressing for topical use in therapies.

1.2 Mathematical modeling of drug release from nanofibers

As mentioned above, quantitative predictions of drug release constitute one of the most critical and complicated issues in drug delivery science (Takeru Higuchi, 1961; Peppas, 1985; J. Siepmann; F. Siepmann, 2008). Release-predicting mathematical models can assist in preventing the need for time-consuming experiments, and generally accelerate the design and development of drug delivery devices (J. Siepmann; F. Siepmann, 2008). Understanding drug release from a particular drug delivery system requires comparing the experimental data with the solution provided by an accurate theoretical model.

Generally, mathematical models that describe the kinetics of the release of substances comprise mechanistic and empirical or semi-empirical models (Grassi et al., 2005; Juergen Siepmann et al., 2012). The fact that the latter approach is merely descriptive and is not based on actual physicochemical processes diminishes both its contribution toward understanding the true essence of release mechanisms and its predictive power. Thus, this approach is often used merely to compare drug release profiles applying specific parameters. Conversely, mechanistic models are constructed based on equations (usually partial differential equations) that describe real phenomena, e.g., dissolution, partition, diffusion, and erosion. Such models provide a more in-depth insight into the essence and relationships between the mechanisms that control the release of drugs from particular dosage forms. Although

numerical and analytical solutions can be used depending on the complexity of the sets of equations obtained and despite the relative ease of using numerical solutions, analytical solutions allow for a more complete understanding of the influence of significant individual variables.

Research on nanofiber-based structures for drug delivery is a relatively new field. Despite this, it has already demonstrated significant progress and potential. It is more than 20 years since the first article on the release of drugs from nanofibers was published by Kenawy et al. (2002). Since that time, a considerable number of experimental studies have been conducted on the kinetics of drug release from nanofibers with concern to a wide variety of combinations of polymer matrices and incorporated drugs (Thakkar et al., 2017; Stack et al., 2018; Ghafoor et al., 2018; Bai et al., 2021). The rapid development of electrospinning technology makes it possible to achieve various release mechanisms such as e.g., immediate (Bai et al., 2021), sustained (Ghafoor et al., 2018), multiple-phase (Chang et al., 2020) or targeted (Ding et al., 2020). However, due to the complexity of nanofibrous structures, the essence of the physicochemical processes of the release of drugs from nanofibers still requires clarification. The overwhelming majority of articles that have described the kinetics of drug release draw their (often mechanistic) conclusions based merely on the fitting of experimental data to empirical or semi-empirical models (Kuang et al., 2018; Preem et al., 2017; Pisani et al., 2019). The conclusions reported to date have been based primarily on the famous Peppas equation (Peppas, 1985) or a simplified form of the Higuchi equation (Takeru Higuchi, 1961; T. Higuchi, 1963), which is essentially a specific form of the Peppas equation relating to early release times.

However, the main difficulty of the theoretical approach lies in the fact that nanofibers reveal a complex system. Unlike most other conventional dosage forms (pellets, spheres, or planar slabs), the electrospun matrices are composed of thousands of infinite cylinders with differing diameters, each of which makes its contribution to the cumulative drug release profile of the nanofiber-based drug delivery device.

The primary considerations behind this study were to fill some of the gaps in understanding the potential restrictions surrounding and the applicability of existing empirical and mechanistic drug delivery models concerning electrospun-based carriers. To clarify the drug release mechanism, we determined the apparent diffusion coefficients for a specific nanofibrous drug-delivery system since diffusivity plays a significant role in the quantitative prediction of drug release. In a similar way to studies by Petlin et al. (2017) and Milosevic et al. (2020), this study considered the significant effect of the fiber diameter distribution on the collective kinetics of drug release. Generally, just a few parameters can be easily determined from micro-graphs. Among them are fiber diameters, fiber orientation, and pore size. Thus, such a model has a significant advantage as the diffusion coefficients can be estimated based on easily obtainable experimental data.

1.3 Nanofibrous orodispersible films

Orodispersible films (ODFs) comprise a relatively new and promising dosage form. This dosage form is suitable for patients with swallowing difficulties (dysphagia), especially for seniors and young children (Preis, 2015; Slavkova et al., 2015; Orlu et al., 2017; Visser et al., 2017). Therefore, pharmaceutical companies are developing various innovative oral dosage forms, one of the most promising of which comprises FDS (Fast dissolving system), which allows for very rapid dispersion in the oral cavity. The significant advantages of these systems concern their simple discrete administration without the need for swallowing or chewing and the rapid onset of action (Bala et al., 2013; Bahrainian et al., 2017). The systems include tablets, films, wafers, and buccal and sublingual patches, which can be used for topical and systemic drug delivery (Bahrainian et al., 2017). According to European Pharmacopoeia, ODFs are defined as "*single or multilayer sheets of suitable materials, to be placed in the mouth where they disperse rapidly*", i.e., within 30 s (O'Malley, 1971). The most commonly used oral film-delivery drugs consist of anesthetics, cough and sore throat medications, antiasthmatics, antihistamines, erectile dysfunction, gastrointestinal, nausea, and CNS medication drugs. Other injectables include caffeine, various vitamins, and sleeping and snoring medications (Borges et al., 2015; Irfan et al., 2016; Mahboob et al., 2016). This dosage form is particularly suitable for highly potent drugs administered in low doses (Hoffmann et al., 2011).

Oral dispersion films are most commonly produced via casting (pouring) and drying, e.g., solvent casting and semi-solid casting. Other fabrication methods include hot-melt extrusion, solid dispersion extrusion, and the 3D printing method (Borges et al., 2015; Irfan et al., 2016; Effiong Daniel Ekpa et al., 2020). Moreover, in recent years, the trend toward fabricating nanofibers via electrospinning has gained considerable momentum in this field. The solvent casting method is based on spreading a polymer matrix over a support substrate and the subsequent drying/removal of the solvent in an oven. The active pharmaceutical ingredient (API) is dissolved or suspended in a solution of polymers, plasticizers, disintegrants, and other soluble components in a volatile solvent, most commonly water or alcohol. However, the disadvantage of this method may be the potential presence of residual solvents in the film if a solvent other than water is used (Borges et al., 2015).

The main advantages of ODFs consist of rapid dissolution and disintegration (with nanofibrous films, this advantage is multiplied) and the subsequent onset of the action of the drug, simple and discreet administration without the need for water, high dosing efficacy and accuracy, etc. (Bala et al., 2013; Irfan et al., 2016; Mahboob et al., 2016; Bahrainian et al., 2017). The disadvantage of these films remains, however, the limitation of the dose of the drug, which is up to 100 mg (Borges et al., 2015); furthermore, due to their good water solubility, ODFs need to be protected from moisture, ideally with aluminum foil or another barrier material.

The main advantage of nanofibrous layers compared to conventional methods concerns their large specific surface, which significantly reduces the dissolution time of the film. However, this may also be a disadvantage in industrial production due to the high susceptibility of such layers to atmospheric humidity and problems with

storage. A further advantage is that the process involves the massive evaporation of solvents; thus, almost no residual solvents remain within the fibers. As with the more commonly used ODF preparation methods, industrial production allows for considerable cost savings.

The choice of polymeric agents (usually a combination of at least two polymers) for forming oral films is crucial. It is necessary to ensure the good mechanical properties of the resulting film, rapid dissolution, and compatibility of the polymers themselves. The stability of the material depends on the polymer and the overall composition of the film. The potential occurrence of phase separation and the crystallization of the polymer or API (active pharmaceutical ingredient) results in the deterioration of the mechanical properties of oral films, which negatively influences post-production processing, including slicing, packaging, and handling during drug delivery.

A study by Samprasit et al. (2015), which investigated the physical stability of nanofibrous PVP oral films containing Meloxicam, demonstrated that the storage of manufactured films under the appropriate conditions (25 °C / 60 % RH) prevents the formation of morphological crystals and ensures that the film remains stable for six months. The tensile strength of the studied oral films ranged from (0.9 ± 0.4) to (1.7 ± 0.7) MPa. Interestingly, a study by Bukhary, Williams, and Orlu (2017) of PVP nanofibers containing Valsartan and amlodipine besylate determined a period of stability of up to 4 months before the occurrence of phase separation. Paaver et al. (2015) addressed the production of controlled-release ODF nanofibers. Their comparison of 3 HPMCs containing Piroxicam determined that the recrystallization of APIs occurs over time and that the process is accelerated at low temperatures and humidity levels. Thus, the quality of nanofibrous films depends on the quality of the HPMC, the solvent system, and the storage conditions. Similar results were obtained by Liew, Tan, and Peh (2014) in their investigation of the effect of HPMC, PVP, and the plasticizer concentration on the production of nanofibrous ODFs with Donepezil HCl. The tensile strength was found to increase with higher HPMC concentrations; the plasticizers acted to decrease the strength. Still, they increased the elasticity (with optimum amounts and types), and the PVP content in the composition of the film enhanced the material's strength and elasticity. Tort and Acartürk (2016) prepared a nanofibrous ODF with HPMC, PEO, and sodium alginate with the addition of glutamine. Birer and Acartürk (2021) achieved the highest degree of elongation for nanofibrous films containing telmisartan and L-Arginine using a PVP matrix. The results revealed that the films produced via electrospinning had a higher Young's modulus E and exhibited a deterioration in their mechanical properties after one month. The nanofibrous films also showed a worsening dissolution rate over time due to the recrystallization of the drug within the fibers.

1.4 Encapsulation of sensitive substances

As discussed in the previous sections, the nanofibers can be functionalized with various bioactive substances. Indeed, encapsulating sensitive bioactive compounds

in nanofibers is complex due to the toxicity of solvents. Therefore, the choice of solvents is limited to water, DMSO, etc., a factor that reduces the choice of potential polymers. In the case of water-soluble polymers, a question arises concerning crosslinking. Moreover, a significant proportion of these polymers are soluble in a variety of other solvents. However, polyvinyl alcohol (PVA), which is soluble only in sufficient quantities in water for high degrees of hydrolysis (Brough et al., 2016), is an exception; it is also non-toxic, cytocompatible, and has been approved for use in the pharmaceutical industry (Baker et al., 2012). Nevertheless, its application in tissue engineering is problematic due to its high degree of hydrophilicity and partial solubility in air moisture (Nyflött et al., 2017; Nuttelman et al., 2002). Although it is suitable for encapsulating bioactive compounds (Huang et al., 2022), PVA capsules still need to be crosslinked or integrated into fibers, which was our case.

One potential method for preparing nano/microcapsules comprises electrostatic spraying, also referred to as electrohydrodynamic atomization. This process differs from electrostatic spinning mainly in terms of the lower concentration of the polymer, which is often of a lower molecular weight, which leads to the generation of droplets in place of fibers under the same operating conditions (Bock et al., 2012). The droplets generated via electrospraying generally have a relatively narrow diameter distribution, which depends primarily on the voltage, the electrical conductivity of the liquid, and the dispensing rate (Duby et al., 2006). Further advantages of the electrospraying method include its so-called "self-dispersion" characteristic, which is caused by the Coulomb repulsion of the charged droplets during the spraying process, thus acting to prevent their aggregation (Duby et al., 2006; A. Gupta et al., 2020). On the other hand, one of the disadvantages of this process concerns the need for an oppositely charged electrode, which poses problems, especially when the polymer must be deposited on structured surfaces or liquids (solvents). However, alternating electrical voltages render the presence of an oppositely charged electrode unnecessary (Pokorny et al., 2014).

Although the first experiments on electrospraying using the AC were conducted several decades ago (Sample et al., 1972; Sato, 1984), this method still lacks a precise physical description, in contrast to its DC counterpart. The first publications on this topic concentrated primarily on the formation of emulsions in liquid-liquid systems. For example, Masayuki Sato experimented with the AC-spraying of liquids into immiscible liquid-acceptors at low frequencies (Sato, 1984). In contrast, a study by Guido Gneist and Hans-Jörg Bart (2002) investigated the AC electrospraying of liquid-liquid systems at high frequencies (30 to 45 kHz). Wang et al. (2006) even noted that at very low frequencies, the behavior of the droplets is similar to that in classical DC spraying in terms of separation and the charge accumulation of the droplets. However, few papers have been devoted to the AC spraying of polymer solutions. For example, Kessick et al. (2004) reported a higher degree of carboxymethylcellulose coverage on semiconducting substrates when comparing the potential of AC to DC, probably due to a reduction in the surface charge accumulation.

In the case of AC electrospraying, in addition to the magnitude of the electrical voltage, other manipulatable parameters concern the frequency and shape of the

signal, as illustrated by the balancing of the Maxwell stress $\varepsilon E^2/2$ by the capillary pressure σ/R at low frequencies, where the Maxwell pressure can be assumed to be independent of the applied frequency (Maheshwari et al., 2009). In addition, resonance may occur in an AC field between the frequency of the input signal and that of the droplet itself. It implies a higher degree of strain and droplet growth with enhanced detachment even when lower voltages are applied. In general, AC electrospraying can be divided into two physical principles in terms of the generation of the resulting droplets, i.e., low frequency ($f < 10$ kHz) (Yeo et al., 2004) and high frequency ($f > 10$ kHz) according to the magnitude of the frequency. However, this paper considers only the low-frequency droplet generation method.

Grigor'ev has provided a theoretical explanation for low-viscosity drops (Grigor'ev, 2000), who inferred that the characteristic time for the relaxation of hydrodynamic drops back to their initial spherical shapes must be significantly longer than the external electric field ($\tau \ll 1/\omega$) period. The time τ can be estimated as required for a stretched spheroidal drop to recover its spherical form under surface tension. The center of mass of the half drop moves with constant acceleration under the influence of constant Laplace force, thus determining the following restriction on the drop parameters.

$$\tau = \sqrt{\frac{\rho R^3}{3\sigma}} \ll \frac{1}{\omega} \tag{1.1}$$

where ρ denotes the density of the liquid, R is the droplet radius, σ is the solution's surface tension, and ω is the frequency of the external electric field. Maheshwari (Maheshwari et al., 2009) considered a similar relationship in his research, albeit for a slightly different geometrical arrangement. Substituting values that corresponded approximately with our parameters ($\rho \approx 10^3$ kg·m^{-3}; $R \approx 10^{-3}$ m; $\sigma \approx 40 \cdot 10^{-3}$ N·m^{-1}) for each parameter of equation (1.1), we determined that $f \ll 55$ Hz. The surface tension was determined approximately for water/ethanol at a ratio of 8:2. This simple estimate led us to hypothesize that to destabilize a droplet, we must apply a frequency in the order of units of Hz. The confirmation of the hypothesis will be demonstrated later on in the text of chapter six.

2 Chapter II: Fabrication of nanofibrous wound dressings

2.1 Introduction

This chapter introduces the pitfalls in the design and fabrication of drug-loaded electrospun nanofibers for use as wound dressings. The effect of the incorporated drug on the electrospun materials' morphology and release kinetics profiles will be discussed. The text of this chapter is based mainly on three papers published in *Scientific reports* (Do Pham et al., 2021), *Biomedical Materials* (Mikeš et al., 2020), and *Journal of Drug Delivery Science and Technology* (Asatiani; Novotný, et al., 2021).

This chapter covers the process of fabrication of a novel nanofiber-based wound dressings with an active antimicrobial/regeneration promoting by means of needless electrospinning. The focus of the study was on the efficient incorporation of the selected substances to the nanofibrous structure and further investigation of their release from nanofibers. It is believed that development of such doped wound dressing and the knowledge of how they are able to release the active agents may provide a pathway to more effective therapies in wound healing.

2.2 Rationale behind implementation of the incorporated substances

This section covers the rationale for choosing the bioactive substances for the incorporation to the nanofibers. Figure 2.1 depicts the SEM micrographs of morphology of the substances selected for incorporation to nanofibrous structures in this study.
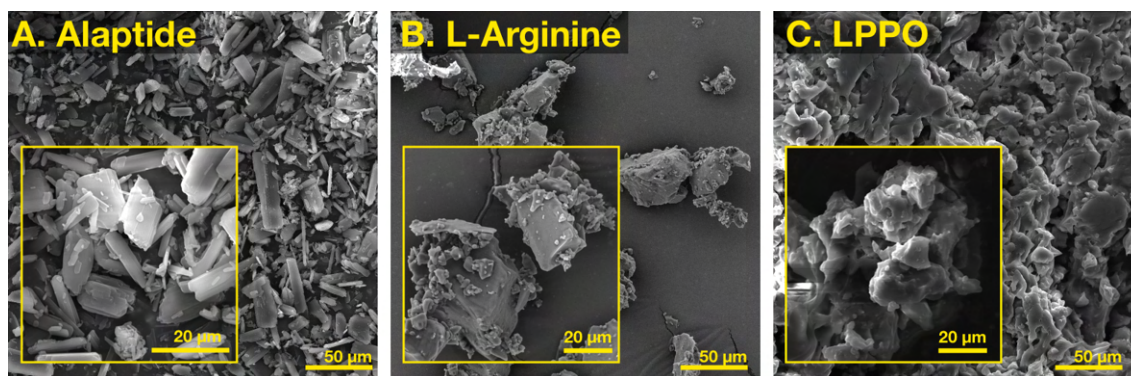
Figure 2.1: The SEM micrographs of encapsulated substances (pure powders) - Alaptide (A), L-Arginine (B), and LPPO (C). The scale bars are 50 μm and 20 μm.

2.2.1 Alaptide

In the introduction chapter, it was already discussed that short peptides represent a promising group of biomolecules for used biomedical application due to their antibacterial properties and its ability to accelerate wound healing process. Thus, the first molecule studied in this thesis is Alaptide. Alaptide, (Figure 2.2), is a spirocyclic synthetic dipeptide which was discovered in the 1980s by Czech chemists Šturc and Kasafírek (Kasafirek et al., 1984). It was developed as an analogue of the melanocyte-stimulating hormone release-inhibiting factor (MIF). This factor, also referred to as macrophage migration inhibitory factor, plays a significant role in wound healing. MIF has been identified as a key effector of beneficial estrogen effects on wound repair (Gilliver et al., 2011) and it induces the proliferation of keratinocytes *in vitro* and *in vivo* (Gesser et al., 2011). Alaptide was selected from among series of other spirocyclic derivatives as the most advantageous MIF analogue from the point of view of its enzymatic stability and due to its pharmacodynamical profile (Kasafirek et al., 1984; Opatrilova et al., 2013).

In the current study, Alaptide was chosen mainly for its favorable results in dermatological experiments: a considerable number of tests have shown that Alaptide can have a positive influence on epidermal regeneration. In vivo experiments, performed on domestic pigs, rats, and mice proved that Alaptide accelerated skin regeneration and the curing of experimental skin injuries (Radl et al., 1990). Moreover, very low acute toxicity was observed in rats and mice, i.e. a 1 g/1 kg dose caused only 20% mortality of female rats (Hlinak et al., 1992; Hliňák et al., 2005). This low toxicity can reduce one of the major disadvantages of transdermal drugs—the possibility of local skin irritation and allergization. Alaptide is currently successfully used as a veterinary 1% hydrophilic ointment under the name ALAPTID® (Bioveta, Czech Republic) for treating warm-blooded animals in order to cure local injuries such as burns, frost-bite, bedsores, etc (Julínek et al., 2010). The release of Alaptide from other formulations, e.g. from cellulose-based hydrogels, has also been studied (Sklenář et al., 2013).
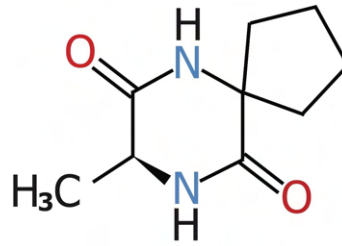
Figure 2.2: Chemical structure of dipeptide Alaptide

2.2.2 L-Arginine

Along with the short peptides, various amino acids are known for its positive effect on the wound healing process. L-Arginine is a non-essential amino acid with a positively charged basic side chain. Its positive effect on wound healing is mainly attributed to the release of nitric oxide and multifunctional free radicals (J.-d. Luo et al., 2005; Stechmiller et al., 2005), see Figure 2.3. Nitric oxide plays a pivotal role in skin repair. It influences the activities of macrophages, fibroblasts and keratinocytes during wound healing. Additionally, L-Arginine is a substrate of arginase, which converts it into ornithine. Ornithine, in turn, is another key player in the process of wound healing, serving as a substrate for synthesis of polyamines, which are crucial for cell proliferation. While proline, which is derived from ornithine, plays a significant role in collagen syntheis (Childress et al., 2008). L-Arginine and its metabolism products are required for tissue repair of acute and chronic wounds. They stimulate the release of growth hormone, and also the release of insulin-like growth factor I (IGF-1), both of which can improve wound healing (Alexander et al., 2014). The body does not provide sufficient amounts of L-arginine for metabolic needs during the healing process. This amino acid is synthetized in healthy humans, but additional L-arginine is needed after injury. A comprehensive review on the L-arginine metabolism and healing has been written by Stechmiller *et al* (2005). Modifying nanofibers with L-arginine has been dealt with in only a small number of papers. Subramaniyan *et al.* coated polyurethane nanofibers with L-arginine for biological *in vitro* testing (Allur Subramaniyan et al., 2018). Other authors have modified the surface of a lignin or cellulose nanofiber gel with L-arginine for wound healing (Reesi et al., 2018; Feizabadi et al., 2018). It is important to mention, that L-Arginine incorporated to the nanofiber-containing gels accelerated the wound healing process better comparing to L-Arginine solution. The suggested explanation for this is the similarity of a nanofibrous layer to extracellular matrix (ECM) (Yoo et al., 2009; Chou et al., 2015).
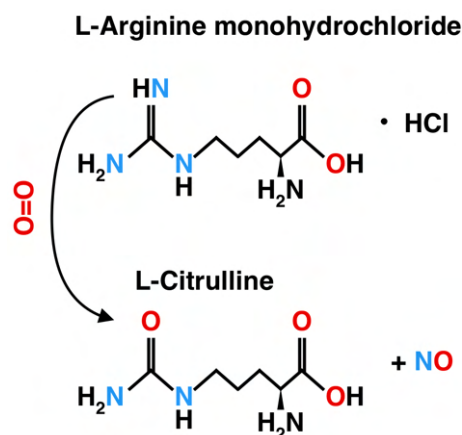
Figure 2.3: Chemical structure of L-Arginine and schematic representation of its hydroxylation to form L-Citrulline with release of nitric oxide.

2.2.3 Lipophosphonoxins (LPPO)

The third molecule which will be described in following chapters is a novel modular compound termed lipophosphonoxins (LPPO) was synthesized by Dominik Rejman's group (Seydlová et al., 2017). From a chemical point of view, LPPO are small amphiphilic molecules bearing positive charge. LPPO has a modular structure, as can be seen from Figure 2.4 (left), consisting of four modules: nucleoside module, a hydrophobic module, an iminosugar module and the phosphonate linker-module, holding all the modules together.

The modifications of the iminosugar module led to developement of second-generation LPPO, which were used in the present study. It was already proved to have a significant antibacterial activities against a wide range of bacteria, both gram-positive and gram-negative, including the strains with a developed multidrug-resistance, with no cytotoxicity on human cells at bactericidal concentrations (Panova et al., 2015). The mechanism of action of LPPO, however, differs remarkably from that of conventional clinically used antibiotics. LPPO act by permeabilization of the bacterial membrane leading to its disruption and, subsequently, to cell death. Taking into account, the unique structure and mechanism of action of LPPO, it is not anticipated that microorganisms will develop cross-resistance as they do with conventional antimicrobial drugs (Seydlová et al., 2017). The use of LPPO as an antimicrobial additive was already successfully evaluated in bone cement (Zbornikova et al., 2020).
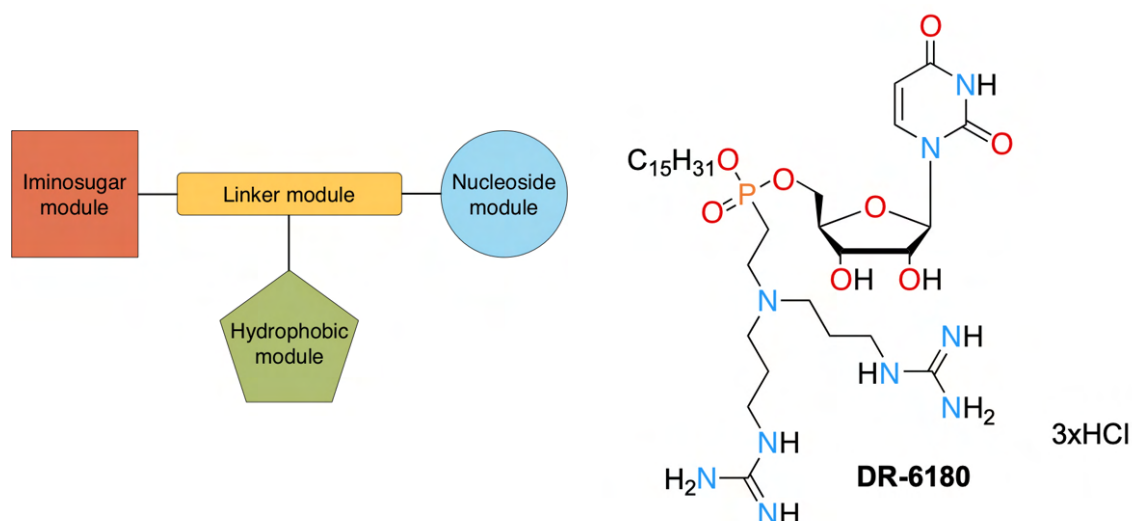
Figure 2.4: Lipophosphonoxins. Scheme of a general modular structure of lipophosphonoxins (left) and the chemical structure of the second generation-LPPO DR-6180 compound used in the present study

2.3 Morphology of drug-loaded wound dressings

2.3.1 Nanofibrous membranes loaded with Alaptide, L-Arginine or their mixture

All polymer/drug formulations were successfully electrospun with two types of additives (dipeptide and amino acid) incorporated into the PCL fibers individually as well as their mixture. The reason of combination of Alaptide and L-Arginine was to verify its possible synergic effect on acceleration of wound healing process. PCL is one of the most promising polymers for use as a wound dressing due to its capacity to tune the biodegradability and cytocompatibility. The morphological analysis of produced nanofibers revealed that the differing drug loading concentrations led to the formation of differing morphologies, as can be seen from micrographs in the Figure 2.5.
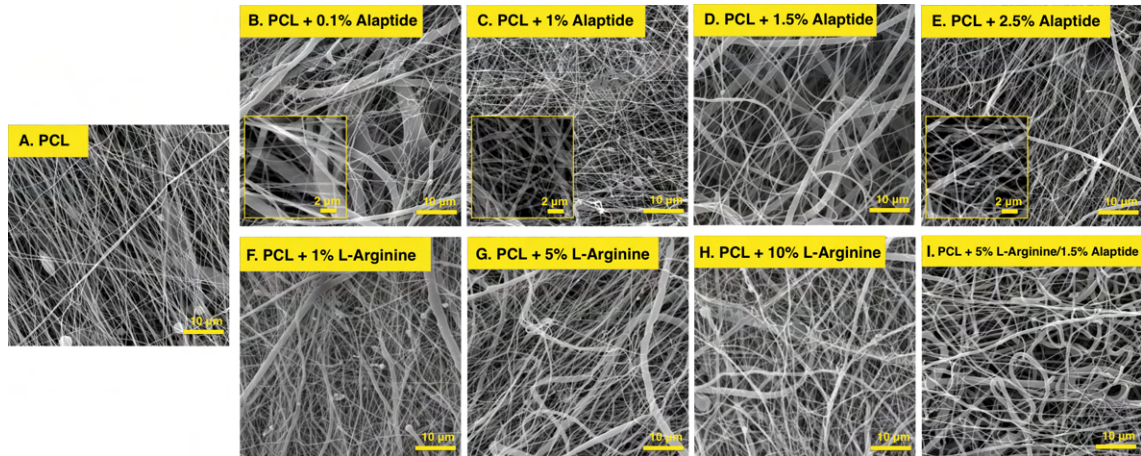
Figure 2.5: Representative SEM micrographs of the electrospun PCL nanofibers loaded with Alaptide or/and L-Arginine. A - pure PCL, B-E – morphology of nanofibrous mats with 0.1, 1, 1.5, and 2.5% of Alaptide. F-I - morphology of nanofibrous mats loaded with 1, 5, and 10% of L-Arginine. I - the nanofibrous mat loaded with mixture of 1.5%Alaptide+10%Arginine. The scale bars are 10 μm (2 μm in the magnified images).

Generally, the fabricated PCL nanofibrous layers had multimodal distributions of fiber diameters (Figure 2.6). This is mainly due to the use of a critical concentration of the polymer that already forms fibers without beads for a given solvent system and molecular weight distribution (Puppi et al., 2010). With increasing concentration of the polymer, or with use of higher molecular weight, monomodal but thicker fibers would be obtained (Mikes et al., 2021). The increase in the loading of Alaptide led to a corresponding decrease in the fiber diameters. Hence, the thinnest fibers were attained from the solution with the highest degree of Alaptide loading (2.5 wt %). However, PCL with 1.5 % Alaptide had the broadest fiber distribution of all the produced materials, which affected the mean value. On the other hand, the increment of the L-Arginine loading led to the increasing fiber diameters. The electrospinning of nanofibers loaded with the mixture of 5 % L-Arginine 1.5% Alaptide resulted in the broad-peak fiber diameter distribution with morphology similar to the material with 1.5% of Alaptide. Comparison of the fabricated doped layers to the control sample (pure PCL) revealed a statistically significant difference for all the drug-loaded samples with exception of PCL + 1.5 wt.% Alaptide and and 10 % of L-Arginine.
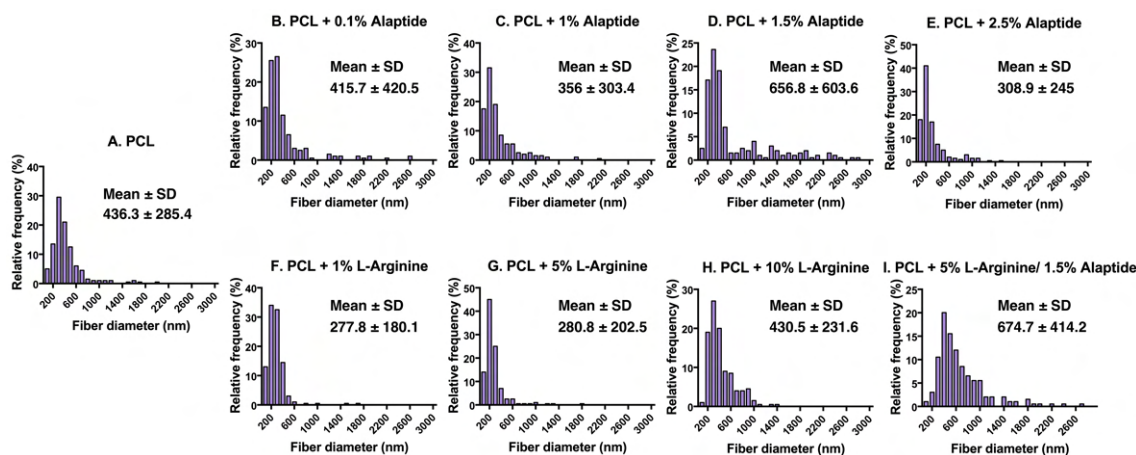
Figure 2.6: Histograms of fiber diameter distribution and mean values of nanofibrous materials loaded with Alaptide and/or L-Arginine (n=200). A - pure PCL, B-E – nanofibrous mats with 0.1, 1, 1.5, and 2.5% of Alaptide. F-I - morphology of nanofibrous mats loaded with 1, 5, and 10% of L-Arginine. I - the nanofibrous mat loaded with mixture of 1.5%Alaptide+10%Arginine.

The differing mat morphologies were partially explained by the differing compositions of the electrospinning polymer solutions in terms of the low solubility of both additives. The solubility of Alaptide in the used solvent system at 20° C was determined experimentally at 3.06 mg/mL (i.e. ∼0.18 %). This finding is in accordance with Figure 2.7), where the relatively sharp transition from solution to suspension is visible between 0.15 and 0.20 % w/w of Alaptide. L-arginine is soluble in water and slightly soluble in ethanol (Bowden et al., 2018). Thus, it was expected that the precursor solution with 0.1 wt% of Alaptide would be fully dissolved so as to form a solution, whereas the rest of the Alaptide or L-Arginine-containing formulations were expected to consist principally of undissolved nano- or micro-particles, thus forming a suspension. Further, it was assumed that electrospinning from the solution would lead to forming a so-called *"monolith solution"* matrix type wherein the drug was homogeneously dissolved throughout the polymer matrix. In contrast, electrospinning from the suspension would result in a *"monolith dispersion"* with a higher degree of heterogeneity and drug particle (crystal) diameters comparable to those of the fibers (Juergen Siepmann et al., 2012). In this regard, some of the defects found on the SEM micrographs of the nanofibrous structure had similar shapes and sizes as L-arginine and Alaptide particles. This is mainly due to electrospinning from suspensions (with the exception of 0.1 wt.% Alaptide).

The particular solvent system (see chapter 7.1) was used for electrospinning because chloroform is a good solvent of PCL. However, chloroform has a moderate dielectric constant and creates fibers with relatively large diameters. The increase in the dielectric constant with the addition of ethanol, methanol or dimethylformamide produces fibers with a more narrow distribution profile of the fiber diameter (C. Luo et al., 2012). Addition of ethanol was chosen due to its relatively low toxicity. Another option is to use the acetic and formic acid solvent system. This system reduces the diameter of the fibers as the dielectric constant increases, however the

polymer solution is unstable and may become degraded over time (Ekram et al., 2017).
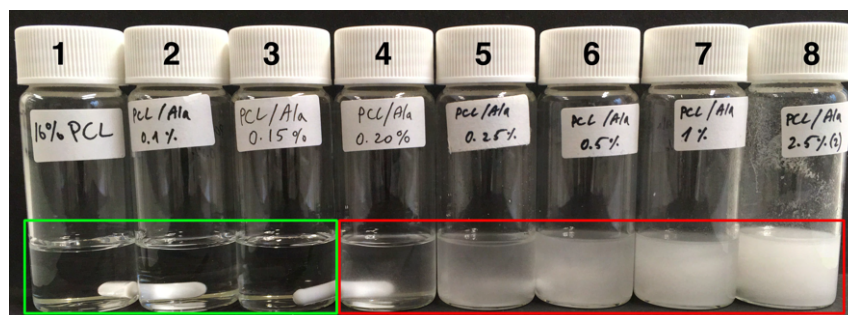

Figure 2.7: Solubility of Alaptide in the polymer solution (16% PCL, CHCl3/EtOH 9:1). Samples 1–8 represent PCL solutions with 0, 0.1, 0.15, 0.20, 0.25, 0.5, 1 and 2.5 wt% of Alaptide, respectively. The green frame indicates the "solution" range, and the red frame indicates the "suspension" range.

2.3.2 Nanofibrous membranes with LPPO

The PCL-based nanofibrous wound dressings were successfully prepared with additions of three different concentration of antibacterial molecule LPPO (DR-6180). The morphology of the fabricated layers is depicted in Figure 2.8 A-D. The morphological analysis of the membranes revealed comparable morphology in terms of fiber diameters, with median values around 300 nm for all the materials (see Figure 2.8 E-H). The multiple comparisons of the LPPO-loaded membranes with the control (pure PCL) showed a statistically significant difference (P-value-based) for the membranes with 2 % and 10 % of LPPO. Despite this, it can be assumed, that the difference occurred mainly from the heterogeneity of the materials itself. However, the slight decrement of fiber size of PCL+10% LPPO layer can be explained by the surfactant-like behaviour of LPPO, which might significantly decrease the surface tension of the polymer solutions. Additionally, as was proved later (see Do Pham et al., 2021 for more details), higher loading of LPPO enhanced wettability and biodegradability of the materials, simultaneously providing significant antibacterial properties.
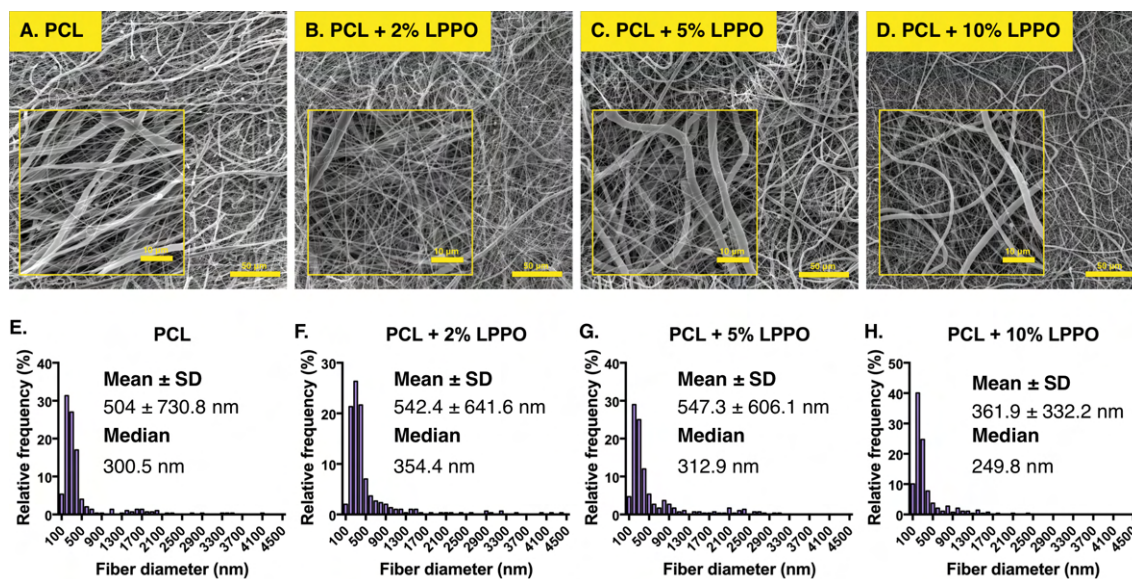
Figure 2.8: Representative SEM micrographs and histograms of fiber diameters of the fabricated PCL nanofibrous layers loaded with LPPO. A - pure PCL, B - PCL+2%LPPO, C- PCL+5%LPPO, D - PCL+10% LPPO. The scale bars are 50 μm (10 μm in the magnified images).

Noteworthy, the distribution of fiber diameters for the LPPO-loaded materials was multimodal as well as the materials loaded with Alaptide and L-Arginine, with most of the diameters distributed around the median value and some highly exceeding the size of one micrometer. Obviously, these thick outliers may significantly shift the mean values and increase the standard deviation. Thus, commonly used statistical software (e.g., GraphPad) often offers various algorithms to obtain the good-looking "cleansed", outlier-free data. However, it will be discussed in the following chapters how important is to take into the account these "outlying" thick fibers (high above one micron), in order to understand the release kinetics of substances from the nanofibers.

2.4   *In vivo* evaluation of the healing capabilities

Performance of drug-loaded membranes fabricated in the current PhD study were tested *in vitro* in terms of antibacterial activity, cell migration and proliferation. Despite this, in order to evaluate the healing capabilities, the drug-loaded materials were tested under *in vivo* conditions in cooperation with First Faculty of Medicine, Charles University (Prague) (Mikeš et al., 2020) and Prague Burn Centre, Third Faculty of Medicine, University Hospital Královské Vinohrady (Prague) (Do Pham et al., 2021). Nanofibrous membranes with Alaptide or Alaptide+L-Arginine mixture were tested on *Female albino* laboratory rats. Particularly, two types of skin wounds were studied - deep skin incicison (15-20 mm in length) and circular skin burns (⌀25 mm) in the dorsal area of the animals. Nanofibrous membranes loaded with lipophosphonoxins were tested on inbred male Balb/c (Balb) mice model.

2.4.1 Burn wounds

Nanofibrous membranes loaded with Alaptide or Alaptide+L-Arginine mixture

Figure 2.9 shows the process of healing of burn wounds which were monitored visually for 7, 14, 21, 28 and 35 days in order to estimate burn recovery. It can be seen from Figure 2.9 that in all cases a burn injury resulted in marked skin necrosis and appearance of erythema (reddening). Instantly after the burn injury, the burns were covered with drug-loaded PCL membrane. On the 7th day after the injury dead tissue pieces (eschar) were noted in all the wounds. It can be seen from the images (second and third row), that the treated wounds the eschar were densely covered with gradually degradation PCL membranes. Important to mention that gradual erosion of the wound dressing, combined with diffusional transport, increased the release of the loaded substances to the wound, thus enhancing the healing process. Over the further days of the study, the burn injuries treated with drug-loaded PCL membranes was found to be significantly different in terms of general wound closure and re-ephitalization, comparing to the control. At the end of the study, day 35, almost completely healed wound was observed for wound treated with drug-loaded PCL membranes. Whereas, the untreated burn injury did not achieve the complete closure within this time period.

The results of time dependence of wound area during the healing of skin burns also demonstrated (Mikeš et al., 2020) the significant difference between treated and untreated wounds. Moreover, synergetic effect of two biomolecules was revealed comparing wounds treated with Alaptide-loaded and Alaptide/Arginine-loaded PCL membranes.

Figure 2.9: Representative images of the healing process (5 weeks) of burn wounds with control membrane without treatment (first row), Alaptide-loaded membranes (second row), 1.5wt%Alaptide+5wt%L-Arginine mixture-loaded membranes (third row). Scale bar is 10 mm. (Reprinted from [Mikeš et al., 2020]).

2.4.2 Skin incisions

Nanofibrous membranes loaded with Alaptide or Alaptide+L-Arginine mixture

The second type of wound for investigation of the healing capabilities was deep skin incisions. The depth of the skin incisions was 4 mm. Figure 2.10 depicts the healing process of control group and the wounds treated with drug-loaded PCL membranes. The control group was not treated over the whole healing process. There is an evident difference in terms of the eschar area within the first seven days after injury. As was discussed previously, the end of first week corresponds to the phase of proliferation. This stage is characterized by the appearance of red granulation tissue with an uneven texture, consisting of collagen and other biomolecules present in extracellular matrix. This granulation tissue serves as a scaffold for the formation of new connective tissue and skin (Gonzalez et al., 2016). The presence of dark granulation may indicate an infection, ischemia, or poor perfusion. During this proliferative stage, the wound continuously shrinks and the new tissues are formed. It can be seen from Figure 2.10 that this process lasted for at least 14 days for the untreated group. At the end of the proliferative stage, epithelial cells reappear on the skin incisions surface. During the last phase the type III collagen is gradually replaced by type I collagen and the wound closes, and the skin area becomes stronger as the thickness of the scar decreases (Gonzalez et al., 2016). It can be seen from Figure 2.10 that for the untreated group the remodeling was observed after third week of the study.

Considering the groups, which were treated with drug-loaded PCL membranes, the significant acceleration of the healing process was observed (Figure 2.10, second and third row). The epithelization phase was observed already after the first week. The gradual reduction of the wound area during the further stages of healing was also much more pronounced for the treated groups. Visible enhancement of the wound healing process can be explained by the specific structure of the nanofibrous wound dressing, which protects the wound from infection and damage, as well as maintain the moisture level and cleanliness within the wound.

Figure 2.10: Representative images of the healing process (4 weeks) of deep incisions with control membrane without treatment (first row), Alaptide-loaded membranes (second row), 1.5wt%Alaptide+5wt%Arginine mixture-loaded membranes (third row). Scale bar is 10 mm. (Reprinted from [Mikeš et al., 2020]).

Generally, both tested compounds used in this study remarkably accelerated the healing process of experimental wounds *in vivo* in rats. The healing process of the burn wounds treated with a combination of Alaptide and L-Arginine lasted 28 days (4 weeks), leading to the wound area close to zero as a result. Whereas for the untreated burn wounds, this process took about 42 days (6 weeks). Considering the incision wounds, the healing process lasted 4 weeks both for the treated and untreated wounds. Despite this, the healing was different in terms of the size (area) of eschar which was formed in the beginning of the healing process. A presence of relatively large eschar was observed during the whole period of healing for the untreated wounds, while rapid decrement of wound size with almost no eshar formation was observed for the membranes treated with Alaptide or with the Alaptide/L-Arginine combination (see Figure 2.10).

It is assumed that the main potential for the use of these modified nanofibrous membranes is in the treatment of relatively large wounds, where supportive material is required. This type of wounds are often infected and thus can cause sepsis, especially in the case of burn wounds. Functionalization of nanofibers not only with wound healing drugs but also with antibacterial drugs is therefore essential for clinical applications of the nanofibrous wound dressings. As will be discussed in the following sections, the second-generation LPPO may serve as a good candidate for such a antibacterial agent to be incorporated to nanofibers.

2.4.3 Infected skin incisions

Nanofibrous membranes with LPPO

An 8-mm disposable skin biopsy punch was used to create a full-thickness skin defect overlying the thoracic spinal column and the adjacent musculature. The open wounds were then infected with *Staphylococcus aureus* strain. The wound experiment was evaluated on post-operative day 7th. As reported, wound infection was clearly visible by the presence of purulent exudate. The nanofibrous PCL wound dressings loaded with 5 wt% and 10 wt% of LPPO displayed a pronounced infection-impairing effect with negligible (from cytotoxicity point of view) systemic levels in liver and/or plasma. Whereas the wound dressing with 2 wt% LPPO had limited antibacterial activity. Additionally, the newly developed PCL wound dressings with and without LPPO slightly improved granulation tissue formation.

2.5 *In vitro* drug release studies

In order to develop an active antibacterial/healing-enhancing wound dressing, the controlled release of the incorporated agent is crucial. Therefore, the produced nanofibrous materials were examined under *in vitro* conditions in order to investigate the kinetics of release of the incorporated substances into a phosphate-buffered saline (PBS) environment.

2.5.1 Nanofibrous membranes loaded with Alaptide or Alaptide+L-Arginine mixture

First of all, in order to verify the efficiency of drug incorporation, the drug loading within the fabricated membranes was determined by means of HPLC. The values of predicted (calculated) and actual (determined) values for both molecules are summed up in Table 2.1.

The predicted drug loading [mg/g], Q, within the fibers was calculated on the basis of the dry mass in the polymer solution under the simple assumption of the complete evaporation of the solvent following electrospinning:

$$Q = \frac{m_{drug}}{m_{fiber}} \tag{2.1}$$

where m_{drug} [mg] is the mass of the incorporated substance added to the corresponding polymer solution and m_{fiber} [g] is the mass of the fibrous sample.

The determined Q (mg/g) values were not significantly different from the predicted values for both incorporated molecules. Table 2.1 shows that with concern to the 2.5 and 1 wt.% of Alaptide, the mean Q (mg/g) values were approx. 16.5% higher than the predicted values with standard deviation of approximately 10 %. Whereas the mean value for the 0.1 wt.% differed by a mere 2.5 %, thus suggesting the more homogeneous distribution of the drug throughout the nanofibrous mats.

Table 2.1: Comparison of the loading of Alaptide and L-Arginine [mg/g] in the nanofibers as determined via HPLC and the predicted values.

L-arginine loading in PCL		
Loading in the solution (% w/w)	Predicted loading in nanofibers (mg/g)	Determined loading in nanofibers (mg/g)
1	58.8	68.2 ± 5.4
5	238.1	299.3 ± 12.7
10	384.6	474.3 ± 55.9
Alaptide loading in PCL		
0.1	6.2	6.3 ± 0.6
1	58.8	71.8 ± 5.6
1.5	85.7	101.6 ± 10.7
2.5	135.1	159.3 ± 15.8

Similarly, the mean Q values for L-Arginine were slightly higher than the predicted values, but also mostly within the standard deviation range.

These differences in loading can be explained by the nature of the electrospinning solutions. It was observed that the suspension of L-arginine tends to be very unstable and the formation of of L-arginine agglomerates was visible over some time. This phenomenon affected the homogeneity of the distribution of the drug in the PCL membrane. The inconsistency relating to the drug loading for the higher loadings of both molecules may have been due to the presence of both the dissolved and undissolved drug within the nanofibrous mats. Moreover, with concern of Alaptide, the difference between the predicted and actual loading could have been caused by the polarity of the Alaptide molecule. The dipole moment of the molecule may lead to the rearrangement of the Alaptide molecules (particles) in the polymer solution as a result of the presence of an electrostatic field during the electrospinning process (Zhuang Li et al., 2014). Thus, it appears that the Alaptide-containing fraction of the precursor PCL solution was spun preferentially over "Alaptide-free" fraction.

On the basis of our preliminary *in vitro* studies (Mikeš et al., 2020), the drug release study of Alaptide from PCL nanofibers was repeated, given the shortcomings of the previous experiment and with emphasis on nature of the Alaptide release from nanofibrous structure. The cumulative drug release profiles of Alaptide (in mg) versus time (mean of the three samples) are depicted in Figure 2.11. The release of all the loadings was found to be biphasic with pronounced burst release at the outset. The PCL+2.5% Alaptide and PCL+1 wt% Alaptide samples exhibited more pronounced burst effects that resulted in the release of almost all the drug content within the first 24 h. The release of the lowest concentration, 0.1%, occurred in a more sustained manner and did not exhibit such a significant burst effect. With respect to the drug loading value shown in Table 2.1, more than half of the initial drug loading content was released within the first 10 h for all the samples (see Figure

2.11, D-F). On the basis of results from repeated experiments on cell metabolic activity, it was assumed that Alaptide loadings higher than 2.5 wt.% could support the healing process (Mikeš et al., 2020). This loading can be even increased, however according to these findings, the majority of drug content will, in any case, be released within the first hours.
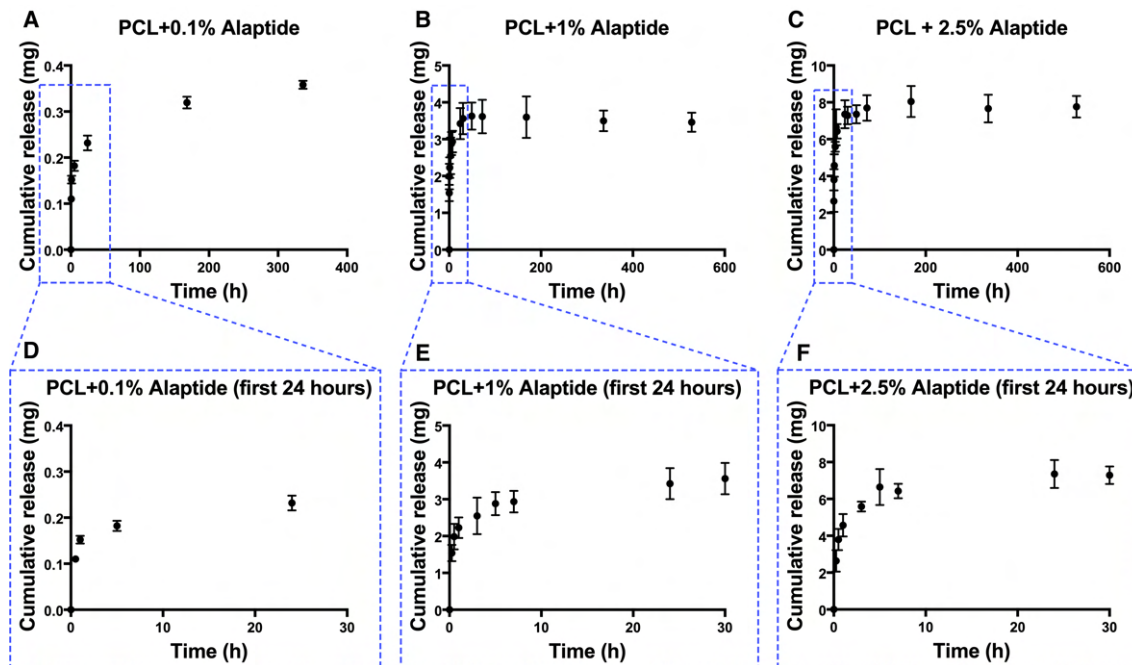

Figure 2.11: Cumulative release of Alaptide (in milligrams) from the PCL nanofibrous mats. The overall release time frame is depicted in the top panel (A-C). The graphs inside the blue dashed borders (D-F) represent the first 24 h of release.

Importantly, the subsequent dissolution of the electrospun mats revealed no residual Alaptide content trapped within the drug-loaded fibers at the conclusion of the release experiment, suggesting that the whole of the loaded Alaptide content had been released within 14 days.

The same method for the investigation of drug release kinetics from nanofibers loaded L-Arginine was applied. However, *in vitro* drug release experiment from Arginine-loaded membranes was rather complicated by the nature of L-Arginine. The cumulative amount of release L-Arginine decreased along with time. Most likely this happened due to the gradual degradation of L-arginine to L-citrulline in the release medium caused by the change in pH, which in turn distorted the HPLC measurement of drug release.

Thus instead of determining cumulative drug release, the change in pH level of demineralized water with immersed L-Arginine-loaded samples was measured (Figure 2.12). Similarly to Alaptide-loaded membranes, a burst release was observed for L-arginine according to a sudden decrement of pH in the first hours. Subsequently, the release kinetics study, confirming this observation by HPLC measurements was subsequently published by the colleagues (Horakova et al., 2020).
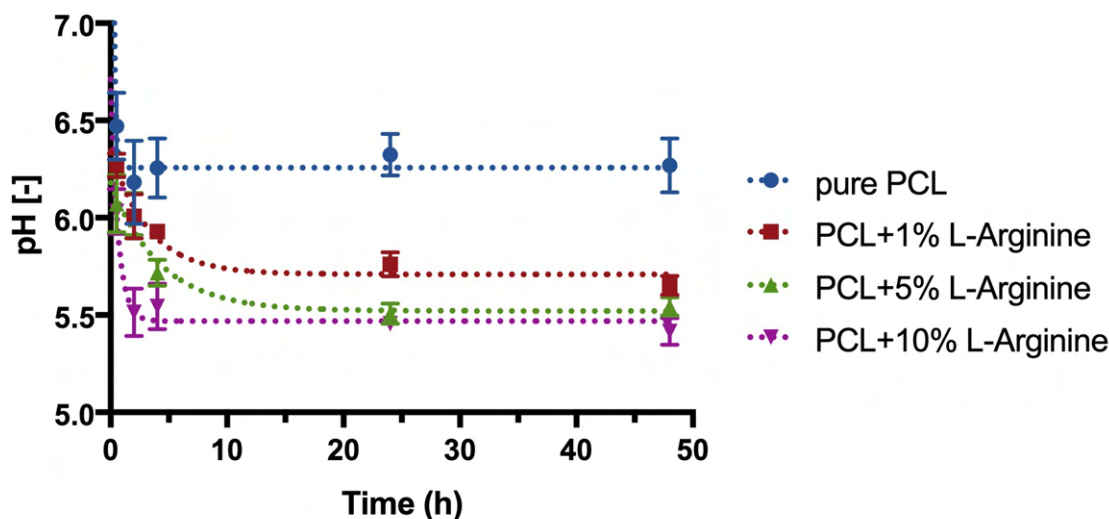
Figure 2.12: The measured change in the pH level of demineralized water after immersing the PCL membrane with various amounts of incorporated L-arginine. The first measurement was made at $t = 30$ min. The data points were fitted with an exponential function (dotted curve).

2.5.2 Nanofibrous membranes with LPPO

In contrast to the measurement of Alaptide/L-Arginine-loaded membranes, the attempt to measure LPPO loading within the nanofibers was unsuccessful due to the complex (surfactant-like) structure of the molecule. Unfortunately, a viable separation method was not developed within the given time frame of the study. The LPPO formed strong bonds with PCL, causing the formation of gel-like aggregates when the LPPO-loaded nanofibers were dissolved. As a result, it was not possible to separate the LPPO fraction for further HPLC analysis. Thus only the loading calculated on the basis of dry mass (see Equation (2.1)) is shown in Table 2.2.

Table 2.2: Actual loading of LPPO [mg/g] in the nanofibers.

LPPO loading in PCL		
Loading in the solution (% w/w)	Predicted loading in nanofibers (mg/g)	Determined loading in nanofibers (mg/g)
2	19.6	n/a
5	47.6	n/a
10	90.9	n/a

The cumulative LPPO-release profiles versus time are shown in Figure 2.13 for three different loadings of LPPO. In the similar fashion to Alaptide- and L-Arginine - loaded membranes, demonstrated biphasic (or even a "threephasic") release char-

acterized by a pronounced initial burst followed by the gradual release over time. The third phase may be distinguished for PCL with 5% and 10% of LPPO with a further stair-like increment in released amount after appx. 500 hours. Although, the detection limit of the developed HPLC method was relatively low, it can be seen that detectable cumulative release of PCL + 2% LPPO started only after 24 hours of experiment. Indeed, according to the predicted loading values (Table 2.2), the LPPO release rate was rather slow for all the examined membranes. Note, that the cumulative amount of released LPPO was proportional to the loading of LPPO. Thereby, the amount (in mg) released from PCL+10% LPPO was approximetely two times larger than that of PCL+5% LPPO and about 5 times larger than that of PCL+2% LPPO. This persisted consistence of the loaded ratios of loaded drug may indirectly indicate the homogeneous distribution of LPPO within the membranes.
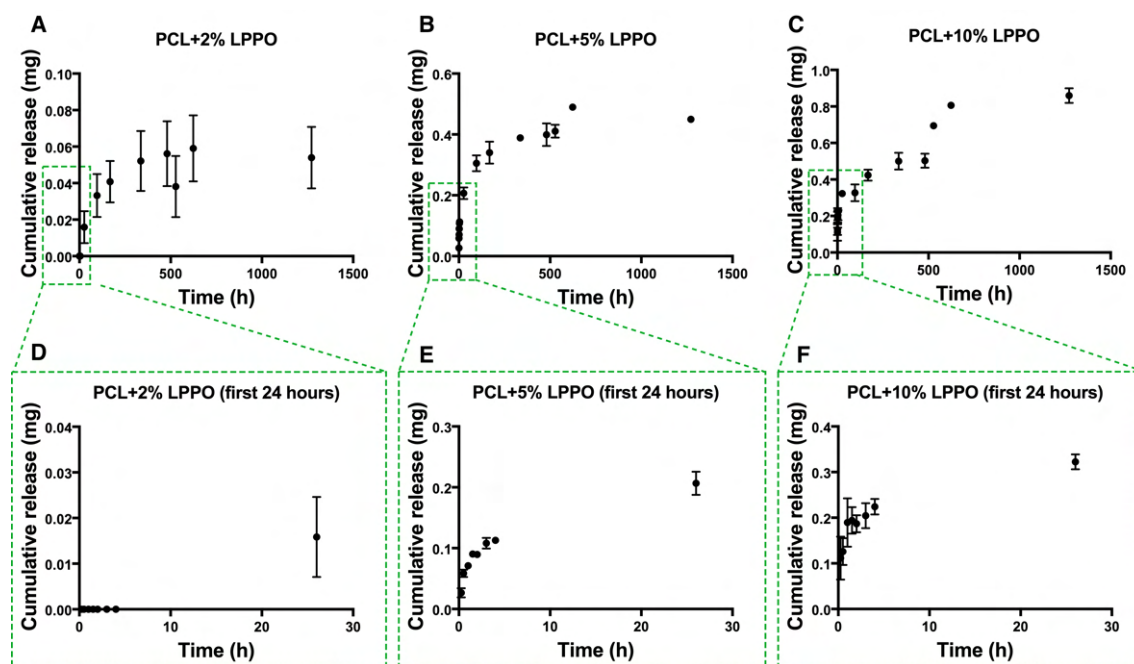

Figure 2.13: Cumulative release of LPPO (in milligrams) from the PCL nanofibrous mats. The overall release time frame is depicted in the top panel (A-C). The graphs inside the green dashed borders (D-F) represent the first 24 h of release.

The findings of subsequent studies (Do Pham et al., 2021) suggested that diffusion may not be the only rate-limiting mechanism for LPPO release from PCL nanofibers, but also an errosion of PCL plays a significant role. The study demonstrated that enzymatically-catalyzed LPPO release from PCL nanofibers in the presence of lipase was concentration-dependent and correlated with the degradation rate of the PCL matrix. This particular feature can be beneficial for an active wound-dressing, as bacteria can enzymatically stimulate the release of LPPO in proportion to the bacterial load within the wound.

2.6 Conclusion

The aim of this chapter was to demonstrate the process of successful functionalization of PCL-based electrospun membranes intended as wound dressings and to evaluate its applicability in wound healing. Three different bioactive molecules were used as a model drugs, namely spirocyclic dipeptide Alaptide, single amino-acid L-Arginine, and the second-generation Lipophosphonoxins. In order to investigate the consequences of drug incorporation, the fabricated drug-loaded materials were characterized in terms of morphology. The release of the incorporated drugs from produced nanofibers was studied under *in vitro* conditions. Finally, the tests on rats/mice were conducted in order to verify the enhanced wound healing capabilities *in vivo* compared to the control group (untreated PCL nanofibers).

The morphology of nanofibrous membranes doped with Alaptide or L-Arginine was dependent on the physical state of the incorporated drug in the polymer solution (or suspension). Some defects found within the structure of the membranes had size and shapes similar to Alaptide and L-Arginine. Whereas, no traces of LPPO on the surface of the nanofibers were found and it is assumed that all of LPPO was dissolved in the electrospinning solution. The release of the incorporated drugs was bi-phasic with a pronounced burst release in the initial stage. Due the complex nature and surfactant-like behavior of LPPO, there was likely other release mechanism involved besides diffusion. All the developed nanofibrous membranes enhanced the wound healing process under *in vivo* conditions.

The findings of this chapter have important implications for the field of wound dressing development, as they demonstrated that the fabricated nanofibrous membranes doped with the selected bioactive agents have a great potential for enhancing wound healing and reducing the risk of the *S. aureus*-induced wound infection (or sepsis). Some important aspects of drug incorporation strategies to electrospun nanofibers are also discussed. Although the studies covered in this chapter provide promising results, the author acknowledge that further *in vitro* drug release studies with modified conditions are necessary in order to obtain reliably reproducible results. Generally, future research could explore the behaviour of releasing substances loaded at close-to-solubility-limit concentrations in order to understand the difference in release mechanisms for monolith-dispersion and monolith-solutions matrices. The combination of developed nanofibrous materials with other suitable formulations (e.g., hydrogels) could be investigated as well as the combination of the wound healing-enhancing molecules and the antibacterial agents in order to achieve a synergy effect of different components.

In conclusion, this chapter has demonstrated the great potential of the developed nanofibrous membranes as a novel approach for accelerating wound healing process and eliminating the risk of microbial infection of the wound. Indeed, the estimation of an appropriate drug loading and prediction of its release behaviour is essential to design and develop a decent wound dressing. Thus, in order to predict the drug release kinetics from nanofibers, use of a mathematical model is needed. The next chapter will cover the development of such a mathematical model for a diffusion-controlled release on the basis of the diffusion equation.

3 Chapter III: Development of the mathematical model of drug release

3.1 Introduction

This chapter will describe the theoretical approach to releasing kinetics of a substance from nanofibrous structures. It will demonstrate how essential specific parameters of the fibrous mat are. The majority of the text that comprises this chapter was previously published in the *Journal of Drug Delivery Science and Technology (2021), volume 63, p. 102492* (Asatiani; Novotný, et al., 2021).

This chapter aims to evaluate the relevance of applying classical mathematical models to nanofiber structures. We will also explore the need for novel approaches, taking into account the specific features of nanofiber-based drug delivery systems. Accordingly, the development of a new mathematical model that describes the diffusion of substances from nanofibers using an analytical solution of the diffusion equation in cylindrical coordinates will be described.

3.2 "Rethinking models": Why do we need a new mathematical model in the first place?

Despite the relatively evident complexity of nanofibrous drug delivery systems, few attempts have been made in recent years to establish a mechanistic approach to the kinetics of drug release from nanofibers. Some authors have reported numerical calculations such as the Finite Elements Method (Nakielski et al., 2015; Kojic et al., 2017; Milosevic; D. Stojanovic, et al., 2018), Method of Lines (Halwes et al., 2018), or simple iterative schemes (Cabrera et al., 2006). In contrast, analytical approaches to addressing such issues have been suggested in studies by Srikar et al. (2009), Gandhi et al. (2009) and Khansari et al. (2013) that advocate the desorption-limited approach, as well as in recent studies by Petlin et al. (2017) and Spiridonova et al. (2019) that describe models controlled by the fiber distribution. Recently, a study has been reported that combines the Finite Elements Computational Method and the fiber-distribution model by Petlin et al. (Milosevic; D. B. Stojanovic, et al., 2020). In addition, only a limited number of these studies attempt to estimate the drug diffusion coefficient Srikar et al., 2009; Gandhi et al., 2009; Spiridonova et al., 2019; Petlin et al., 2017; Chung et al., 2019 within the nanofibers, which may

differ significantly from the apparent diffusion coefficients estimated for the same polymer but other geometries (e.g., polymeric slabs or pellets) Rosenberg et al., 2007; Muschert et al., 2009.

In the study by Srikar et al. (2009) a case in which the release of the drug is significantly below 100% is described. However, it is possible to misinterpret this model, particularly in cases where the percentage amount of the released drug is merely calculated (from the polymer solution) rather than determined experimentally, i.e., it is possible to determine a drug release count of less than 100 % in cases where the incorporation efficiency is less than 100 % (e.g., due to the insufficient stirring of the polymer solution).

The results of the studies conducted by Petlin et al. (2017) are limited by the assumption of a monolithic solution-type drug delivery system. In the case of monolithic dispersion, the model will not necessarily function when electrospinning proceeds from a suspension. Although work by Petlin et al. (2017) was based on real experimental data, the nanofibrous mats examined had a relatively homogeneous distribution of fiber diameters. In particular, the value of the coefficient of variation (CV) of the fiber diameter distribution would typically have higher values (Colmenares-Roldán et al., 2017), especially concerning polycaprolactone fibers.

Nowadays, it is customary in modern scientific literature to characterize the mechanisms of release from nanofibers by applying widely-used empirical models such as the Korsmeyer-Peppas (3.1) and the simplified form of the Higuchi equation (3.2):

$$\frac{M_t}{M_\infty} = kt^n \tag{3.1}$$

$$M_t = k_H t^{1/2} \tag{3.2}$$

where M_t and M_∞ are the absolute cumulative amounts of the drug released at time t and at infinite time, n is the diffusional exponent, k is the pre-exponential factor incorporating the characteristics of the macromolecular network that forms the drug carrier, and k_H is the Higuchi dissolution constant.

The Korsmeyer-Peppas model, also widely known as the "power law", is valid for the first 60% of a normalized cumulative fractional release of a substance. This model takes into account substance release deviations from Fick's law following anomalous release behavior. The n value is related to the geometry of the matrix. It indicates the transport mechanism: particularly, if $n = 0.5$, drug release takes the form of Fickian diffusion; if $0.5 < n < 1$, drug release takes the form of non-Fickian diffusion due to the combination of erosion and diffusion, and $n = 1$, case II (relaxational) transport (Peppas, 1985). It should be noted that the Higuchi equation generally represents a special case of the Peppas model for $n = 0.5$

However, is using these models for such a complex system as nanofiber membranes appropriate? These models were originally derived for more familiar dosage forms – i.e., cylinders of known length (pellets), slabs (or thin films), or spheres, whereas nanofiber systems, in fact, comprise an assembly of infinite cylinders of various diameters. Unfortunately, such simplified models tend to

"hide" too much physical meaning in one equation parameter and are often misinterpreted. For example, the release mechanism is frequently attributed to a diffuse character based merely on the exponent value n<0.5 for slabs or n<0.45 for cylinders (Kuang et al., 2018; Preem et al., 2017; Pisani et al., 2019), whereas the original article (Peppas, 1985) states that "*the exponent n may take only values greater than* 0.5*; n < 0.5 is a clear indication of a statistical analysis problem*".
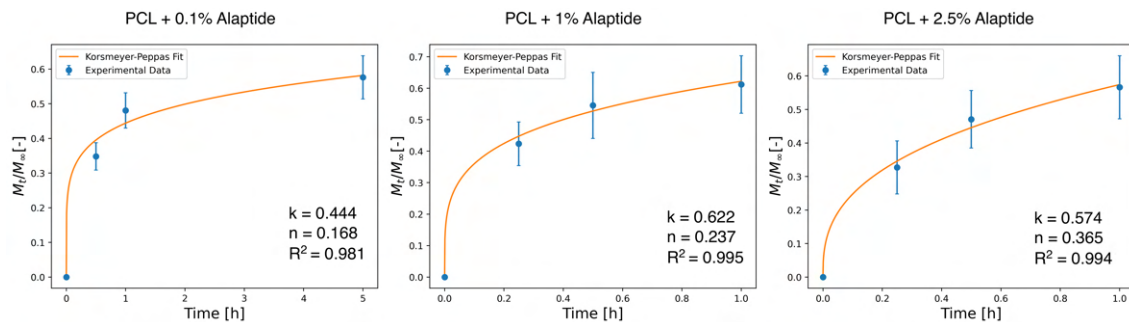

Figure 3.1: Representative results of fitting the experimentally obtained results of Alaptide release to the Korsmeyer-Peppas model.

Among others, nanofibrous drug delivery systems' burst release is a common issue. Sometimes, a significant part of the drug is released within a very short time frame, making it very complicated to withdraw aliquots consistently. Thus, if the preliminary study is being conducted, this can result in a lack of data points within the first 60 % range to be fitted with the Korsmeyer-Peppas model. Figure 3.1 shows an example of fitting the experimentally obtained drug release results to Korsmeyer-Peppas model. It can be seen that the goodness of the fit of all three data sets is high, i.e., 0.981, 0.995, and 0.994, respectively. However, the obtained values of the exponent n, 0.168, 0.237, and 0.365 do not make much sense or are just out of the acceptable range. As mentioned above, values lower than 0.5 might indicate an error in the data or the system assumptions in the first place.

3.3 Development of a new mathematical model

3.3.1 Establishing a problem

First, it is important to ask, ***what*** *is a nanofibrous membrane*? At least, what is it from the geometrical point of view? Depending on what the answer is, different approaches and the establishment of a mathematical problem will be applied. One can approximate a nanofibrous mat just as a thin slab (plane sheet). Another option can be considering nanofibrous membranes as porous mesh. This study will consider nanofibrous membranes a rather complex system of infinite cylinders. For this assumption, solving the diffusion equation in cylindrical coordinates with appropriate initial and boundary conditions is necessary.

Generally, three main cases can be considered when solving the problem of drug diffusion through cylindrical solids: a) solid cylinder of finite length, b) hollow cylinder of infinite length, and c) solid cylinder of infinite length (Vergnaud, 1993; Crank, 1979). We will focus on the last case, as the length of nanofibers can be assumed to be infinite. Moreover, this is the simplest case due to axial symmetry, as the diffusion is radial only; thus, the edge effects are negligible. The concentration of a drug $u(r, t)$ is dependent only on time t and the radius of a fiber, r. The diffusion equation in cylindrical coordinates for $0 \leq r \leq R$ and for $0 \leq t \leq \infty$, assuming axial symmetry, is:

$$\frac{\partial u(r,t)}{\partial t} = D \frac{1}{r} \frac{\partial}{\partial r} \left(r \frac{\partial u(r,t)}{\partial r} \right) \tag{3.3}$$

where D is the diffusion coefficient. Note, in our particular case, we assume that D does not depend on concentration changes (i.e., is constant).

It is assumed that at $t = 0$, the concentration of the drug in the fiber is uniform and equal to U_0 for $0 \leq r \leq R$, thus the initial conditions can be written as follows:

$$u(r, 0) = U_0 \qquad\qquad \frac{\partial u}{\partial r}\bigg|_{r=0,t} = 0 \tag{3.4}$$

3.3.2 Choice of boundary condition

Before choosing the boundary condition for $r = R$, one more aspect of diffusion-controlled drug release should be clarified. Although it may not be obvious, the release of drugs from nanofibers is conceptually similar to the evaporation problem of a liquid. It can be mathematically described with the same equations. Analogically to the evaporation of a liquid, in some cases, the boundary conditions relate to the rate of mass transfer of a drug across the surface of the medium. Crank (1979) describes this boundary condition as follows: during the evaporation, if the solid is initially dry and the air contains water vapor, the solid takes up moisture from the air. Such exchange of moisture at any time, t, will depend on the air's relative humidity and the actual concentration of the moisture on the surface of the solid. Crank (1979) provides a simple, reasonable assumption that the rate of this moisture exchange is then directly proportional to the difference between the actual concentration $u_0(r)$ at the surface at any time and the concentration U_∞ which would be achieved in the equilibrium with the vapor pressure in the atmosphere remote from the surface.
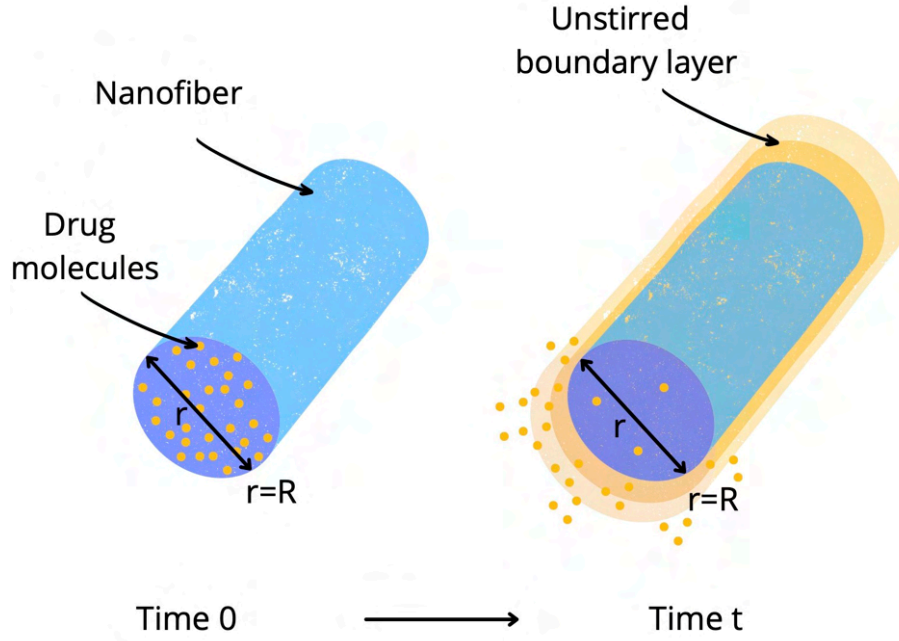
Figure 3.2: Illustration of drug release from a nanofiber involving unstirred boundary layer close to nanofiber surface. Initially, the drug is homogeneously distributed within the nanofiber (left) and the drug is released over time t from the nanofiber surface (right).

Similarly, when a nanofibrous matrix is immersed into a release medium, an unstirred boundary-layer mass transfer resistance may exist at the surface of the matrix (L. Fan et al., 1989) as illustrated in Figure 3.2. Most importantly, such a boundary layer may exist even in well-agitated release systems (L. Fan et al., 1989; J. Siepmann; Lecomte, et al., 1999; Muschert et al., 2009), giving rise to additional resistance. Simplified, in a well-agitated release medium, there is a region of a "completely unstirred liquid layer," where the mass transfer occurs only via diffusion, and then a "well-stirred bulk fluid," in which the mass transfer occurs mainly via convection (J. Siepmann; F. Siepmann, 2013). The mass transfer exchange is then analogical to the exchange of moisture described by Crank (1979).

It is worth mentioning that the real-life systems are rather complex, and these transitions are not that steep (Brunner, 1904). Despite this, two kinds of boundary conditions can be considered. The first one is when the mass transfer on the surface is so high (i.e., the mass transfer resistance is so low) that the concentration of the released substance on the fiber's surface reaches the constant value at equilibrium immediately after release starts. The second case assumes a finite mass transfer on the surface, which leads to concentration variations during the release process from the initial value to the value after reaching the equilibrium (Vergnaud, 1993). Mathematically, this boundary condition can be expressed as follows:

$$-D\frac{\partial u}{\partial r}\bigg|_{R,t} = h\left[u(R,t) - U_\infty\right]\bigg|_{R,t} \tag{3.5}$$

where h is a boundary layer mass transfer coefficient $[cm/s]$, which depends on the partition coefficient of the drug between the nanofibers and the release medium, as well as the thickness of the unstirred boundary layer (which is a function of agitation speed of the release medium) (L. Fan et al., 1989; J. Siepmann; F. Siepmann, 2013). Note that if this rate is large, the boundary condition should be $u(R,t) - U_\infty = 0$ (i.e., sink condition).

3.3.3 Solving the diffusion equation

Now, in order to solve the diffusion equation (3.3) with the given initial (3.4) and boundary (3.5) conditions, let us first introduce a new variable:

$$\tilde{u}(r,t) = u(r,t) - U_\infty,$$

where $\tilde{u}(r,t)$ represents the concentration of the diffusing substance in time t, and $u(r,\infty) = U_\infty$ is the concentration of the substance, which is trapped inside the polymeric matrix by means of intermolecular interactions at time $t \to \infty$. With this definition, we obtain a new boundary condition at $r = R$

$$\tilde{u}(r,0) = U_0 - U_\infty \qquad\qquad -D\frac{\partial \tilde{u}}{\partial r}\bigg|_{R,t} = h\tilde{u}(R,t) \qquad (3.6)$$

The problem (3.3) can be solved by the method of separation of variables $\tilde{u}(r,t) = T(t)R(r)$ (Crank, 1979), leading to the following solution:

$$\tilde{u}(r,t) = Ce^{-\lambda^2 Dt}J_0(\lambda r) \qquad (3.7)$$

We now apply this solution (3.7) to the boundary condition at $r=R$ (3.6), using the relation of Bessel functions that $dJ_0(x)/dx = -J_1(x)$, to obtain the following equation:

$$-\frac{hR}{D}J_0(\beta) + \beta J_1(\beta) = 0 \qquad (3.8)$$

with $\beta = \lambda R$.

The roots of this equation give the eigenvalues $\lambda_n = \beta_n/R$, which are dependent on the value of hR/D. The parameter hR/D will be discussed in more detail in the section 3.3.5. For the first ten positive roots of the equation (3.8) for various values of hR/D, the reader is referred to Table 3.1 (section 3.3.5).

With the eigenvalues β_ns, the general solution to the differential equation for $u(r,t)$ is the sum of $\tilde{u}(r,t)$ and U_∞.

$$u(r,t) = \sum_m C_m e^{-\left(\frac{\beta_m}{R}\right)^2 Dt}J_0\left(\frac{\beta_m}{R}r\right) + U_\infty \qquad (3.9)$$

The constant C_m can be found by the integration of initial condition that $\tilde{u}(r,0) = (U_0 - U_\infty)$.

$$\tilde{u}(r,0) = U_0 - U_\infty = \sum_m C_m J_0 \left(\frac{\beta_m}{R} r \right), \text{ we multiply and integrate}: \int_0^R r J_0 \left(\frac{\beta_n}{R} r \right) dr$$

$$(U_0 - U_\infty) \int_0^R r J_0 \left(\frac{\beta_n}{R} r \right) dr = \sum_m C_m \int_0^R J_0 \left(\frac{\beta_m}{R} r \right) r J_0 \left(\frac{\beta_n}{R} r \right) dr$$

From the orthogonality condition for the Bessel functions, we know that for $n \neq m$, the integral is equal to zero thus we can express the integral as follows:

$$(U_0 - U_\infty) \int_0^R r J_0 \left(\frac{\beta_m}{R} r \right) dr = C_m \int_0^R r \left[J_0 \left(\frac{\beta_m}{R} r \right) \right]^2 dr$$

Following the integration of both sides from $r = 0$ to $r = R$ we attain the result for the constant C_m:

$$C_m = \frac{2(U_0 - U_\infty)}{\beta_m} \frac{J_1 (\beta_m)}{[J_0 (\beta_m)]^2 + [J_1 (\beta_m)]^2}$$

Now we substitute this result into the general solution (3.9) of the problem for $u(r,t)$ to obtain the final solution of the problem for concentration of the diffusing (released) substance on fiber surface expressed in terms of series:

$$u(r,t) = U_\infty + \sum_m \frac{2(U_0 - U_\infty)}{\beta_m} \frac{J_1 (\beta_m)}{[J_0 (\beta_m)]^2 + [J_1 (\beta_m)]^2} e^{-\left(\frac{\beta_m}{R} \right)^2 Dt} J_0 \left(\frac{\beta_m}{R} r \right). \quad (3.10)$$

3.3.4 Amount of diffusing (released) substance

We have obtained the final solution in the form of a concentration profile. However, it is considered more appropriate to use the amount of the diffusing substance, M_t, from the fibers instead to simplify the comparison with the experimental data. To obtain the desired parameter, we will use Fick's first law, which postulates that the diffusive flux, j, goes from regions of high concentration to regions of low concentration, with a magnitude that is proportional to the concentration gradient (Fick, 1855; Crank, 1979).

$$j_R(t) \Big|_R = -D \frac{\partial u}{\partial r} \Big|_{R,t}$$

The amount of a diffusing substance $M(\tau)$ from the fibers after time τ is related to a flux of the substance through the boundaries (surface) of the fibers:

$$M(\tau) = 2\pi RNl \int_0^\tau j_R(t)dt = -2\pi RNlD \int_0^\tau \frac{\partial u(t)}{\partial r}\Big|_R dt, \qquad (3.11)$$

where Nl is a total length of fibers and $2\pi RNl$ is its total surface area. By substituting from equation (3.10), and using the following relation between Bessel functions:

$$\frac{d}{dr}\Big|_R J_0\left(\frac{\beta_m}{R}r\right) = -\frac{\beta_m}{R}J_1\left(\frac{\beta_m}{R}R\right)$$

with further integration we obtain the following equation for the amount of the diffusing substance from the fibers:

$$M(t) = 4\pi R^2 Nl\left(U_0 - U_\infty\right) \sum_m \frac{[J_1(\beta_m)]^2}{\beta_m^2\left([J_0(\beta_m)]^2 + [J_1(\beta_m)]^2\right)}\left(e^{-\left(\frac{\beta_m}{R}\right)^2 Dt} - 1\right).$$

As it is always easier to work with dimensionless numbers, we can now express the fractional release of the substance at time t with respect to total amount of substance release at time $t \to \infty$. The total amount of released substance at time $t \to \infty$ equals to $M(\infty) = (U_0 - U_\infty)\pi R^2 Nl$ and for $t = 0$ the amount of released substance is $|M(0)| = 0$. By using the expression $J_1(\beta_m)\beta_m/R = h/DJ_0(\beta_m)$ and simple algebra we obtain the final form of the solution for $r = R$.

$$\frac{M(t)}{M(\infty)} = 1 - 4\sum_m \frac{1}{\beta_m^2\left[1 + \left(\frac{D\beta_m}{hR}\right)^2\right]}e^{-\left(\frac{\beta_m}{R}\right)^2 Dt} \qquad (3.12)$$

3.3.5 Mass transfer coefficient in the boundary layer

Now let us focus our attention on the final solution (Equation (3.12)). In the boundary condition we introduced a parameter of proportionality h, called mass transfer coefficient in the boundary layer. Together with the diffusivity, D, and characteristic size of the system, R, it comprises a dimensionless parameter L, known as *Sherwood number* or also *the mass transfer Nusselt number*, which is a ratio between mass transfer resistance at the surface and the diffusional resistance throughout the polymer matrix (Vergnaud, 1993; Arifin et al., 2006):

$$L = \frac{h}{D}R, \qquad (3.13)$$

It is evident from the already presented equations that the parameter L has a strong effect on the final solution as it appears in the very beginning for the calculation of individual eigenvalues, β_ns, (Equation (3.8)). Thus, for the estimation of diffusion coefficients, D, we need to investigate the behavior of the Sherwood number in more detail.

If we plot Equation (3.8) as a function of β, we can see how the distribution of the roots β_ns, changes with varying values of L. However, we can see from the plots that the amplitude of changes between individual β_ns eventually descends with the increasing L. It is even more evident from Table 3.1, where the first ten eigenvalues β_ns are summed up.

Table 3.1: Roots of equation 3.8 for different values of dimensionless parameter L

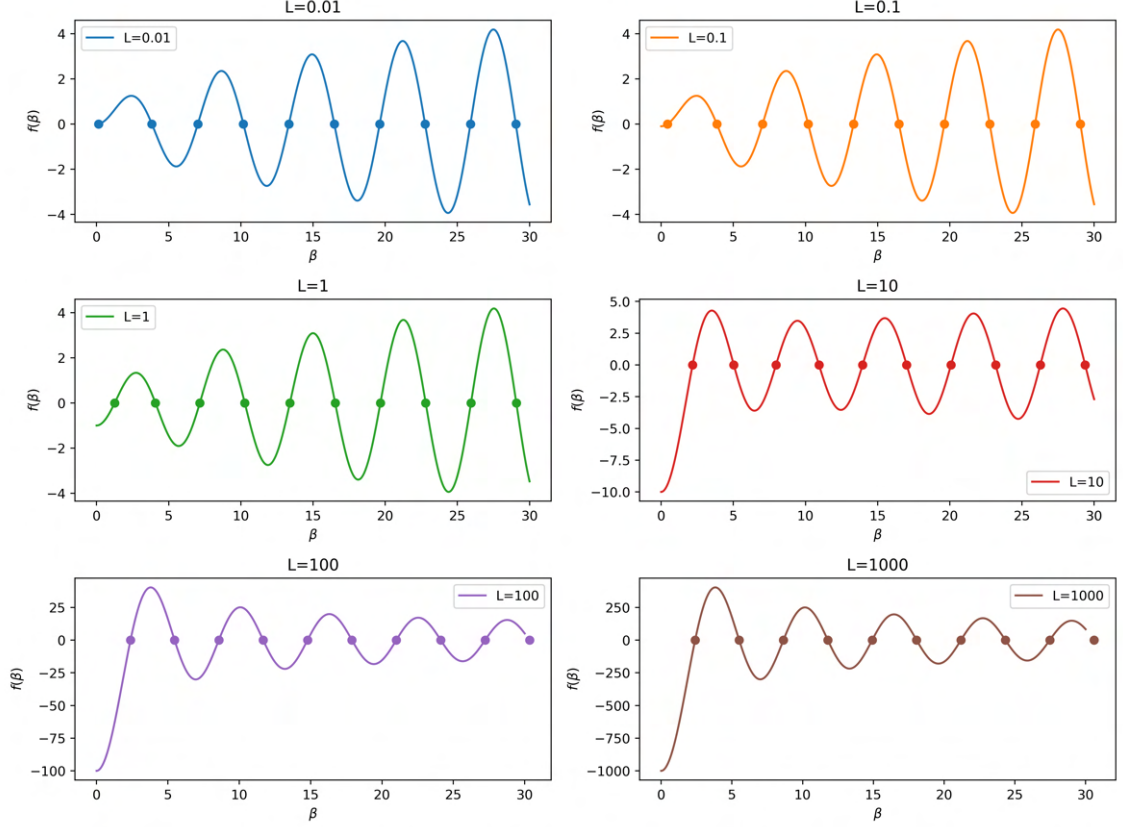| | Roots of $-LJ_0(\beta) + \beta J_1(\beta) = 0$ with $L = hR/D$ | | | | | | | | | |
L	β_1	β_2	β_3	β_4	β_5	β_6	β_7	β_8	β_9	β_{10}
0.01	0.141	3.834	7.017	10.174	13.324	16.471	19.616	22.761	25.904	29.047
0.1	0.442	3.858	7.030	10.183	13.331	16.477	19.621	22.764	25.908	29.050
1	1.256	4.079	7.156	10.271	13.398	16.531	19.667	22.804	25.942	29.081
10	2.179	5.033	7.957	10.936	13.958	17.010	20.083	23.171	26.270	29.377
100	2.381	5.465	8.568	11.675	14.783	17.893	21.004	24.115	27.226	30.339
1000	2.402	5.515	8.645	11.780	14.916	18.053	21.190	24.328	27.466	30.604
∞	2.405	5.520	8.654	11.792	14.931	18.071	21.213	24.354	27.496	30.638

Figure 3.3: Profiles of function $f(\beta) = -LJ_0(\beta) + \beta J_1(\beta)$ for different values of dimensionless parameter L. Dots are depicting first ten positive roots, β_ns, of Equation(3.8) (summed up in Table 3.1).

Indeed, if we now plot dependency of fractional release $M(t)/M(\infty)$ (Equation (3.12)) as a function of square root of dimensionless time $\sqrt{Dt}/R$ for various values of L (Figure 3.4) we can see that the fractional release profiles differ from each other significantly for L values below 100. However, there is no remarkable difference between $M(t)/M(\infty)$ profiles for L=100 and L=1000. Thus, the result is equivalent to the case of a constant concentration on the surface with negligible resistance of the boundary layer. In other words, large L effectively means *perfect sink* conditions.
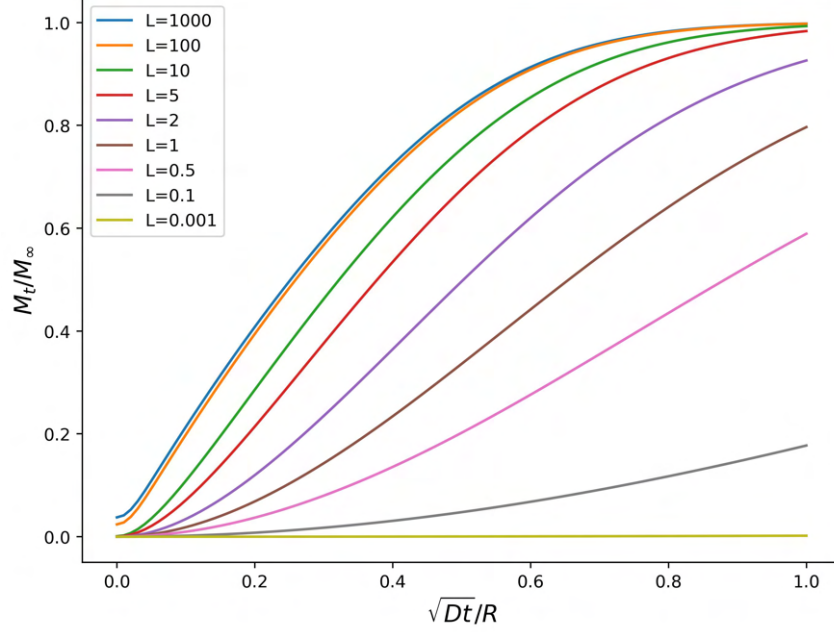
Figure 3.4: Fractional amount of substance released through the surface of a nanofiber as a function of the square root of dimensionless time, for various values of Sherwood number, L

Thus, at this point, it is necessary to consider the orders of magnitude for h, R, and D. The order of magnitude of the nanofiber radius is typically in the range of $10^{-4} - 10^{-5}$ cm. The diffusion coefficient of substances may vary significantly but is mainly reported to be $10^{-10} - 10^{-15}$ cm^2/h. Finally, the mass transfer coefficient h, can be determined from the tangent at the origin of the curve $M(t)$ expressed as a function of time (3.12)(Vergnaud, 1993). At the beginning of the process, the concentration on the surface remains the same as the initial concentration $u_0(r)$:

$$\frac{dM(t)}{dt} \cong h(U_0 - U_\infty) \quad pro \quad t \to 0.$$

This estimation of h, however, is difficult to approach experimentally. Another approach of determining h is related to the fact that the rate of mass transfer, h, in the boundary layer is proportional to the thickness of this boundary layer (Etters, 1995) as schematically depicted in Figure 3.5. Chien (1975) reported an experiment on estimating the mass transfer resistance by varying the rotational speed of release medium agitation and determining the thickness of a boundary layer. The experiment demonstrated a strong correlation between the agitation speed and the release rate of ethynodiol acetate from a silicone matrix. More frequently, however, the mass transfer coefficient is determined utilizing non-linear regression (Levenberg Marquardt method) of experimentally obtained data and the solution of the diffusion equation. Studies conducted by J. Siepmann (1999) and later by S. Muschert (2009) demonstrated that for polymer systems of various geometries the mass transfer coefficient was very high, in a range of $10^{-9} - 10^{-12}$ cm/h (leading to $L \approx 100$),

so that the mass transfer resistance within the boundary layer was considered negligible compared to the resistance within the polymer bulk. Despite this, in extreme cases, especially when dealing with an active agent of low solubility or high affinity to the polymer matrix, an unstirred boundary layer can become saturated with the diffusing substance and hinder (or even stop) the release from fibers.
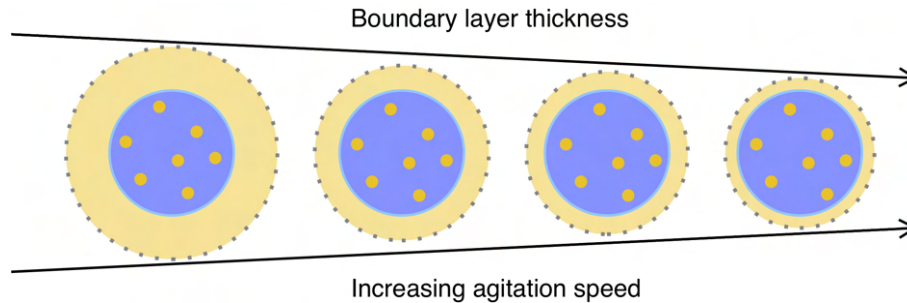

Figure 3.5: Schematic representation of dependency of boundary layer thickness on the speed of agitation of release medium (adapted from Etters, 1995). The Blue circles represent cross section of a fiber, yellow dots represent drug particles and the yellowish area around the fiber is the boundary layer.

To summarize, although the findings on total mass transfer resistance at the matrix surface can be contradictory, one must be aware of its potential ability to alter the release profile even of a well-designed drug delivery device. Moreover, the *in vitro* experiments conducted in a well-agitated medium do not necessarily reflect the situation at *in vivo* conditions (Roseman et al., 1976). Finally, one should consider that the behavior of systems can often change significantly when their components operate together(Anderson, 1972; Bar-Yam, 2019). Therefore, the specific complexity of the nanofibrous structure, which comprises a mesh of densely entangled fibers, may potentially escalate the thickness of the unstirred boundary layer at the surface of individual fibers.

Thus, implementation of the boundary layer resistance to the developed mathematical model might help reveal the physical nature of the release from the nanofibrous structures and avoid obstacles within the design process of a drug delivery system. Otherwise, if there is a firm belief that the effect of mass transfer resistance at the surface of a particular delivery system can be omitted (for large L) the boundary condition of a constant concentration can be applied: $u(R, t) - U_\infty = 0$.

3.3.6 Importance of fiber diameter distribution

We are approaching perhaps the most exciting part concerning the unique features of nanofibrous structures. It can be demonstrated that the results of the solution of the diffusion equation (3.12) are highly dependent on the input value of the fiber radii R. The particular impact of this value on the equation solution is evident from the following graph (Figure 3.6), which illustrates the dependencies of fractional release profiles, $M(t)/M(\infty)$, over time t for various values of fiber radius R [nm].
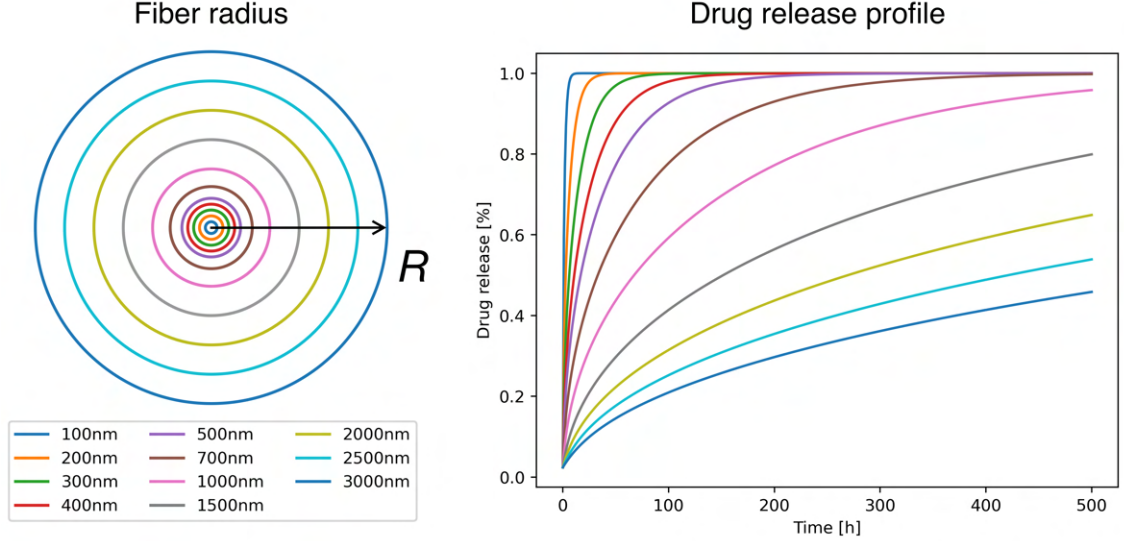
Figure 3.6: Dependency of fractional drug release profile, $M(t)/M(\infty)$, on fiber radius value as a function of time. The circles on the left represent different values of R from 100 to 3000 nm. The aspect ratio is preserved. The plot on the right depicts the drug release profile for the corresponding values of R over time. The diffusion coefficient is set to be 10^{-11} cm^2/h, and Sherwood number L equals 100.

For real nanofibrous systems, it is evident that even for exceptionally homogeneous fibrous structures there is always a certain distribution of fiber diameters. Subsequently, fibers with smaller diameters will exert a more pronounced effect on the mass transfer of a substance at the initial stage of release. In contrast, the thicker fibers will contribute to the release of the substance at later times. Hence, it is important to take into account the variability of the diameters of the fibers. The total drug release profile can then be considered a sum of individual "sub-profiles" (i.e., solutions of equation (3.12)) for various fiber fractions with a particular diameter. Depending on how broad the diameter distribution of a particular fibrous system is, it is necessary to determine the appropriate width of the group (bin width) from the histogram of the distribution of the fiber diameters and the probability or weight of their occurrence is then determined depending on the relative frequency of the particular fraction (bin):

$$p\left(R_i\right) \cong \frac{n\left(R_i\right)}{n_{\text{total}}} \tag{3.14}$$

where $p(R_i)$ is the probability of the occurrence of the i-th class of averages, $n(R_i)$ is the frequency of the averages of the mean radius R_i of the given class, and n_{total} is the total number of measurements.

Nevertheless, it should be considered that each fraction (bin) of the distribution of the fiber diameters in the classical histogram is weighted equally. On the other hand, even though the thick fibers may represent an extremely low percentage of the total number of fibers, this is not the case when one considers their volume. As

famous South Asian philosopher Sir Muhammad Iqbal once said, *"Democracy is a system where people are counted, not weighed."* (Ahmad et al., 2021). Indeed, is it appropriate to consider the individual fibers equally, taking the average value based just on their number?
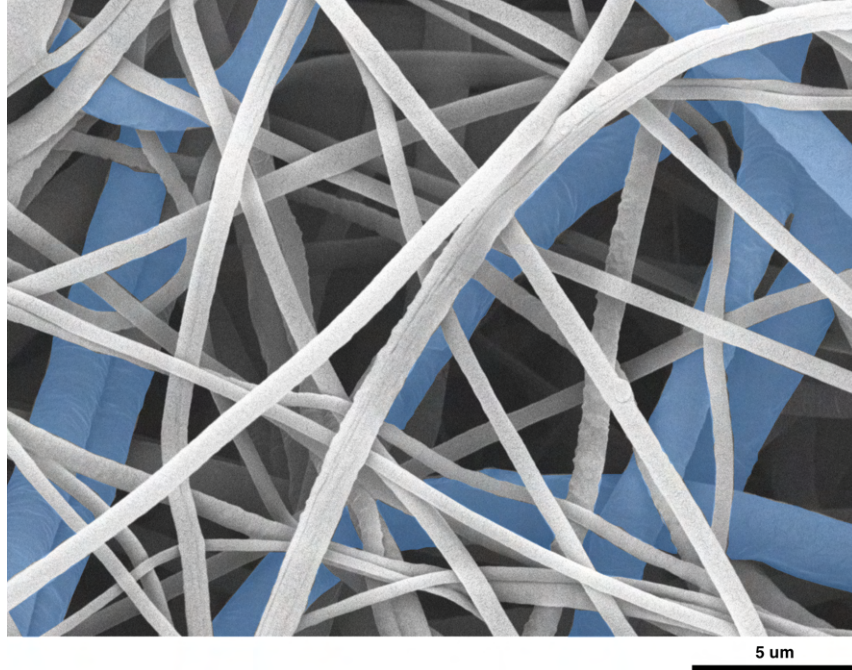

Figure 3.7: Representative SEM image of a typical submicrofibrous layer. The fibers with significantly larger diameters are highlighted in blue. The scale bar is 5 um.

To answer this question, consider a typical SEM image of an arbitrary submicrofibrous layer (Figure 3.7). In this figure, we can observe a bimodal distribution of fiber diameters. The thick fibers highlighted in blue are often treated as outliers due to their small number. On the other hand, it is clear that on a single selected section of the nanofiber mat, thick fibers will occupy much more space than thin nanofibers, even if the number thereof is orders of magnitude higher. Taking this fact into account and considering the infinite length of the nanofibers, a probability $P(R_i)$, firstly introduced by Petlin et al. (2017), has to be applied. It also considers the surfaces of individual fibers from the general distribution:

$$P_i\left(R_i\right) = \frac{n_i \pi R_i^2 l}{\sum n_i \pi R_i^2 l} \tag{3.15}$$

As previously discussed, the length of fibers within non-woven fibrous structures, l, can be assumed to be infinite. Thus, we can reduce πl expression both in the nominator and denominator to obtain the following expression:

$$P_i\left(R_i\right) = \frac{n_i R_i^2}{\sum n_i R_i^2} \tag{3.16}$$

The next chapter will demonstrate how this weighing significantly transforms a classical histogram of fiber diameter distribution. Now, if we include the volume-weighed probability of the nanofibrous radii into Equation 3.12, we finally obtain the desired solution for the diffusion equation:

$$\frac{M(t)}{M(\infty)} = \sum_i P\left(R_i\right) \left[1 - 4\sum_m \frac{L^2}{\beta_m^2 \left[\beta_m^2 + L^2\right]} \exp\left[-\left(\frac{\beta_m}{R_i}\right)^2 Dt\right]\right] \qquad (3.17)$$

This extended volume-weighted solution contains the separate groups of fiber radii and their significance coefficient (weight) based on their frequency of appearance within a given fibrous layer.

3.4 Conclusion

To conclude, we have seen that the complexity of nanofibrous drug delivery systems makes it inappropriate to use the mathematical models developed for the conventional dosage forms. Therefore, it is necessary to look for new approaches that consider the specifics of such systems.

The chapter demonstrated the process of the development of a mechanistic model for drug release kinetics from nanofibers. It is clear now that the complexity lies in how the drug interacts with the fibers and how the fiber interacts with the environment. Thus, many questions regarding assumptions for developing a model that adequately reflects reality remain unanswered.

Nevertheless, in the next chapter, the developed model will be applied to real experimentally-obtained data of drug release from nanofibers to determine the diffusivities of the drugs and assess the adequacy of the model.

4 Chapter IV - Application of mathematical model of release kinetics

4.1 Introduction

In the previous two chapters, we explored the application of electrospun nanofibrous wound dressings as drug delivery systems. It was demonstrated that to understand and to be able to predict the drug release kinetics, an appropriate mathematical model is needed. Nevertheless, conventionally used mathematical models describing the release of drugs may fail due to the complex morphology of nanofibrous drug delivery systems. Thus, the development of the new mathematical model for fibrous drug delivery systems was demonstrated in the previous chapter. This chapter will cover the application and verification of the developed model on the experimentally obtained data of drug release kinetics.

This chapter aims to demonstrate the developed mathematical model's efficiency in estimating diffusion coefficients of model substances in the nanofibers. The model was verified on experimentally obtained drug release kinetics data of Alaptide and LPPO (described in chapter 2.2). Unfortunately, a strong interaction between the PCL matrix and LPPO resulted in the non-diffusional behavior of its release from nanofibers. Thus, the diffusion coefficients for the LPPO-loaded materials were not obtained within the scope of this study, and the experimental solution to this problem will be suggested later in the chapter.

The text that comprises this chapter was published in *the Journal of Drug Delivery Science and Technology (2021), volume 63, p. 102492*

4.2 Results and discussion

4.2.1 Alaptide-loaded nanofibers

Fiber morphology before and after release

To verify the developed mathematical model concerning fiber diameter distribution, a more precise investigation of Alaptide-loaded nanofibers was conducted. This time, 300 diameters were measured in order to obtain reliable (confident) descriptive statistics. Analogically to the study by Petlin et al. (2017), the coefficient of

variation was used to express the homogeneity of the nanofibrous layers. The general descriptive statistics of the individual diameter distribution of the fibers are shown in Table 4.1). Additionally, to confirm the hypothesis of the diffusion-controlled release of Alaptide from nanofibers, the morphology of the nanofibrous layers at the end of the release experiment was evaluated (see Figure 4.1).
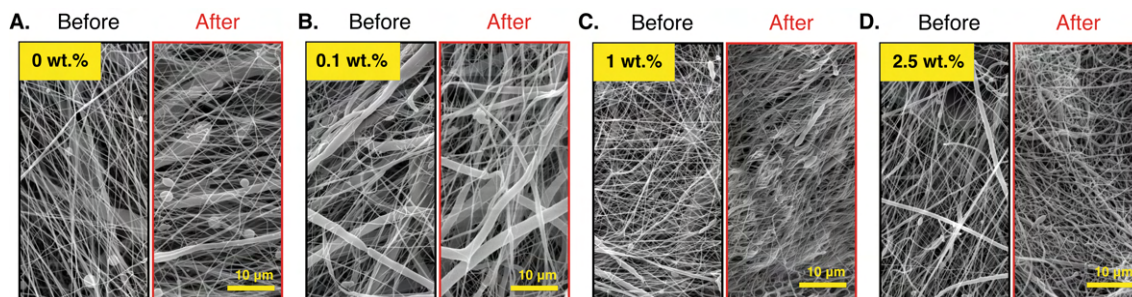

Figure 4.1: Representative SEM images of the electrospun PCL nanofibers. A-D – morphology of nanofibrous mats with 0, 0.1, 1 and 2.5 wt% of Alaptide before and after the drug release experiment.

An investigation of the electrospun layers following incubation (after 21 days) revealed a statistically significant difference in fiber diameter distributions for pure PCL and 2.5 wt.% samples with p=0.0009 and p=0.0018, respectively. However, despite this fact, the difference in the distribution of fiber diameters was mainly due to the heterogeneity of the material. The vast majority of fibers were up to about 500 nm, which is at least 75 to 90 % of all measured values (n=300). A deviation of the curves is visible in the quantile graphs (Figure 4.2 A, D). However, this deviation corresponds to approximately 10 % of 300x measured diameters.

Moreover, the median difference between the samples before and after incubation is on two tens of nanometers with IQR 100-300 nm. Together with simple observation of SEM images, these results might indicate that no fiber collapse or significant thinning proceeded during the release of the drug. Indeed, several samples with 1 and 2.5 % of Alaptide had fibers that were "stuck" together (see Figure 4.1).

Table 4.1: Selected descriptive statistical values of the fiber distributions of the Alaptide-loaded nanofibrous mats (n=300).

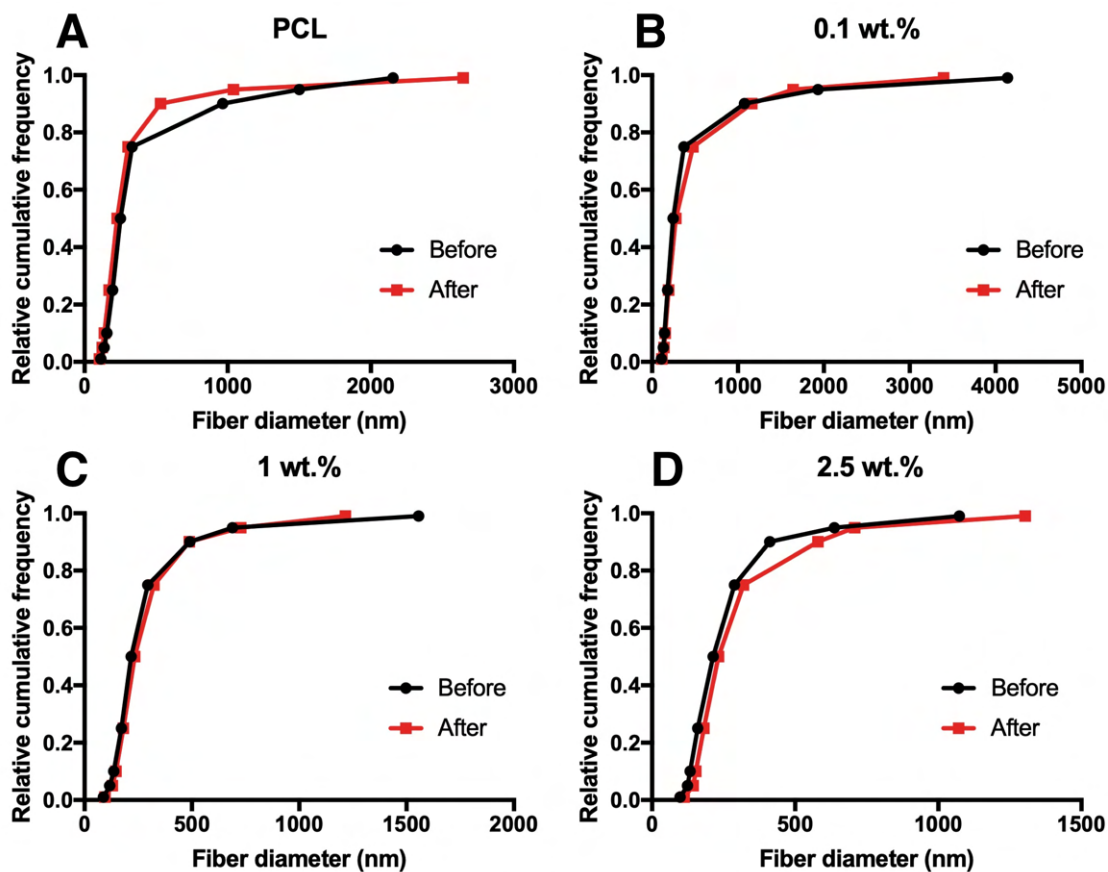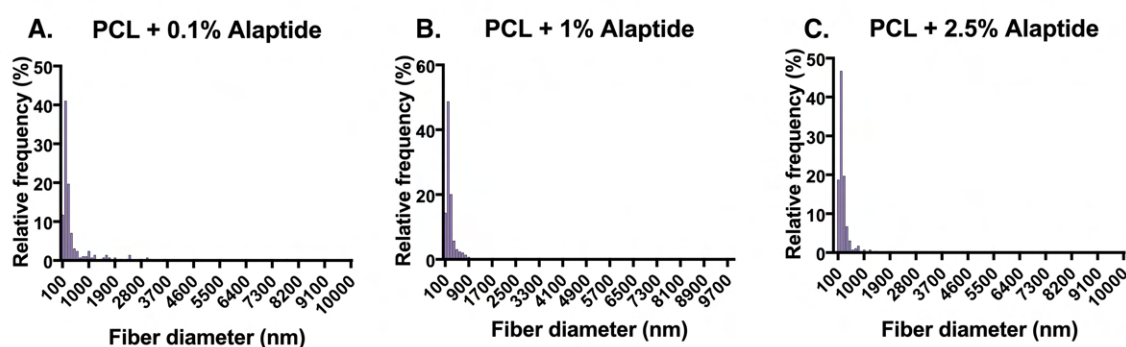| Alaptide loading [wt%]	Fiber diameter (mean ± SD) [nm]		Fiber diameter (median, IQR) [nm]		Coefficient of variation, CV [−]	
	Before	After	Before	After	Before	After
0	404.3 ± 453.8	338.3 ± 433.1	256.0 (137.6)	227.2 (133.1)	1.12	1.28
0.1	513.4 ± 919.8	499.2 ± 614.2	244.6 (188.7)	244.6 (290.5)	1.79	1.23
1	290.6 ± 315.2	296.6 ± 227.4	217.1 (123.6)	217.1 (141.7)	1.09	0.77
2.5	261.9 ± 180.1	303.1 ± 230.2	214.0 (102.5)	214.1 (138.6)	0.69	0.76

Figure 4.2: Quantile plots (cumulative relative frequencies) of fiber diameter distributions before and after 21 days of incubation of the fiber samples in PBS. The plots show the proportion of fiber diameters that are less or equal to particular values. A – pure PCL (without Alaptide), B – sample with 0.1 wt% of Alaptide, C- sample with 1 wt% of Alaptide, D - sample with 2.5 wt% of Alaptide.

Transformation of the fiber distributions

Following what was discussed in the previous chapter, the diameters of individual nanofibers significantly affect the overall release from a nanofibrous membrane. Therefore, to appropriately determine the apparent diffusion coefficient, the distribution of fiber diameters must be considered. Accordingly, the fiber diameter distributions were transformed by assigning the corresponding weights based on the fiber volume using relation (3.16). The transformed distributions are depicted in Figure 4.3. It is evident from the transformed histograms how the thickest fibers have the lowest abundance in the analyzed layers before the transformation and, on the other hand, the highest quantity after. These newly obtained probabilities (abundances) were subsequently used for the fitting of experimental data to the model (Eq. 3.17).
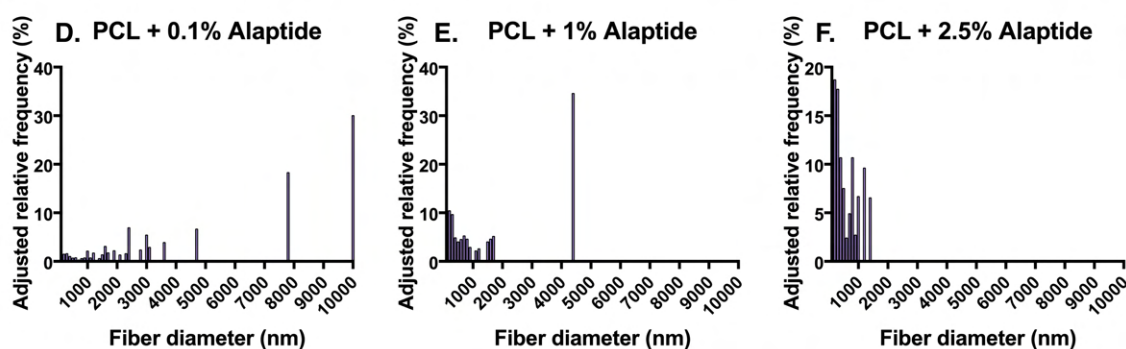
Figure 4.3: Fiber diameter distribution of Alaptide-loaded fibers. The original histogram (A, B, C) and the volume-adjusted distributions corrected according to the volume of the individual fibers (D, E, F).

Estimation of the apparent diffusion coefficient

All the experimentally-obtained cumulative release profiles were substituted into the final solution (3.12) of Eq. (3.3) with the boundary and initial conditions (3.6) and (3.4). The results of the fitting process are shown in Figure 4.4. It is important to note that even though the histograms show the values of the fiber diameters, the equation involves the radii, R. Since the value of the substituted radius was taken as the bin center of the histogram, the number of groups was particularly important. In this case, a bin width of 100 nm was adopted, and the number of corresponding fiber bins (fractions) was automatically calculated from this assumption.

It is worthy of note that the large error bars and the values above 100 % were due to a propagated error caused by the determined value of the initial drug loading of the samples (see Table 2.1). Otherwise, the deviation between the release data of the individual replicates was mostly within approx. 5 % (see Figure 2.11).

Table 4.2: Diffusion coefficients of Alaptide estimated using non-linear regression of experimental data.

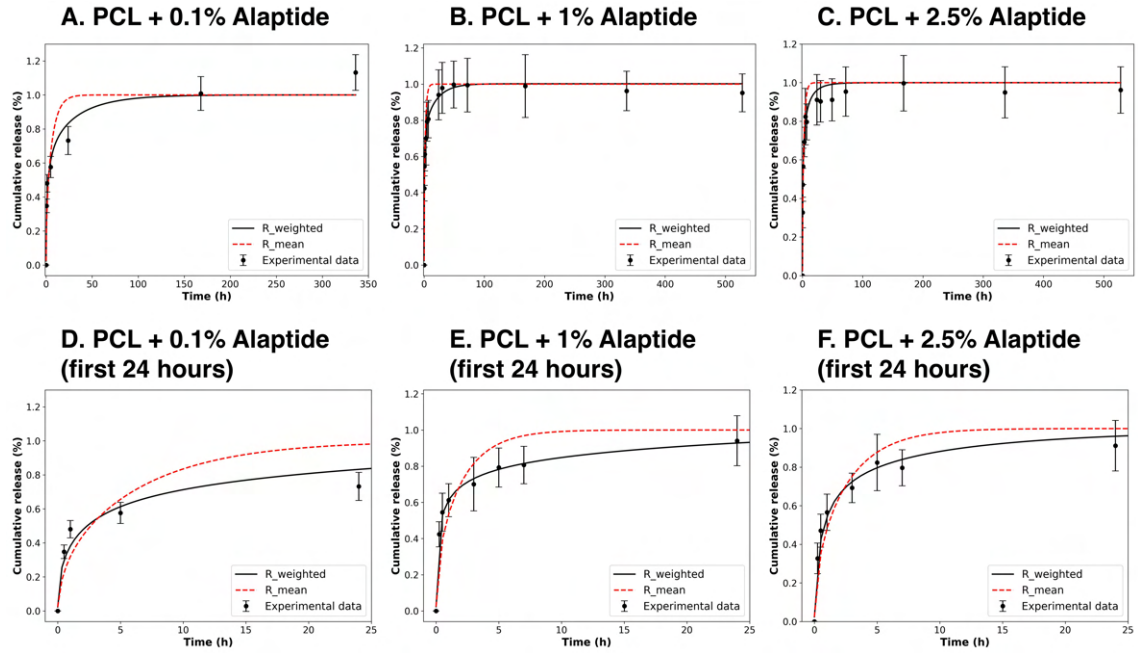| Alaptide loading in the solution (% w/w)	Estimated diffusion coefficient, D (cm^2/s)	R^2
0.1	$(3.10 \pm 1.07) \cdot 10^{-13}$	0.988
1	$(1.18 \pm 0.10) \cdot 10^{-13}$	0.999
2.5	$(1.11 \pm 0.14) \cdot 10^{-14}$	0.997

Figure 4.4: Results of the fitting of the experimental data to the solution of the diffusion equation for the three differing Alaptide loadings. The dashed curves represent fitting using the mean value of the fiber radii. The solid lines represent fitting applying the effect of the fiber radii distribution.

The estimated diffusion coefficients were the same order of magnitude for both the 0.1 and 1wt% loadings, i.e., $(3.10 \pm 1.07) \cdot 10^{-13}$ and $(1.18 \pm 0.10) \cdot 10^{-13}$ cm^2/s respectively. However, with respect to the 2.5 wt% loading, the value was one order of magnitude lower, i.e., $(1.11 \pm 0.14) \cdot 10^{-14}$ cm^2/s.

The graphs (Figure 4.2) illustrate that the curve plotted by fitting with the constant (mean) value of the fiber radii (the red dashed curve) does not describe the release profile sufficiently well. It is also evident from the graph that the application of fitting with the mean fiber diameter value always leads to higher release rates, which is explained by the underestimated effect of the thicker fibers, which is common concerning nanofibrous mats. Moreover, it is visible from Figure 4.4 that the curve corresponding to the volume-adjusted radii distribution (the black solid

curve) fits the experimental data significantly better, with coefficients of determination that are close to a value of 1 (see Table 4.2). It is due mainly to the effect of the rare but still voluminous thick fibers. A more severe deviation of the fitting function from the experimental data is observed concerning the 0.1wt% concentration. This deviation is due primarily to the displacement of the data points due to the normalization of the experimental data (to obtain the dimensionless fraction $M(t)/M(\infty)$. Since the loading was more extensive than expected (see Table 2.1), the values did not saturate at 100 %. However, this problem is difficult to avoid in cases where the drug distribution in the nanofibers is uneven; since the nanofibers do not allow for the calculation of their length, it is impossible to use the value of the total mass of the drug in mg in order to plot the function. Generally, for the same reason, applying the Higuchi equation for such kinds of drug delivery systems is impossible. It is also worth noting that it is essential to consider the influence of the coefficient of variation, the highest value of which is related to the 0.1 wt% loading.

From the calculated values of the diffusion coefficient given in Table 4.2, we can see a decreasing trend of D with increasing concentration of Alaptide in the fibers. From this, it can be concluded that in the case of 0.1% concentration, the fastest release of Alaptide occurred due to its complete dissolution in the polymer solution. The drug was present in the fibers in the form of uniformly distributed individual molecules, which were released by simple diffusion. In the case of higher concentrations, the drug was already present in the form of solute and individual undissolved particles. The release, in this case, was more gradual. It is believed that the solute was released first, followed by a gradual dissolution of the solid particles by penetration of the solvent through the polymer pores and their subsequent release by simple diffusion (L. Fan et al., 1989). This fact is supported by subsequent analysis, which showed no change in fiber morphology after drug release.

4.2.2 LPPO-loaded nanofibers

Fiber morphology before and after release

In order to investigate the mechanism controlling the LPPO release from the fibers, the morphological changes of nanofibrous membranes after the drug release were studied. Analysis of the morphology of the LPPO-loaded layers on the 174th day revealed significant changes in terms of fiber diameters for all the fibrous layers. Generally, the mean and median values have shifted towards higher values for all the membranes except the PCL+2% LPPO. However, the statistical significance based on p-value may be arguable for such heterogeneous nanofibrous membranes. Thus, the cumulative relative frequency (quantiles) was analyzed. As can be seen in quantile plots Figure 4.5 (A-D), no remarkable difference was determined for the control sample of PCL and PCL+2%LPPO. However, a significant shift towards thicker fibers is observed for the membranes with higher loading of LPPO (i.e., 5 and 10%).

Additionally, certain changes in terms of morphology were observed on the SEM micrographs of the fibers (Figure 4.5 (E-H). Certain type of anomalies were spotted throughout the layers loaded with LPPO - Figure 4.5 F and H (indicated with red triangles). These anomalies were present as core-shell-like structures, where the thick fibers revealed a much thinner fiber from within. Notably, no such anomalies were spotted on the control PCL layer without LPPO. It may be speculated that this "shell-" or "envelope-like" structure is LPPO covering the PCL fiber. However, no evidence to prove it is provided within the scope of the current study.
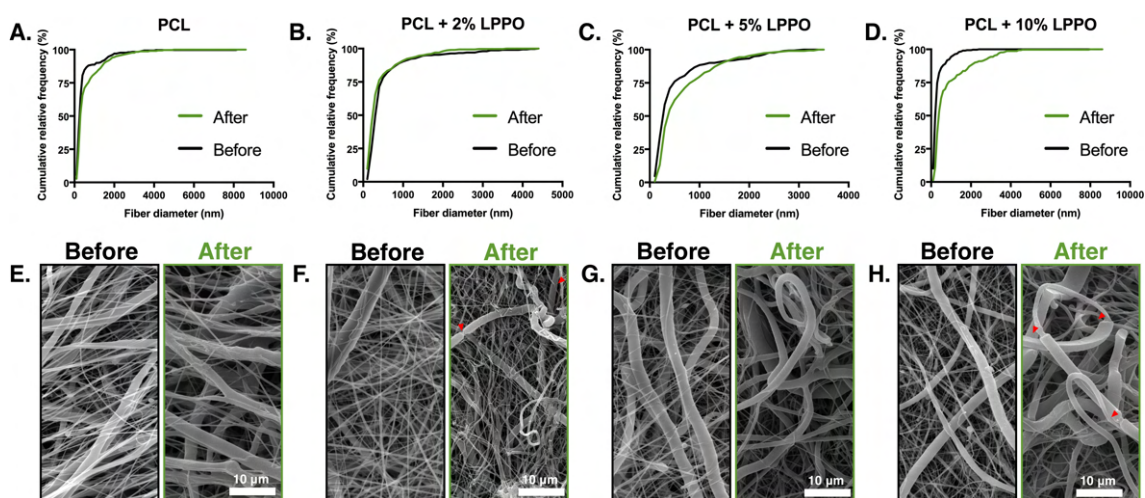

Figure 4.5: Comparison of fiber morphology before and after the LPPO release experiment (after 174 days). Panels A-D depict quantile plots (cumulative frequencies) of fiber diameter distribution for all the fibrous layers. The panels E-H depict comparison of SEM micrographs of the fibrous structures before and after the experiment. The scale bar is 10 μm.

Taken together, these morphology changes indicate a certain degree of swelling of the produced fibers after incubation in PBS. Even though the PCL is considered

Table 4.3: Selected descriptive statistical values of the fiber distributions of the LPPO-loaded nanofibrous mats.
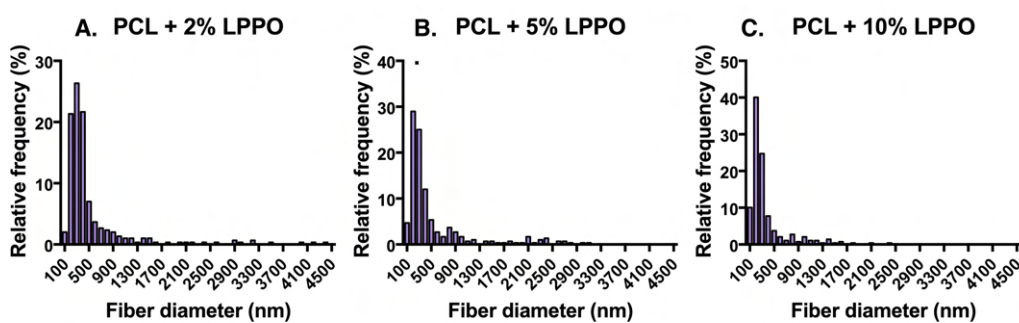
LPPO loading [wt%]	Fiber diameter (mean ± SD) [nm]		Fiber diameter (median, IQR) [nm]		Coefficient of variation, CV [−]	
	Before	After	Before	After	Before	After
0	504.0 ± 730.8	652.3 ± 745.8	300.5 (181.1)	342.5 (441.4)	1.45	1.14
2	542.4 ± 641.6	444.4 ± 481.2	354.4 (240.1)	278.5 (244.7)	1.18	1.08
5	547.3 ± 606.1	681.1 ± 607.1	312.9 (292.9)	410.0 (588.4)	1.11	0.89
10	361.9 ± 332.2	871.2 ± 1011.7	249.8 (171.5)	417.8 (598.6)	0.92	1.16

to be an almost non-swelling polymer, several publications report the increasing mass of PCL nanofibers by swelling (Zahedi et al., 2013; Renkler et al., 2021). It is important to say that swelling is an essential parameter for wound healing as it characterizes the ability of the nanofibrous mat to absorb the exudate in the wound (Sethuram et al., 2023).

Transformation of the fiber distributions

To determine the diffusion coefficient of LPPO within PCL nanofibers, the histograms of fiber diameter were adjusted based on fiber volumes (see Eq. (3.16)). Figure 4.6 shows the transformation of the relative frequency distribution once the correction is applied. We again see how significantly transforms the shape of the histogram, and the change is, obviously, more pronounced with a more significant number of thick fibers. The newly obtained weight for individual fiber diameter fractions was substituted to the mathematical model, and the non-linear regression analysis was applied.
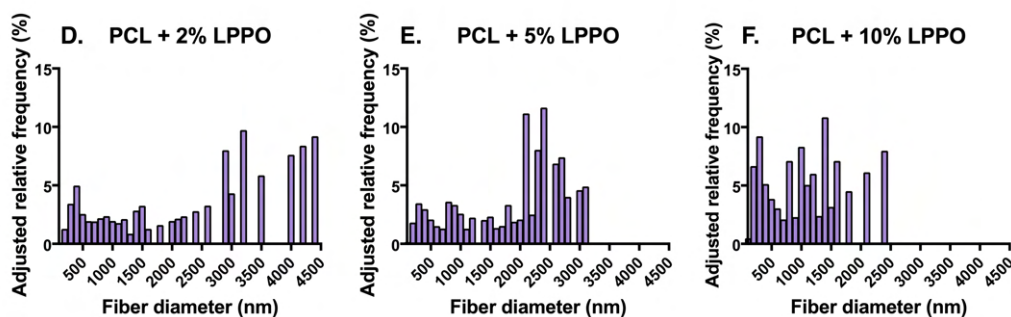
Figure 4.6: Fiber diameter distribution of LPPO-loaded fibers. The original histogram (A, B, C) and the volume-adjusted distributions corrected according to the volume of the individual fibers (D, E, F).

Estimation of the apparent diffusion coefficient

Unfortunately, the mathematical model could not describe the release of LPPO from the nanofibers. The coefficient of determination was low for all the tested materials.

Thus, random normalized fiber diameter distributions were generated in the same diameter range and with the same number of groups (bins) for the histograms to investigate the effect of adjusted diameter distribution on the goodness of fit. The release data of PCL+10% LPPO were used for evaluation. Figure 4.7 shows nine randomly generated distributions, with the 10th distribution being the actual distribution for PCL+10% LPPO membrane (see Figure 4.6-F, highlighted in blue frame). The bottom panel of Figure 4.7 demonstrates the results of the experimental data's fit (R^2 values) to the model considering the corresponding distribution.
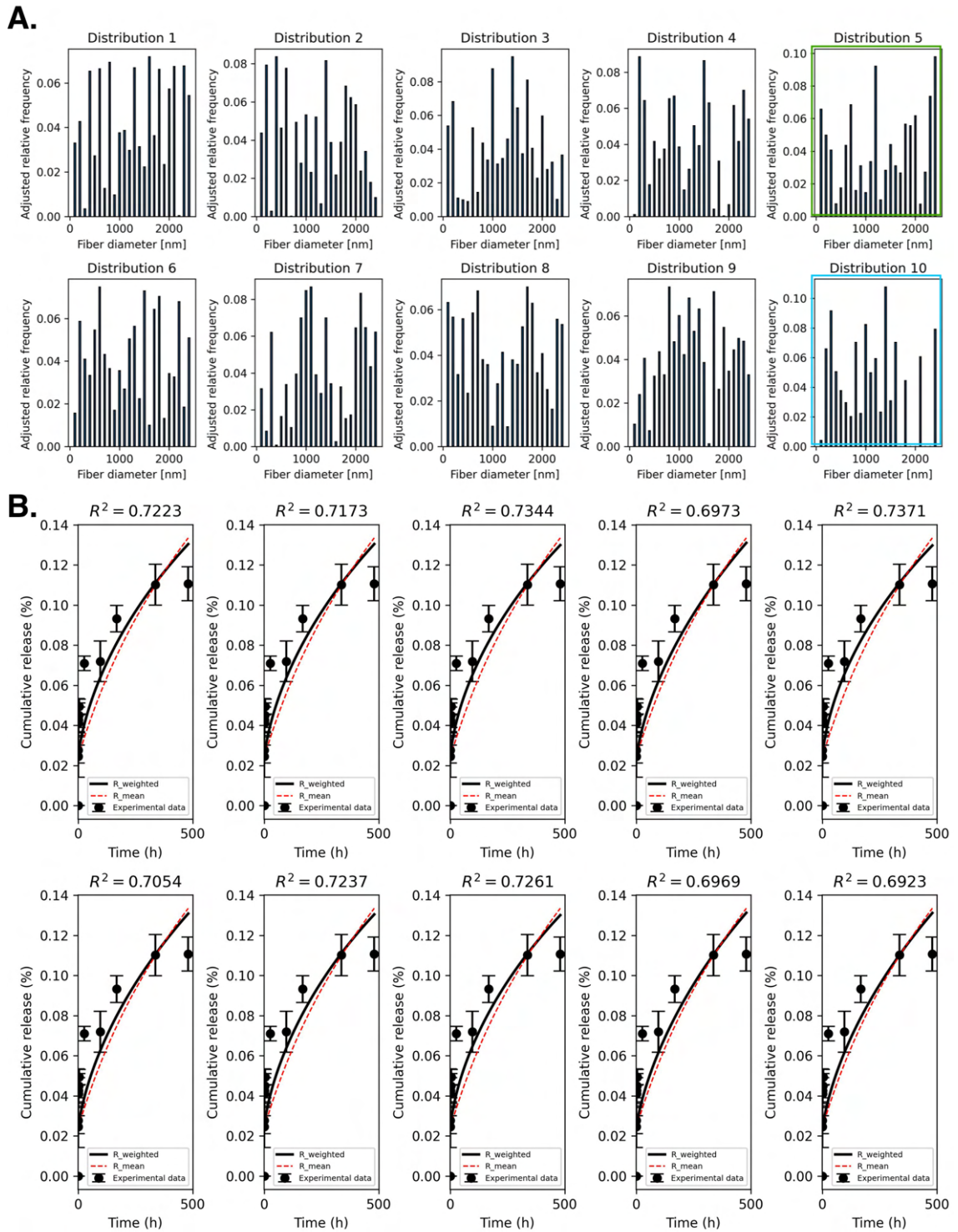
Figure 4.7: Various volume-adjusted ditributions and the corresponding non-linear fit of experimental data. Panel A demonstrates nine fiber diameter distributions (1-9) and the actual one (10). Panel B depicts the result of non-linear fit of the experimental data to the mathematical model considering the given distribution of diameters. R^2 indicates the coefficient of determination.

It can be seen from the graphs that the best fit ($R^2 = 0.7344$, highlighted in green frame) was obtained for Distribution 5. Nevertheless, tests with various random distributions did not demonstrate fit with R^2 values higher than 0.75. Indeed, the values of R^2 for fit with weighted (volume adjusted) distribution were consistently higher than those with a mean fiber diameter value ($R^2 = 0.6309$). The total overall fit differences for the different distributions and the mean value of fiber diameters can also be seen in Figure 4.8.
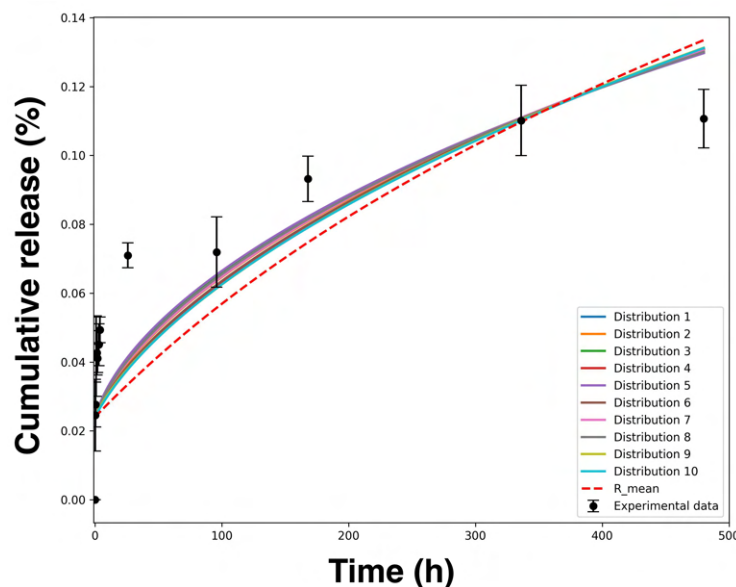

Figure 4.8: Comparison of overall fit differences for various generated fiber diameter distributions and the average fiber diameter value.

Taken together, the analysis of release kinetics suggests that diffusion was not the only rate-controlling mechanism for releasing LPPO from nanofibers. Accordingly, it is well known that PCL significantly changes its wetting properties over time once electrospun due to gradual depolymerization. The tested LPPO materials described above were immersed in PBS freshly after electrospinning; thus, the hydrophobicity of PCL+LPPO membranes could still be high, making it difficult for water to fill the pores of the nanofibrous membrane. On the other hand, when the release experiments were repeated with PCL+10% LPPO materials, the significantly increased release in a burst manner was observed.

4.3 Conclusion

The idea behind the study was to attempt to form an understanding of the mechanism that governs the release of substances from nanofibrous mats designed in the form of wound dressings. Moreover, the intention was not only to provide a characterization of the drug release data obtained but also to predict the subsequent kinetics by determining the diffusion coefficient of the drug in the nanofibers.

It was hypothesized that the higher loadings would be evenly dispersed inside the fibers. At the same time, the lowest concentration was expected to be fully dissolved in the polymer, thus resulting in molecular dispersion. To determine the diffusion coefficient, the experimentally obtained drug release kinetics data was evaluated using a mechanistic model on the basis of the solution of the diffusion equation in cylindrical coordinates. Notably, the model considered the weighting of the distribution of the fiber diameters inside the nanofiber membrane.

This chapter demonstrated the successful estimation of diffusion coefficients of Alaptide released from nanofibrous layers by applying an analytical diffusion equation solution to experimental data. Alaptide's release strongly depended on the fiber diameter distribution of the obtained materials. Also, the values of the estimated diffusion coefficients correlated with the concentration (and physical state) in which Alaptide was present in the fibers; the higher the concentration of the drug in the fibers, the lower was the release rate, which can be explained by the gradual dissolution of Alaptide in the nanofibers and its subsequent release via simple diffusion. The decrease of the estimated values of the diffusion coefficients with the increase of the drug loading supports this hypothesis. Moreover, no residual Alaptide in the fibers nor noticeable changes in the morphology of the fibers were found at the end of the experiment.

On the other hand, the mathematical model could not describe the release of LPPO from the nanofibers. The obtained results suggest there might be a strong interaction of LPPO molecules to the PCL matrix, leading to significantly slowed release. Even after approximately half a year of release, not more than 20% of the substance was released. Unfortunately, due to the absence of new samples and the limited time scope of the current study, we could not estimate the necessary parameters (e.g., U_∞) to adapt the mathematical model. This model evaluation, however, can be suggested as the direction of a new extended study.

Despite the limited ability to thoroughly verify the model on both molecules, it is anticipated that this model will help to enhance the versatility of the approach to quantifying the amount of released drug since it can be applied to highly heterogeneous nanofibrous layers with high CV values. Moreover, introducing the mass transfer coefficient, h, into the model may help attain even more accurate results concerning the prediction of kinetics in the future. These results also bring up a discussion of whether it is appropriate to consider the mean as a good representative of a "typical value" within the diameters distributions and how to treat outliers.

5 Chapter V - Effect of polymer parameters on electrospun matrix

5.1 Introduction

In the previous chapters, we discussed the aspects and effects of the polymer solutions (or suspensions) for fabricating electrospun wound dressings. In this chapter, however, we will try to depict the importance of the raw polymer material and its effect on the reproducibility of the electrospinning process. The case study will be described where the nominally same or very close cellulose derivatives behaved differently depending on the manufacturer.

This chapter summarizes the testing of several HPMCs, for which a high-productivity polymer system was specially designed based on non-toxic solvents. We show that sourcing polymers with the same parameters from different manufacturers can significantly influence the mechanical properties of the fabricated layers. The following abbreviations were used throughout this chapter: **E5** = Methocel E5, **PH606** = Pharmacoat 606, **T605** and **T606** = Tylopur 605 and 606, respectively. For more detailed information on the particular HPMCs used, the reader is referred to the section 7.2.1. We hypothesize that even slight differences between arrangements of substituted methoxy- and hydroxypropyl groups of HPMC can dramatically alter the critical properties of electrospun ODFs. In the previous study by Švára et al. (2022), APIs, specifically tadalafil, were added to the nanofibrous layer, and several properties were studied with an emphasis on mechanical properties. In this chapter, only the matrix has been studied to exclude inter-molecular interaction between the polymers and the API.

The text that comprises this chapter was published in *Cellulose (2023), volume 30, pp. 4527–4541*, (Asatiani; Filipová, et al., 2023).

5.2 Results and discussion

5.2.1 Characterization of the morphology

Electrospun nanofibrous layers

The electrospinning processing parameters and the ambient conditions were kept constant during the study to ensure that the type of HPMC was the only variable parameter that affected the fiber morphology. The nanofibrous layers produced appeared to be regular and without any remarkable defects or significant differences in the macroscopic structures of the layers. Figure 5.1 shows representative SEM images of the obtained fibrous layers (A-D) and the distributions of the fiber diameters within the structures.
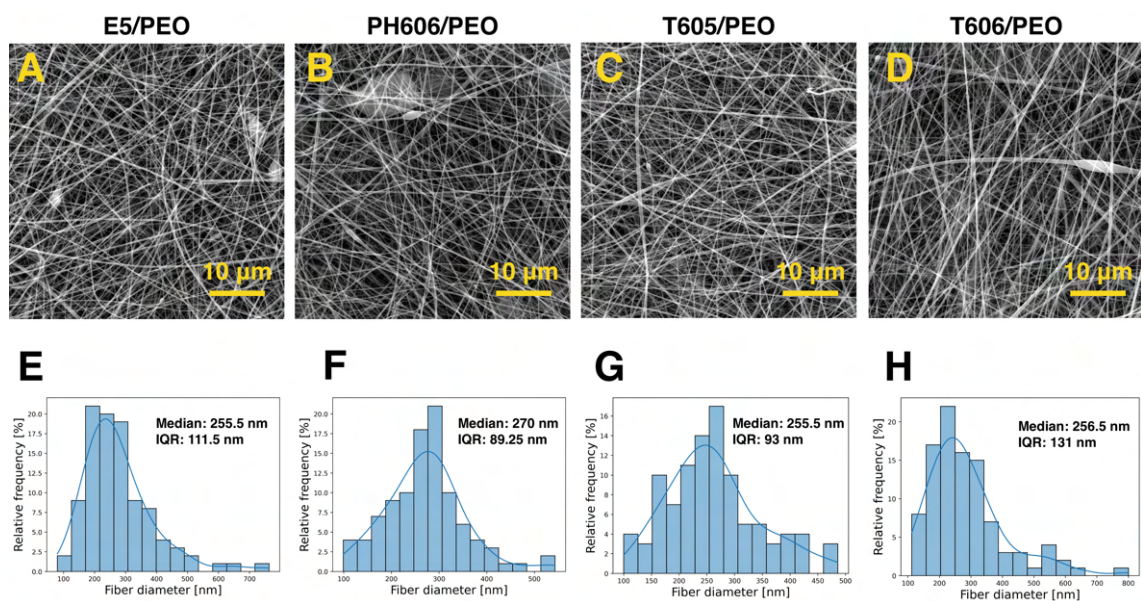

Figure 5.1: Morphology of the electrospun HPMC layers. SEM images (A-D) and histograms (with KDE) of the fiber diameter distributions of the electrospun fibers produced from the various HPMCs with PEO.

The analysis of the SEM images revealed that all the resulting electrospun fibers were free of beads and evinced fiber diameters of around 250 nm (median value, n=100) with relatively limited fiber diameter distributions (generally up to 650 nm).

The observations were similar to those suggested by the earlier data for various electrospun HPMCs with differing PEO ratios (Aydogdu et al., 2018). On the other hand, the diameter values obtained in this study were approximately four times smaller than the HPMC/PEO fiber values obtained by Balogh et al. (2016) using DC electrospinning. Balogh et al. (2016), however, considered significantly lower PEO 100k ratios (up to 5 % w/w). Since none of the material fiber distributions displayed a normal distribution, the Kruskal-Wallis test was applied, which

confirmed the absence of statistically significant differences (p=0.7492) between the fiber diameter distributions. A marked difference was observed in the productivity (mg/cm^2) of the fibrous layers produced. The highest productivity, (3.27 $\pm$ 0.16) mg/cm^2, was determined for the T605/PEO layer, which corresponds to a high fiber density (see Figure 5.1 – C). The productivity of the PH606/PEO and T606/PEO layers was comparable at (2.93 $\pm$ 0.20) and (2.96 $\pm$ 0.21) mg/cm^2, respectively, and the E5/PEO layer evinced the lowest productivity, i.e. (2.44 $\pm$ 0.24) mg/cm^2. The productivity was determined by weighing 2.2 x 2.2 cm samples stamped at three randomly selected locations for each polymer on the fabricated layer. The nanofiber layer production parameters were the same for all the nanofibrous layers.

Solvent-cast ODFs

Thin films (solid dispersions) of the same polymer formulations were solvent-cast on glass slides and analyzed by means of crossed-polarized microscopy aimed at obtaining visualizations of the phase and state transitions of the polymers used in the studied HPMC/PEO matrices. All the HPMC/PEO formulation samples revealed two distinct phases following complete drying. Three HPMCs, i.e. PH606/PEO, T605/PEO, and T606/PEO (Figure 5.2 B/F, C/G, D/H) evinced similar macroscopic structure patterns with highly-defined dispersion phases and dispersed bubble-like structures within. However, the E5/PEO sample (Figure 5.2 -A/E) was more homogeneous and lacked a well-defined separated phase size and shape.
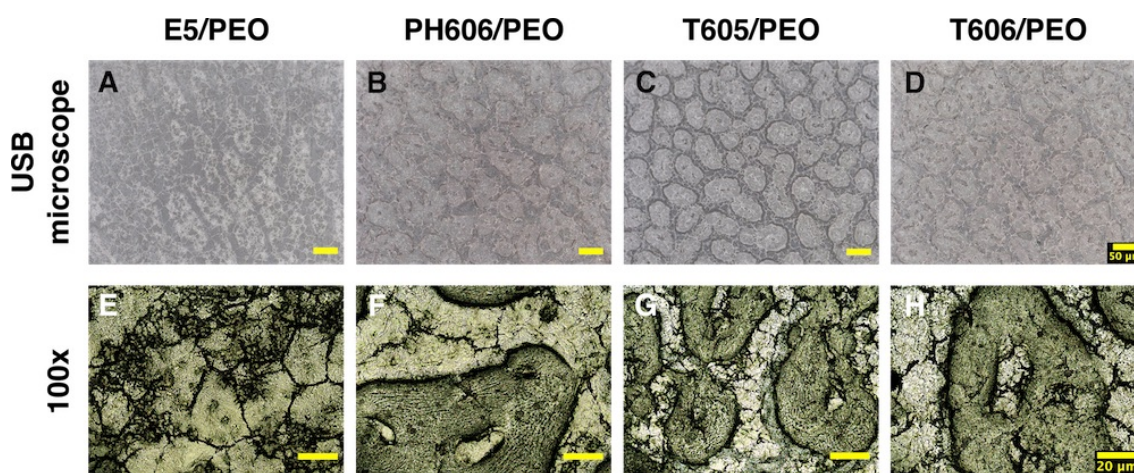

Figure 5.2: USB-microscopy (A-D) and polarized light microscopy (E-H) images of the solvent-cast HPMC/PEO films follodwing complete drying. The scale bar is 50 µm and 20 µm for the USB microscope and 100x magnifications, respectively.

Solutions with differing ratios of HPMC/PEO were subsequently prepared aimed at the investigation of this aspect of microphase separation in more detail. The microscopic analysis revealed that the phase separation changed markedly for both the E5/PEO and PH606/PEO samples. Obvious microphase separation occurred

at a ratio of 9/1, with HPMC particles that were comparable to the PEO nuclei. Moreover, the particles from the separated HPMC microphase dispersed in the PEO increased intensively with the increasing ratio of PEO. With respect to both the E5/PEO and PH606/PEO samples, the separated amorphous HPMC domains were significantly larger and were densely dispersed within the easily distinguishable crystal PEO phase. Moreover, a comparison of the 7/3 ratios for both the E5 and PH606 samples (Figure 5.3 - D, H) revealed that the shape of the PEO crystals and their distribution throughout the film was not as regular for the E5/PEO as for the PH606/PEO sample. This observation may indicate the higher degree of compatibility (miscibility) of the polymers in the E5/PEO formulation. The morphology of the PEO crystals was consistent with the results determined by Lovinger and Gryte (1976).
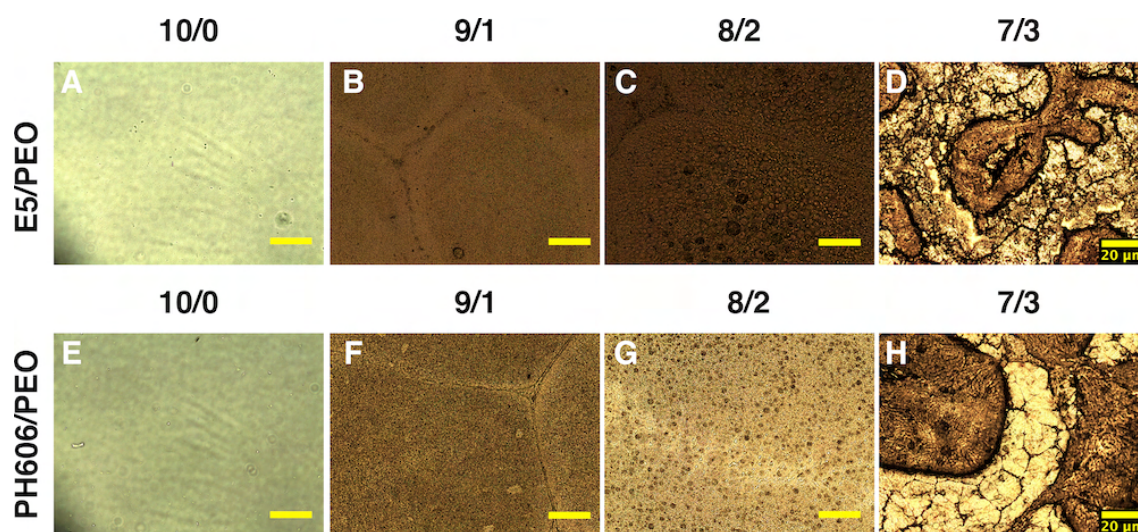

Figure 5.3: Polarized light microscopy images of the E5/PEO (A-D) and PH606/PEO (E-H) solvent-cast films with differing ratios of PEO.

It is clear from the images shown in Figure 5.3 that the PH606/PEO, T605/PEO, and T606/PEO sample HPMC domains exhibit a specific orientation in terms of the interconnections within the grains, whereas no evidence of anisotropy was observed from the E5/PEO images. This observation was partially confirmed via the plugin OrientationJ in ImageJ software (Figure 5.4) which was used for the analysis of the local orientations of typical HPMC domain fragments. As can be seen from the histograms of the distribution of the local orientations and the color-coded maps, no defined peak was evident for the E5/PEO, whereas more or less narrow well-distinguishable peaks were observed for the PH606/PEO, T605/PEO, and T606/PEO samples. Despite the presence of isotropic or multimodal areas on the PH606/PEO, T605/PEO, and T606/PEO domains, the coherency was in most cases higher than that of the E5/PEO. This may indicate differences in terms of the miscibility of the polymers due to variations in the interactions that occur between the PEO and the HPMC, as well as differing degrees of the interruption of the PEO crystalline phase by the HPMC.
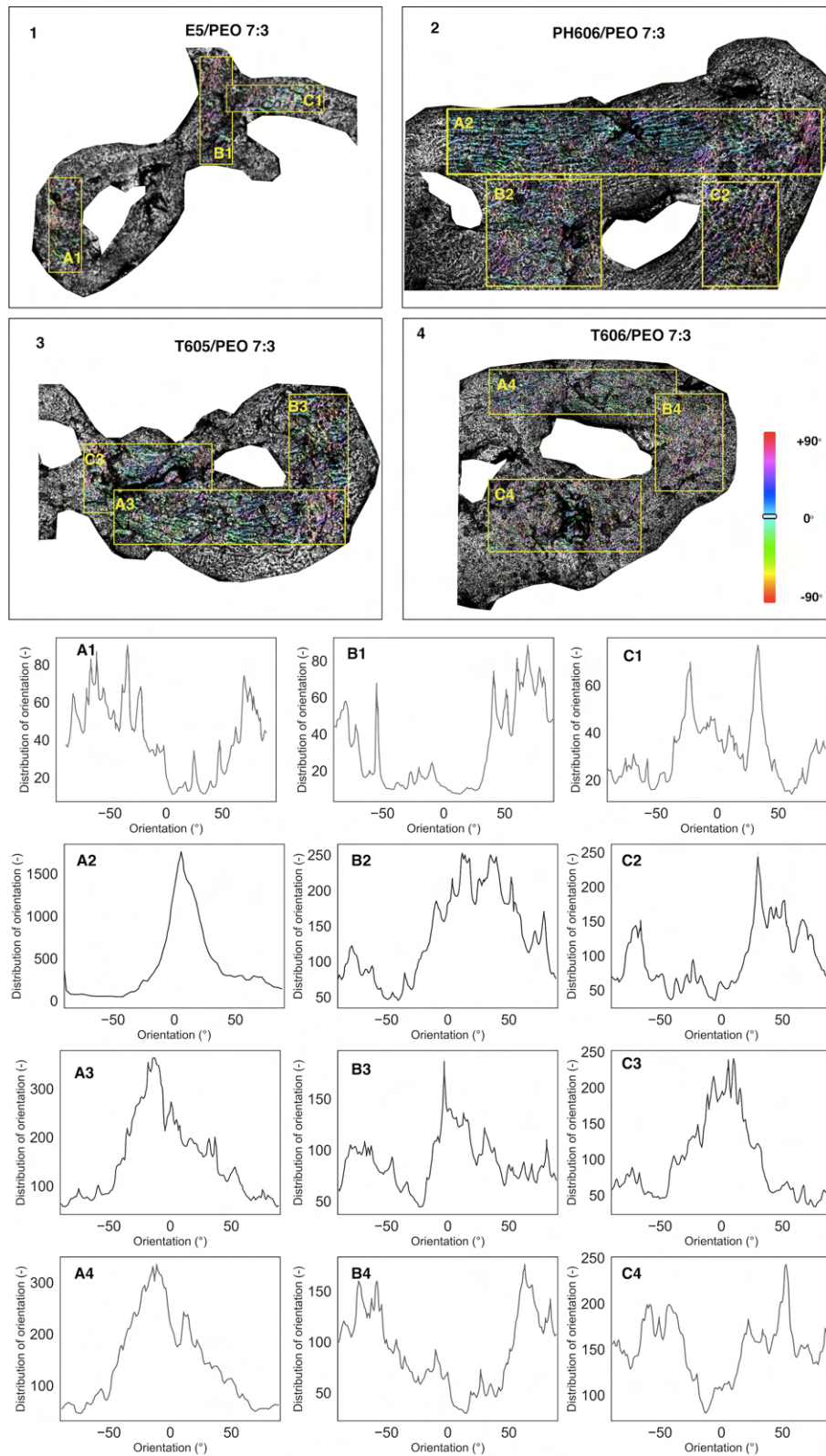
Figure 5.4: Representative results of the analysis of the orientation and coherency of the PEO crystalline phase in the HPMC domains. Each frame (1-4) presents a typical HPMC domain cut from the polarized light microscopy image, three color-coded measured areas, and the corresponding histograms of the orientation distributions.

5.2.2 DSC characterization

Figure 5.5 presents the DSC thermograms of various HPMC/PEO nanofibrous layer samples recorded at a heating/cooling rate of 15° C/min. All the blended samples exhibited pronounced endothermic peaks during heating and sharp pronounced exothermic peaks during cooling. The exothermic peak corresponded to the cold crystallization temperature of the PEO, while the endothermic peak corresponded to the reported values of the PEO melting point (Nijenhuis et al., 1996; Money et al., 2013; Aydogdu et al., 2018; Meruva et al., 2020) The lowest exothermic peak and enthalpy of cold crystallization values were determined for the E5/PEO sample (35.82 °C and 27.33 J/g, respectively), whereas the highest temperature and enthalpy of cold crystallization values were observed for the PH606/PEO sample. All the thermograms featured a broad peak at approx. 95° C, which may indicate the dehydration of the humidity absorbed by the samples during storage. The comparative DSC analysis of the physical mixtures stored under normal conditions and the physical mixtures dried before measurement revealed the high degree of hygroscopicity of the materials, as evident from the DSC thermograms, i.e. the enthalpy of the melting of PEO changes significantly with increased water content. On the other hand, the glass transition temperature of the HPMC was not detected for any of the HPMCs during the measurement process, which is consistent with the observations reported earlier for the electrospun HPMC/PEO nanofibrous formulations (Balogh et al., 2016); the glass transition temperature of pure HPMC is reported as 155° C in the literature (Nyamweya et al., 2000). Due to the absence of detectable temperatures and enthalpies for the cold crystallization/melting of HPMC, a summary of these values with respect to the PEO of selected samples is presented in Table 1.

A noticeable trend is evident in the decrement of the temperature of the melting of PEO from the pure PEO powder toward the electrospun samples. Table 1 indicates an approximately 7% decrement for the physical mixtures and an approximately 10% decrement for the nanofibers. Moreover, the enthalpy of melting decreased dramatically i by up to 90 % and the enthalpy of cold crystallization by up to 30%. The depression of the melting point may have been due to the inter-reference of the PEO crystallization process by the HPMC domains. Taken together, this appears to serve as a good indicator of the higher degree of interaction between PEO and HPMC in nanofibers (Rathna et al., 2011; Bianco et al., 2013). Similar observations have been reported previously for HPMC/PEO (Aydogdu et al., 2018) and PCL/PEO nanofibrous blends (Lowery et al., 2010). The lower temperature of the cold crystallization of PEO in the nanofibrous samples than in the physical mixtures comprises an important aspect. The depression of the cold crystallization temperature indicates the enhanced crystalline ability of PEO and appears to suggest that HPMC domains serve as nucleation sites for PEO (Y. Li et al., 2012).

Table 5.1: DSC characterization of the pure polymers, nanofibrous samples, and physical mixtures of HPMC/PEO. The temperature and enthalpy of the cold crystallization/melting of PEO for selected samples.

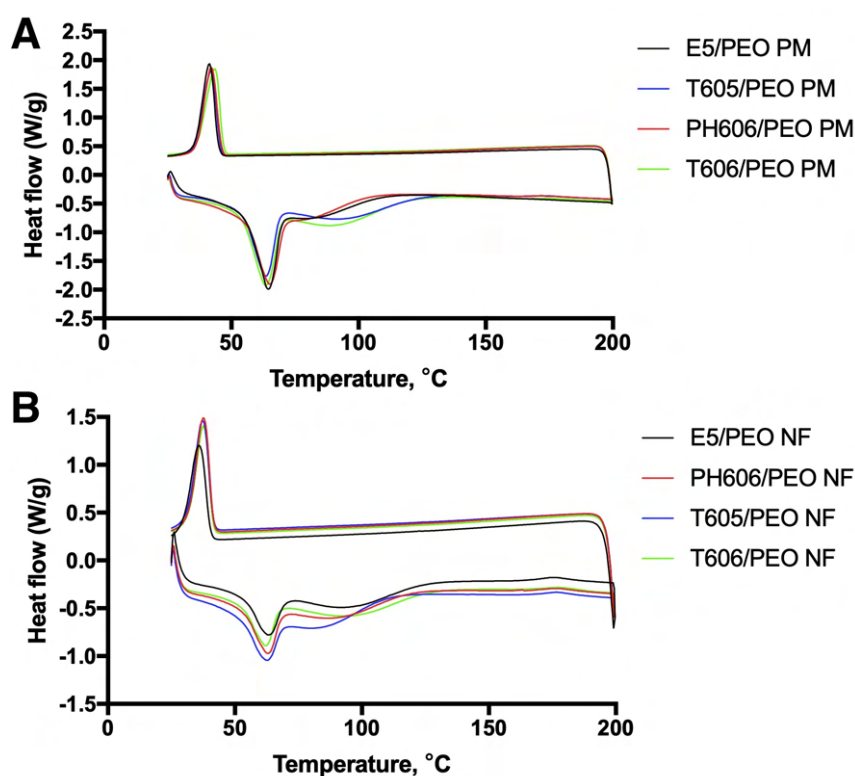| Sample	Temperature of Cold Crystallization (°C)	Enthalpy of Cold Crystallization (J/g)	Melting Temperature (°C)	Enthalpy of Melting (J/g)
Nanofibrous samples				
E5/PEO NF	35.82	27.33	63.26	-17.69
PH606/PEO NF	37.66	30.20	62.95	-18.15
T605/PEO NF	37.40	29.75	62.42	-18.66
T606/PEO NF	37.65	28.51	61.97	-17.20
Physical mixtures				
E5/PEO	41.22	37.97	64.46	-46.96
PH606/PEO	42.00	37.79	65.18	-43.21
T605/PEO	41.75	37.43	63.45	-41.94
T606/PEO	43.53	36.94	67.37	-46.28
Pure polymer				
PEG 100k powder	31.91	41.74	69.88	-174.11

Figure 5.5: DSC curves for the HPMCs/PEO (7/3) physical mixtures (A) and the nanofibrous layers (B) heated at 15 °C/min and subsequently cooled at 15 °C/min. The peaks that appear above the baseline represent the endothermic peaks.

5.2.3 Mechanical properties of the nanofibrous layers

The properties of oral films are type-dependent (fast dissolving, gradual release, etc.). However, all the various types of films are required to fulfill certain property requirements, i.e. they should be thin, efficiently and rapidly dissolvable, have an acceptable taste, and, most importantly, must allow for the ease of handling during production and subsequent administration (Bala et al., 2013; Borges et al., 2015). Of the various properties, priority is accorded to the mechanical properties of the film, which should remain stable. Gupta and Kumar (2020), when describing the mechanical properties of oral films, suggested the ideal tensile and puncture properties of orodispersible films as follows: tensile strength of greater than 2 N/mm^2, elongation at break of greater than 10 % and Young's modulus of less than 550 N/mm^2.

Table 5.2: Tensile profiles of the electrospun HPMC/PEO nanofibrous layers

Sample	Young modulus (MPa)	Tensile stress at maximum load (MPa)	Elongation at break (%)
E5/PEO NF	75.85 ± 13.91	1.60 ± 0.63	2.88 ± 0.96
PH606/PEO NF	57.10 ± 2.31	1.76 ± 0.04	6.43 ± 0.94
T605/PEO NF	75.42 ± 2.67	2.12 ± 0.13	5.48 ± 0.86
T606/PEO NF	63.41 ± 2.51	1.89 ± 0.05	7.05 ± 0.68

Figure 5.6A shows the typical tensile stress-strain curves of electrospun HPMC/PEO nanofibrous layers. Figure 5.6B compares Young's modulus of the various HPMC/PEO fibrous layers. The Young's modulus values of the E5/PEO and T605/PEO were comparable, i.e. (75.85 ± 13.91) and (75.42 ± 2.67) MPa, respectively. These values were significantly higher than that of the PH606/PEO and similar to that of the T606/PEO layers. Figure 5.6C compares the tensile stress of the materials at maximum load. The highest value, (2.12 ± 0.13) MPa, was determined for the T605/PEO layer; this was significantly higher than for the PH606/PEO and comparable to the E5/PEO and T606/PEO layers. Figure 5.6D shows the differences in the ultimate elongation of the tested materials before fracture. The lowest elongation value, i.e. (2.88 ± 0.96) %, was attained by the E5/PEO layer; this was lower than that of the T605/PEO (5.48 ± 0.86) % and significantly lower than those of the PH606/PEO (6.43 ± 0.94) % and T606/PEO (7.05 ± 0.68) % layers.

The relatively low Young's moduli of HPMC-containing formulations have been reported previously (Alopaeus et al., 2020; Shi et al., 2020). The comparison of the tensile properties of the materials tested in this study revealed a specific pattern of similarity between the materials spun from HPMCs with the same nominal viscosity. Generally, in terms of elastic deformation, the tensile behavior of E5/PEO and T605/PEO (5 mPa·s) was similar, as was that of the PH606/PEO and T606/PEO (6 mPa·s) layers. However, a significant difference was evident concerning the

E5/PEO layer in terms of the plastic deformation – the elongation at break of the E5/PEO was almost 2-times lower than that of the other tested layers. As suggested previously (Puppi et al., 2010), this may indicate the presence of a significant amount of the PEO crystalline phase, which hinders the mobility of the various polymer chains during stretching. Shi et al. (2020) reported the significant suppression of elongation with increases in the content of additives in the HPMC matrix, which was attributed to the possible agglomeration of the additives. As demonstrated by Shi et al. (2020), an increase in the HPMC chain length may act to enhance the mechanical properties due to the presence of a higher number of intermolecular bonds between the polymer chains. The results of the comparison of the elongations at a break in this study, however, suggest that higher viscosity (a higher molecular weight) plays a role primarily during the plastic deformation phase (see Figure 5.6 - A, D).
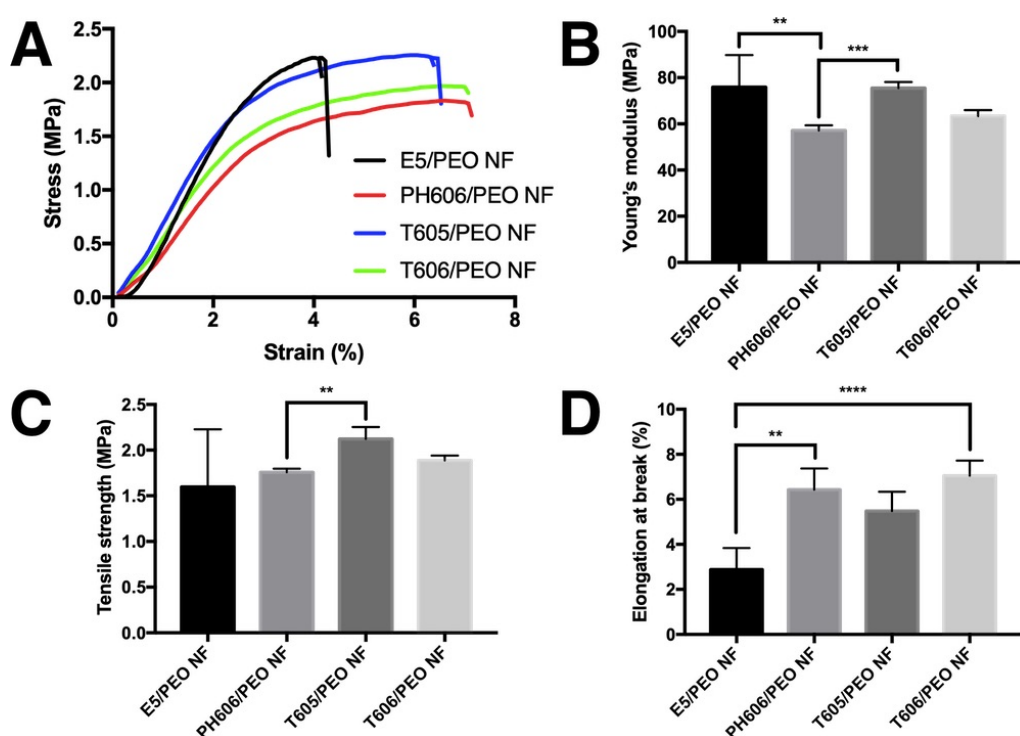

Figure 5.6: Tensile properties of the electrospun HPMC/PEO layers. Representative stress-strain curves (A), Young's modulus (B), tensile stress at maximum load (C) and elongation at break (D) of the various electrospun HPMC/PEO layers. The asterisks (*) indicate a statistically significant difference ($p < 0.05$) between the two materials; none of the other comparisons were statistically significant.

5.2.4 Fourier-transform infrared spectroscopy (FTIR) and Raman Spectroscopy

The FTIR and Raman spectroscopy analyses served to provide important information on the macromolecular structures and functional groups of the HPMCs, which

helped in terms of revealing the nature of the interactions between the various HPMCs and PEO. Four HPMC powder samples were analyzed and compared using FTIR and two samples were analyzed by means of Raman spectroscopy.
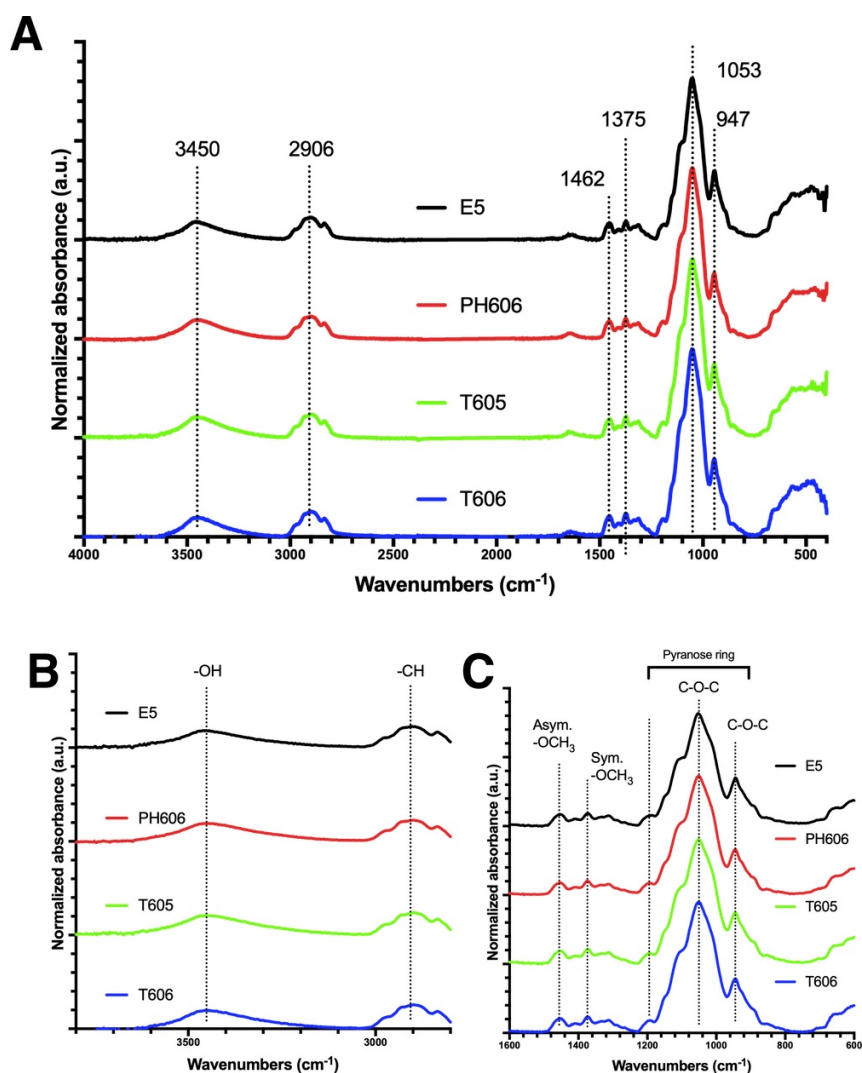

Figure 5.7: FTIR spectra of the pure HPMC powders (A). Magnified FTIR spectra of HPMC with a wave number range of 2800-3800 cm^{-1} (B) and with a wave number range of 600-1600 cm^{-1} (C).

Figure 5.7 shows the FTIR spectra obtained for the four differing HPMCs. The wave number of the OH (-hydroxy) strain was 3450 cm^{-1} and that of the C-H aliphatic strain was mainly 2906 cm^{-1}. The C-O-C stretching vibration of the PH606 was observed to comprise the strongest peaks (at 1052 cm^{-1} and 947 cm^{-1}). The broad peak from 1.200 cm^{-1} to 800 cm^{-1} was identified as a pyranose ring vibration. The smaller peaks at 1375 cm^{-1} and 1461 cm^{-1} corresponded to the symmetric and asymmetric bending vibrations of the –OCH$_3$ group (-methoxy), respectively. No noticeable differences were observed in the fingerprint region for the analyzed HPMC spectra (Figure 5.7 C). The FTIR spectra obtained for the

79

HPMCs under study were consistent with the spectra presented in the literature (Akinosho et al., 2013; Aydogdu et al., 2018).

Raman spectroscopy, which is generally more sensitive to C-H stretching, was used to define the potential differences that were not determined via the FTIR analysis. The spectra of two HPMCs with enlarged CH stretching regions are shown in Figure 5.8.
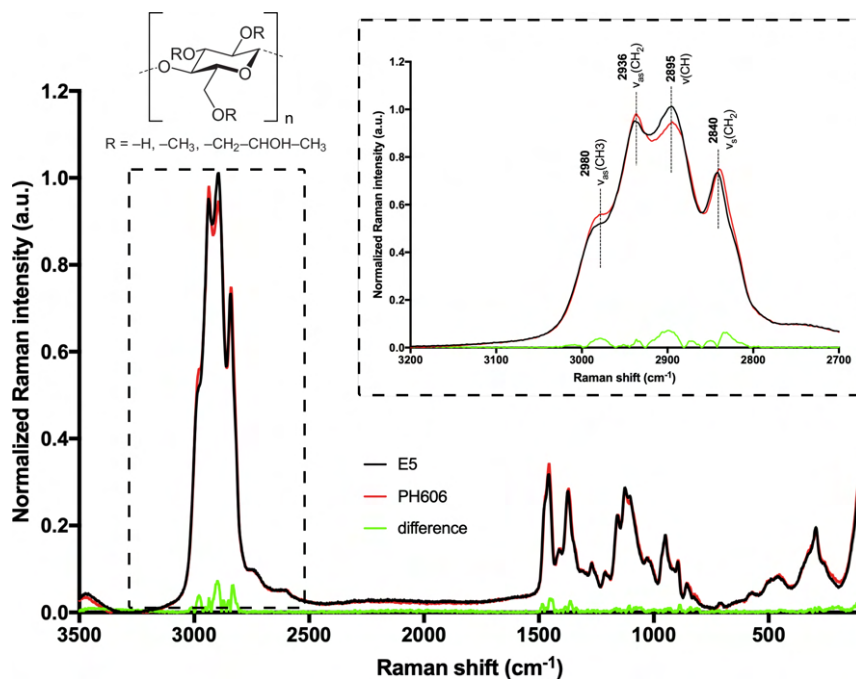

Figure 5.8: Superimposed Raman spectra of pure HPMC Methocel E5 and Pharmacoat 606 powder samples with a chemical structure of HPMC in the upper right corner of the figure. The spectra have been enlarged in the CH-OH region to highlight the differences.

The comparison of the Raman spectra in Figure 5.8 revealed a slight difference in the signal intensity primarily in the CH stretching region. The most intensive peaks at 2840, 2936, and 2895 were assigned to symmetric and asymmetric CH_2 stretching and the acyclic CH groups, respectively. The shoulder at around 2980 was assigned to asymmetric CH_3 stretching (Socrates, 2004). The Raman spectra revealed differences in the structures of the analyzed samples, mainly in terms of the linearity and length of the aliphatic chains. The signal intensity differences suggest that the E5 macromolecules evince a more branched structure and are generally shorter. On the other hand, PH606 is assumed to have longer and more linear macromolecules. These proposed properties are consistent with the fact that E5 has a lower viscosity, i.e., molecular weight, than PH606.

5.3 Conclusion

Using nanofibers as ODFs has several advantages, including relatively simple and inexpensive production, fast solubility, the absence of residual solvents, simple modifiability, etc. On the other hand, their large-scale use is limited primarily due to their poor mechanical properties and long-term stability issues.

This chapter aimed to show how even a relatively small variation in the parameters of the input polymers can significantly affect the mechanical properties of nanofibrous layers. We selected a polymer used widely in the pharmaceutical industry, HPMC, to prepare the ODF films. Two groups of polymers with the same inherent viscosity produced by different manufacturers were tested concerning various parameters. The study revealed that while the higher viscosity group displayed similar characteristics for both polymers, this was not the case for the lower viscosity group. Even though no significant difference was observed between the two polymers, the mechanical properties of Methocel E5 were approximately half as good as the rest of the tested polymers. The calorimetric measurements did not reveal any areas of significant crystallinity, nor did the morphology and infrared spectroscopy suggest any significant differences. The examination of the optical microscope images of the layers produced by the solvent casting method confirmed the orderliness of specific regions in the Methocel E5 combined with PEO compared to the other HPMCs.

The Raman spectroscopy analysis suggested that the main differences between the samples consisted of the linearity and length of the aliphatic chains of the macromolecules. The E5 macromolecules were assumed to have more branched and generally shorter aliphatic chains, while the PH606 was assumed to have more extended and linear macromolecules. Thus, it is reasonable to speculate that these slight differences can affect interactions between the macromolecules and thus lead to a significant deterioration in the mechanical properties of the fabricated layer.

The characterization of the input polymers is of significant importance. Even a slight change in the isomerism can significantly affect the parameters of the fabricated layer. This study demonstrated a series of analytical methods that enhance understanding of the behavior of mixed polymer solutions intended for electrostatic spinning.

6 Chapter VI - New approach on incorporation of sensitive bioactive substances to nanofibrous structures

6.1 Introduction

By this time, we have dicsussed the problems related to incorporation of bioactive molecules to nanofibers by relatively simple techniques as blend electrospinning, which results in production of monolith (or matrix-type) drug delivery system. However, plenty of bioactive molecules are too sensitive for incorporation by these techniques as they may be damaged (or destroyed) by the harsh organic solvents used for dissolving a polymer for electrospinning. On another hand, most of the water soluble polymer matrices are unstable without cross-linking. Thus, new approaches toward incorporation of bioactive substances to polymeric nanofibers such as polycaprolactone is demanded.
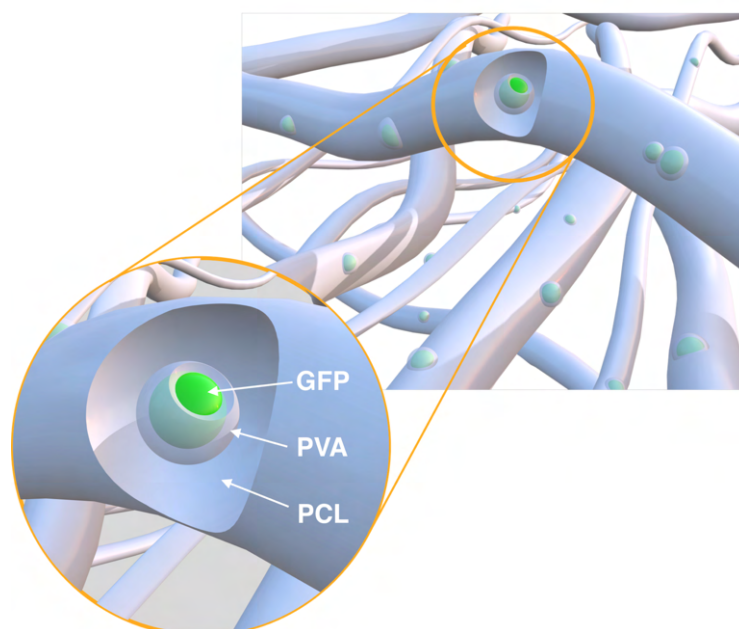
Figure 6.1: Schematic representation of the desired structure of the modified fibers with the encapsulated active ingredient.

The main subject of this study concerns the use of alternate current electrospraying to create a suspension consisting of polyvinyl alcohol capsules that contain a bioactive substance dispersed in a solvent system suitable for non-water-soluble biocompatible polymers. A suitable polymer is dissolved in such a suspension and subsequently spun using electrostatic spinning. This results in the production of a fibrous structure into which PVA capsules containing the bioactive agent are integrated. The PVA capsules protect this bioactive substance from the organic solvents required to dissolve the selected polymer.

6.2   Results and discussion

In order to confirm the accuracy of our hypothesis, it was necessary to verify the efficiency of the encapsulation of the active substance, which is also sensitive to the solvent. In addition, the substance should be of a sufficiently high molecular weight so that it does not diffuse out of the formed polymer capsules into the solvent. Organic solvents can alter the native structure of proteins by disrupting the hydrophobic interactions between the non-polar functional groups of individual amino acids (Herskovits et al., 1977). Chloroform, for example, is frequently used in molecular biology for the controlled denaturation of proteins during DNA or RNA isolation (Chomczynski et al., 2006; Xiong et al., 2014). The absorption and fluorescence spectra of green fluorescent protein (GFP) change dramatically in the presence of organic solvents (even at relatively low concentrations), and GFP completely loses its ability to fluoresce during denaturation. The isolated chromophore GFP (4-(p-hydroxybenzylidene) imidazolidin-5-one, or HBDI) is not fluorescent per se (Park et al., 2016), thus suggesting that the protein environment of the so-called β-Barrel of GFP appears to play a key role in the photophysics of HBDI. Therefore, the loss of GFP fluorescence is often used to indicate the degree of GFP denaturation (Penna et al., 2005; Shin et al., 2009). Tsuboyama et al. (2020) reported the successful use of "Hero"-proteins as protective agents to shield proteins from harsh conditions, including exposure to organic solvents. Their work reported that unprotected GFP exposed to chloroform lost up to 90 % of its original fluorescence intensity after 30 minutes. Hence, GFP was chosen as a suitable candidate for encapsulation in nanofibers since it has been well characterized and can be used to establish or refute our hypothesis.

PVA with various degrees of hydrolysis was selected to encapsulate the bioactive compounds. This polymer is characterized, in particular, by its low solubility in non-aqueous solvent systems and, therefore, has the potential to provide sufficient protection for the encapsulated substance from the solvents used for dissolving the polymer employed for the formation of the nanofibers (Yaqoob et al., 2021). PCL dissolved in a mixture of chloroform and ethanol was chosen for the preparation of the nanofibers due to its high cytocompatibility and the long-term experience of its use in the field of tissue engineering (Mondal et al., 2016). The main idea of this study was to combine the two polymers mentioned above to create a composite nanofibrous structure, concerning which the main carrier polymer is PCL

with PVA capsules containing the bioactive substance. To create the structure, a novel method was developed to prepare the polymer suspension/solution by combining several technologies. AC electrospraying technology was used to prepare the nano/microcapsules. As described in the introductory chapter, this method does not require a counter electrode and is, therefore, suitable for spinning/spraying into the solvent. It was first necessary to determine a PVA with appropriate molecular weight and degree of hydrolysis to optimize the droplet generation via AC electrospraying to the maximum extent. Two PVAs with differing degrees of hydrolysis were selected to generate the droplets. These polymer solutions were subsequently tested for the morphological analysis of the produced samples.

The PVA polymer solution containing the bioactive agent was first 'sprayed' into the PCL solvent. The particles in the polymer solution displayed a tendency to aggregate; the equation gives the rate of the aggregation of the particles (Gardner et al., 1996):

$$\frac{dn_k}{dt} = \frac{1}{2}\alpha\beta_{ij}n_in_j - n_k\sum_{i=1}^{\infty}\alpha\beta_{ij}n_i \tag{6.1}$$

where α is the collision efficiency factor, i.e., a dimensionless quantity that expresses the ratio of the number of collisions involved in the aggregation process to the total number of collisions of the individual particles. The quantities n and β_{ij} denote the density of the individual particles and the collision frequency function, respectively. In our case, collisions due to Brownian motion dominated, where the frequency function is based on Fick's first law with the particle diffusion coefficient given by the Stokes-Einstein equation. The collision rate parameter is described by (Dhont, 1996)

$$\beta_{ij} = \frac{2k_BT}{3\eta}\left(\frac{1}{r_i} + \frac{1}{r_j}\right)(r_i + r_j) \tag{6.2}$$

where η denotes the viscosity and r_i and r_j are the radii of the particles. The aggregation rate can be significantly retarded by reducing the collision factor, for example, by adding a surfactant or by increasing the viscosity of the solution. Since the addition of a surfactant could disturb the encapsulation of the active agent and affect the wetting process, it is advisable to increase the viscosity of the solution to reduce the frequency function value.

The chloroform container was placed in the ultrasonic bath. It is known that ultrasound is suitable for breaking the attractive forces between particles by increasing their Brownian motion, which acts to break down the aggregated particles (Kachanoski et al., 1988). Moreover, ultrasound can be used for the dissolution of polymers. However, due to the application of high-energy ultrasonic waves, care must be taken not to reduce the molecular weight by breaking the bonds between the monomers (K. Li et al., 2015). It is also known from the literature that even repeated sonication should not act to damage the GFP (Peternel et al., 2010). Therefore, PCL 80k was added to the container of chloroform and ethanol and gradually dissolved during the spraying period. This approach served to increase the solution's

viscosity and significantly reduce the degree of particle aggregation. The entire solution/suspension was thus rendered stable, and no aggregation nor sedimentation of the particles was observed over the two weeks in which the solution/suspension was followed. A diagram of the whole experiment and an image of the suspension are shown in Figure 6.2.
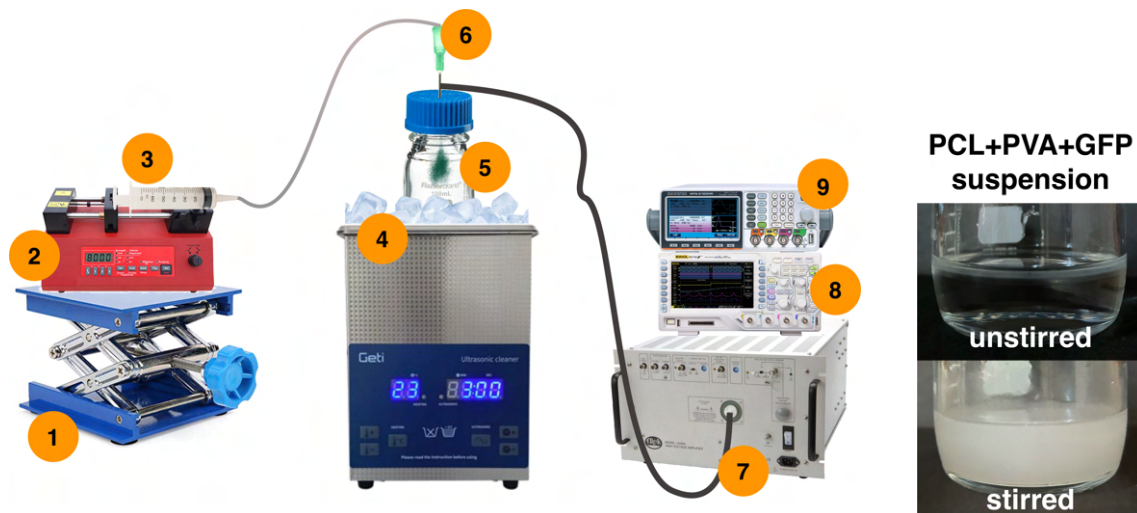

Figure 6.2: Schematic of the AC electrospraying apparatus for suspension preparation. The figure illustrates the following components: 1. Laboratory lifting platform, 2. Linear pump with a syringe (3.) holding a stock solution of PVA and GFP, 4. Ultrasonic bath filled with iced water, 5. Vial containing solvent and PCL polymer, 6. Needle with applied AC voltage, 7. High voltage amplifier, 8. Oscilloscope, and 9. Signal generator. The resulting suspension is depicted on the right side of the figure.

The electrostatic spraying process was conducted throughout the dissolution of the PCL. A nanofibrous layer was subsequently prepared from the solution containing the encapsulated bioactive agent via needleless electrostatic spinning using an NS 1S500u Nanospider. The machine parameters were selected so that the layer could be sufficiently manipulated. The resulting nanofibrous layer was then subjected to a morphological analysis.

6.2.1 Characterization of morphology

Our experiments revealed that using low-molecular-weight polymers for electrospraying is advisable. It is known that the stability of PVA increases with the increasing degree of hydrolysis, where PVA with a high degree of hydrolysis is soluble even in water only at an elevated temperature of 80 °C (Q. Fan, 2008). Hence, two PVA polymers with low molecular weights and two differing degrees of hydrolysis (88 % and 98 %) were selected for the GFP encapsulation. The two polymers at suitable electrospraying concentrations were dissolved in water with ethanol at

a ratio of 8:2 and then sprayed onto the target for the SEM analysis. The micrographs in Figure 6.3 (A and B) show that spherical particles with sizes in the range of nano- to micro-meters were obtained in both cases. The histograms illustrate the remarkably different distributions of the two polymers. The PVA98 evinces a narrower relative frequency peak with around 70 % of the diameters lying in the range of 50-200 nm (mean = (177 ± 229) nm). In contrast, the distribution of the PVA88 evinces a broader distribution, the mean value of which has shifted towards 500 nm (mean = (413 ± 247) nm). Moreover, the density of the particle coverage of the substrate, which corresponded to the productivity of the solutions, also differed significantly. In the case of the PVA88, various areas of beads were observed to partially or entirely overflow into the fibers. However, no such fibrous structures were observed for the PVA98.
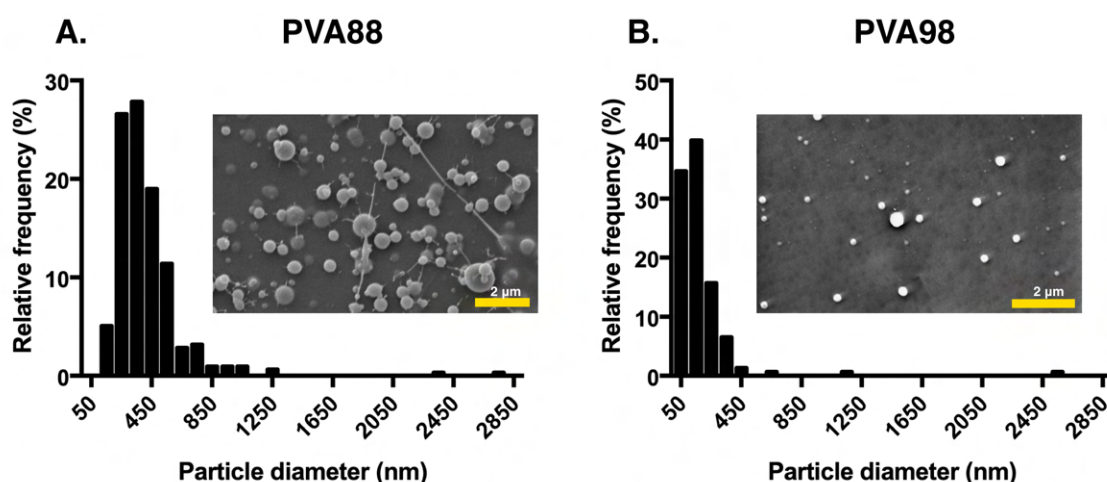

Figure 6.3: Histograms of the diameter distributions of the particles produced via AC electrospraying from the two polymers – PVA88 (A) and PVA98 (B).

The SEM micrographs of the obtained nanofibers were subsequently analyzed. The overall morphologies and histograms of the fiber diameter distributions of all the fabricated layers with and without the addition of GFP are shown in Figure 6.4 (A-E). Generally, the fibers obtained had diameters in the range of around 1000 nm. Moreover, the layers without PVA were observed to have considerably finer fibers, while the layers with the added PVA contained a more significant number of thick fibers (above 1 μm). It is also evident that the productivity of the electrospinning process was reduced with the addition of PVA particles to the solution. The addition of PVA also led to a decrease in the density of the obtained nanofibrous meshes. The reduction in productivity and increase in the fiber diameters was due mainly to the presence of water in the PCL solution that originated from the PVA solution. Water is a non-solvent for PCL; thus, it prevents its dissolution in wetting solutions or causes coagulation.
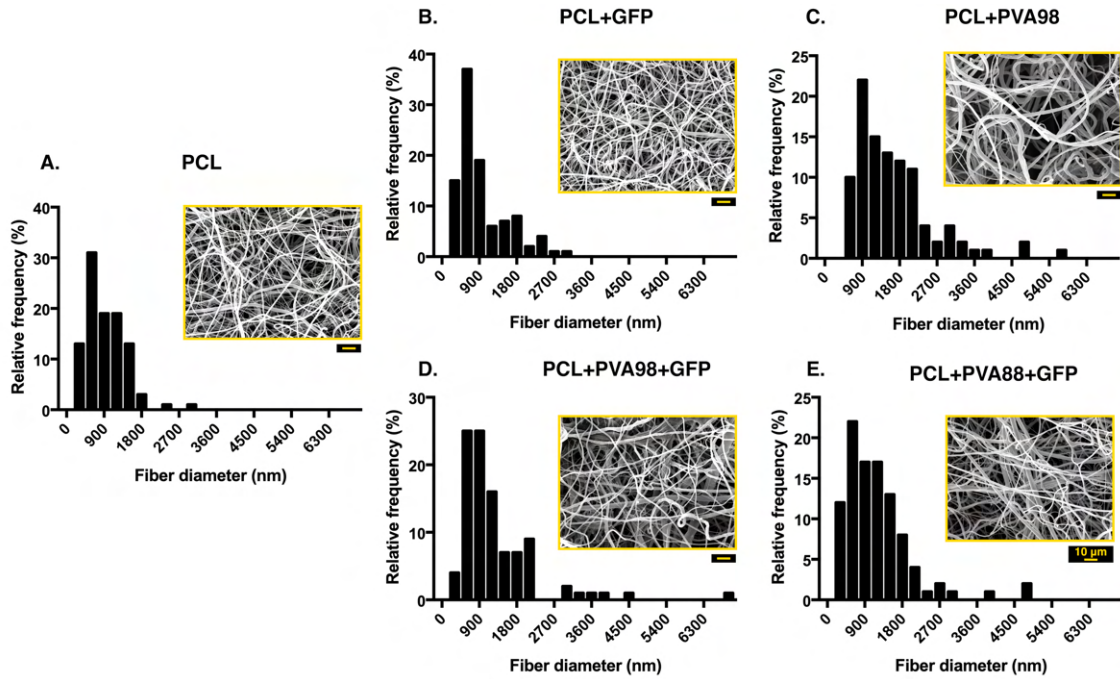
Figure 6.4: Histograms of the fiber diameter distributions (n=100) for the produced fibrous materials with representative SEM micrographs (scale bar = 10 μm).

The fibers made from PVA-free PCL solutions are homogeneous, have predominantly smooth surfaces, and have no visible defects. However, the micrographs of the fiber surfaces (Figure 6.5 C and D) show fibers that are covered mostly with several hundred nanometers in size spherical particles. The coverage of the fibers by these particles can be described as relatively uniform. No difference is visually apparent between the PVA capsule materials containing and not containing GFP. Despite the large number of particles on the surface, unfortunately, we have not yet been able to determine with the techniques available how effective the incorporation of the PVA particles inside the PCL fibers is. It can also be seen from Figure 6.6 that in terms of the resulting fiber diameter distribution, the materials produced using PVA88 and PVA98 differed significantly. On the other hand, the intensity of the coverage of the fiber surfaces by the PVA particles was considerably higher for PVA98.

Adding GFP directly to the electrospinning solution did not affect the electrospinning process or the resulting fiber morphology, as seen in Figure 6.5 (B) and Figure 6.6. Moreover, no traces of GFP were observed on the PCL fibers. It may indicate that the GFP suspension immediately denatured in the PCL solvent system (i.e., mainly chloroform) and did not affect the polymer solution. Representative images of the fiber surfaces with and without PVA encapsulation are shown in Figure 6.5 (A-E).
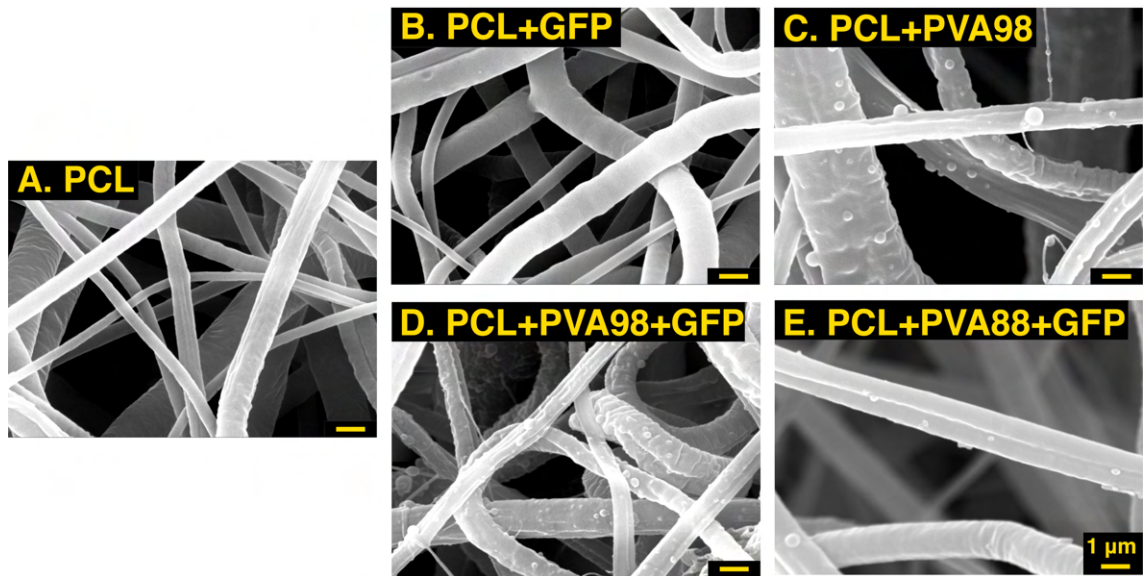
Figure 6.5: Representative images of the surfaces of the fabricated fibrous materials obtained via scanning electron microscopy. PCL (A), PCL+GFP (B), PCL+PVA98 (C), PCL+PVA98+GFP (D), and PCL+PVA88+GFP (E). The scale bar is 1 um.
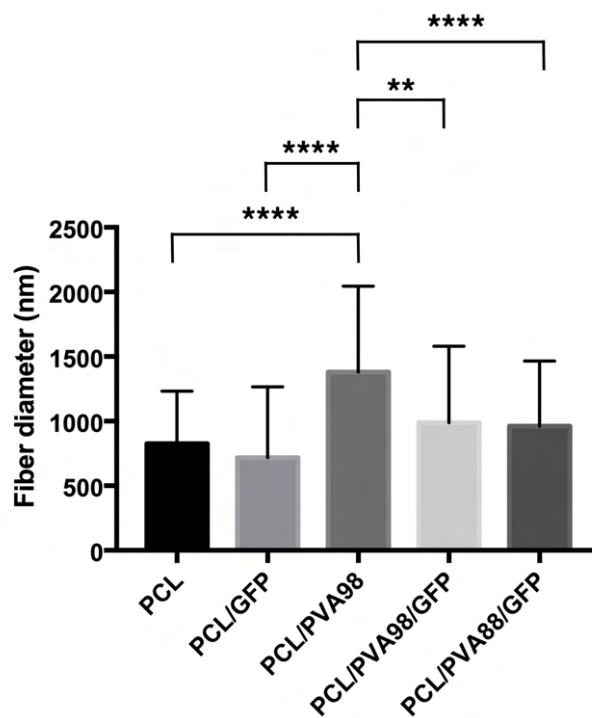

Figure 6.6: Bar plot of the fiber diameters (Median and IQR) for the produced fibrous materials (the asterisk indicates statistically significant differences at p 0.05).

6.2.2 Epifluorescence microscopy

The degree of denaturation of the GFP was challenging to measure quantitively due mainly to the matrix effect of the polymer bilayer, which distorts spectrophotometric measurement methods. A further reason was the material's lack of a continuous GFP layer. In contrast to studies that considered the direct incorporation of GFP into the nanofiber structure (Putthanarat et al., 2006; Acikgoz et al., 2016; Koeda et al., 2016), the GFP was contained in the PVA particles in our experiment and constituted around 10 % w/w of the resulting fiber material. However, it was shown that the GFP added directly to the PCL solution in the system lost its fluorescence properties. In contrast, the GFP protected in the PVA capsules retained fluorescence after spinning, as depicted in Figure 6.7 (D and E).
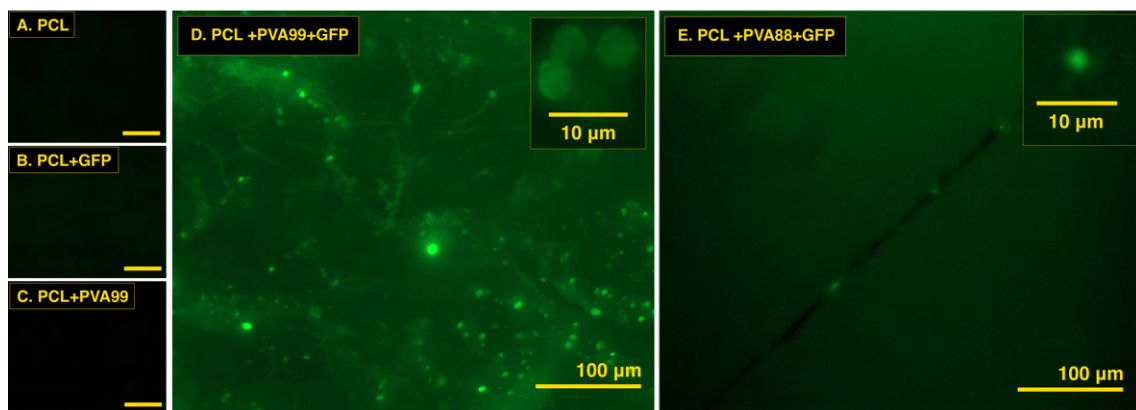

Figure 6.7: Representative epifluorescence microscopy images. A – negative control (PCL fibers), B – PCL fibers with GFP blended directly into the spinning solution, C – PCL fibers with electrosprayed PVA98 capsules, D – PCL fibers with GFP incorporated into the electrosprayed PVA98 capsules, and E - PCL fibers with GFP incorporated into the electrosprayed PVA88 capsules. The scale bar is 100 um (10 um for the magnified micrographs).

Figure 6.7 presents the epifluorescence microscope images. Images A, B, and C show no fluorescence. In contrast, fluorescent spherical particles of a size in the order of micrometer units and less can be observed in images D and E. The fluorescent particles exhibit a similar size and spatial distribution to the PVA particles observed in the electron microscope images. Since these fluorescent particles are not evident on the control layers of the pure PCL or the PCL sample with sputtered PVA particles, it was assumed that they comprise native GFP. The fact that such particles are not observed on the sample for which the GFP was incorporated directly into the PCL (Figure 6.5 B) is indicative of the effectiveness of the procedure and that PVA capsules are capable of sufficiently protecting the GFP molecule exposed to the solvent system of the polymer solution. On the other hand, fluorescence intensity differs between the PVA88 and PVA98 supplemented layers. Moreover, the epifluorescence microscopy analysis observed the gradual decay in the fluorescence of the PVA88-supplemented layers. Together, these observations indicate that the

stability of PVA88 is insufficient in protecting the GFP molecule. It is assumed that the reason concerns the gradual diffusion of chloroform into the PVA88 particles, leading to the denaturation of the GFP in the PCL nanofibers.

6.3 Conclusion

Incorporating sensitive biomolecules in nanofibrous structures remains challenging due to the bio-incompatibility of most of the solvents used for electrospinning. Therefore, more complex approaches are being explored that ensure the retention of the nanofibers' properties while maintaining the molecules' bioactivity.

For the first time, this study applied the low-frequency AC electrospraying technique to incorporate a sensitive biomolecule in nanofibers *in situ*. A model bioactive molecule, green fluorescent protein (GFP), was successfully encapsulated within polyvinyl alcohol capsules, followed by their incorporation in the structure of polycaprolactone nanofibers using needless electrospinning. The morphological analysis of the scanning electron microscopy micrographs confirmed the presence of uniformly distributed PVA particles on the surface of the fibers. Further, fluorescence microscopy revealed the presence of fluorescent, nondenatured GFP on the PVA capsule-loaded samples. Moreover, the absence of fluorescence was observed for the samples with GFP incorporated directly in the PCL fibers without encapsulation, suggesting the denaturation of the unprotected GFP in the PCL solvent system. The comparison of PVA with two different degrees of hydrolysis confirmed the hypothesis that, despite electrospraying's higher productivity, PVA88 is unstable enough to protect the GFP sufficiently. On the other hand, smaller particles with narrower diameter distributions and higher stability were produced from the PVA98.

The findings of this study demonstrate the effectiveness of a novel approach to creating a complex nanofibrous structure using low-frequency electrospraying. The experimental setup used in this study illustrates the significant advantages of AC electrospraying for this incorporation technique. One significant benefit is that it eliminates the need for an opposite electrode to act as a collector, thus allowing the particles to be incorporated directly into the dissolving polymer matrix. Such nanofibrous structures with incorporated capsule carriers can be used as controlled drug delivery systems for proteins and other sensitive biomolecules in biomedical applications, e.g., wound healing.

Nevertheless, due to the complex composition of such multi-component matrices, we could not quantify the encapsulated GFP within the confines of this study, and only qualitative results that confirm the presence of protected GFP following electrospinning are provided. Consequently, further advancements in the sample preparation methodology are required to ensure the accurate quantification of the incorporated GFP by means of fluorometric analysis.

In conclusion, this study successfully demonstrated a novel approach to creating complex structures by combining low-frequency AC electrospraying and needless DC electrospinning. The study's findings provide insights into the control of aggregation through the manipulation of the viscosity of the medium. In addition, our study establishes the basis for further investigation of the impact of the degree of hydrolysis and the molecular weight of PVA on the size of the produced nano- and microparticles. Thus, this research serves as a framework for methodological advancements in the field and opens up new horizons concerning the potential use of AC electrospraying in a wide range of biomedical applications.

7 Materials and methods

7.1 Preparation of drug-loaded nanofibrous materials

This last chapter covers the key methods and materials, which were utilized for fabrication and further investigation of produced nanofibrous materials.

7.1.1 Nanofibrous materials loaded with Alaptide and/or L-Arginine

Nanofibrous wound dressings were prepared by blending electrospinning technology (Zhang et al., 2017). PCL (Merck, KGaA 704 105) with average molecular weight Mn 45.000 was dissolved in a chloroform/ethanol (Penta s.r.o., Czech Republic) solvent mixture at a weight ratio of 8:2 (L-Arginine-loaded mats) or 9:1 (Alaptide-loaded mats). Ethanol was used as a less volatile solvent (in comparison with chloroform) to control the evaporation rate of the solvent system. The polymer concentration used for obtaining continuous fibrous meshes was 16 wt.%. The L-arginine-modified PCL meshes were prepared by adding 1, 5 or 10 wt.% of L-arginine monohydrochloride (Merck KGaA, Germany) in the form of a cryomilled powder. First, 0.075 wt.% of sodium lauryl sulphate (SLS) was dissolved as a stabilizer in the same solvent system mentioned above for PCL. A given amount of L-arginine was then dissolved/dispersed in this solvent system for 30 min; this was followed by 10 min of sonication to ensure the homogeneity of the L-arginine suspension. Following the addition of PCL pellets, the resulting solution was stirred constantly until the PCL had completely dissolved, whereupon it was immediately electrospun. The addition of 1 wt.% of L-arginine led to the formation of electrospinning solutions, whereas the addition of 5 and 10 wt.% gave rise to a suspension containing partly undissolved L-arginine particles. The same procedure was performed for Alaptide, and later for the Alaptide/L-arginine mixture. Nanonized Alaptide was synthesized by means of the standard procedure (Kasafírek et al., 1992) and then milled according to Cernikova et al. (Cernikova et al., 2014). In this study, we used 0.1, 1 and 2.5 wt.% of Alaptide added into the PCL solution, and for membranes with the Alaptide/L- arginine combination, the loading was 1.5 wt.% of Alaptide and 5 wt.% of L-arginine in the PCL solution. The concentrations of the additives mentioned throughout this study were calculated with respect to the polymer solution from which the nanofibrous membrane was spun. The concentrations of the additives in

the nanofibers therefore have to be recalculated with respect to the dry content only. For example, 1 wt.% in the PCL solution means that 1 g of the drug was added to 16 g of PCL and was dissolved in 83 g of the solvent. This finally yields 6.25 wt.% of the drug in the dry PCL nanofibrous membrane. For electrospinning, a positive voltage was applied to the wire (i.e. the spinning electrode) and a negative voltage was applied to the collector; the potential difference was 40 kV. The distance between the spinning electrode and the collector was 160 mm. The temperature during the experiments was (22 ± 5) °C, with relative humidity of (40 ± 5) %.

7.1.2 Nanofibrous materials loaded with LPPO

The second generation LPPO DR-6180 (Figure 2.4) was synthesized in multigram quantities according to the procedure reported previously (Seydlová et al., 2017). Nanofibrous wound dressings were prepared by blending electrospinning technology (Zhang et al., 2017). Four nanofibrous (polycaprolactone—PCL) materials with different concentrations of LPPO were prepared (0, 2, 5, and 10 wt%). All concentrations were calculated for dry matter (excluded solvent). Firstly, LPPO was dissolved in chloroform/ethanol (Penta s.r.o., Praha, Czech Republic) solvent mixture at a weight ratio of 8:2 (solution for preparation of PCL supplemented with LPPO 2% was prepared by dissolving 0.32 g of LPPO in 84 g of solvent mixture; solution for preparation of PCL supplemented with 5% LPPO was prepared by dissolving 0.8 g of LPPO in 84 g of solvent mixture; solution for preparation of PCL supplemented with 10% LPPO was prepared by dissolving 1.6 g of LPPO in 84 g of solvent mixture). The ultrasound (40 kHz, 50 W) was then applied for 30 min to enhance the solubilization of LPPOs and ensure homogeneity of the spinning solutions using an ultrasonic bath (Shesto, Watford, UK). Then 16 g of polycaprolactone (Merck, Praha, Czech Republic) with an average molecular weight Mn 45,000 was dissolved in each solution. The polymer concentration used for obtaining continuous fibrous meshes was 16 wt% (LPPO is not included in this ratio). All materials were electrospun using Nanospider NS 1WS500U (Elmarco a.s., Liberec, Czech Republic) on polypropylene spunbond microfiber nonwoven (Pegatex S; 20 g/m^2; fiber diameter 20 m; PFNonwovens Czech, Czech Republic). For electrospinning, a positive voltage was applied to the wire (i.e., the spinning electrode) and a negative voltage was applied to the collector; the potential difference was 40 kV. The distance between the spinning electrode and the collector was 160 mm. The temperature during the experiments was (22 ± 5) °C, with a relative humidity of (40 ± 5) %. Produced samples were finally sterilized in the flow box using a UV light for 10 min for each side.

7.1.3 Nanofibrous materials loaded with GFP-encapsulated PVA particles

Electrospinning was performed using a laboratory-scale NANOSPIDER NS 1W500U (Elmarco, Czech Republic) device. The process parameters were set at a temper-

ature of 20° C and a relative humidity of 40%. The potential difference between the electrode and the collector was 50 kV, with a positive charge applied to the electrode and a negative charge to the collector. The distance between the collector and the electrode was 160 mm. The same procedure was subsequently employed so as to produce modified materials with the presence of GFP. The solution of PCL with PVA and GFP was stored in aluminum foil at 8 °C. Subsequently, the solutions were magnetically stirred for around 30 minutes prior to electrospinning. The electrospinning of the PCL+PVA+GFP required a higher potential difference (60 kV) and a lower relative humidity (30 %).

7.2 Preparation of ODFs

7.2.1 Nanofibrous ODFs

Polyethylene oxide with a molecular weight of 100 kDa was purchased from Sigma Aldrich. Hypromellose Methocel E5 was purchased from JRS Pharma (Rosenberg, Germany); the viscosity value of aqueous 2% (w/v) solution at 20 °C was 5 mPas. Pharmacoat 606 was purchased from Shin-Etsu Chemical (Tokyo, Japan); the viscosity value of aqueous 2% (w/v) solution at 20 °C was 6 mPas. Tylopur 605 and 606 were purchased from SE Tylose (Wiesbaden, Germany); the viscosity value of aqueous 2% (w/v) solution at 20 °C was 5 and 6 mPa s, respectively. Methoxyl content was 28–30 % and a hydroxypropoxyl content of 7–12 % for all the tested HPMCs. The purified water and Isopropyl alcohol were obtained from Penta chemicals (Czech Republic).The spinning solutions were prepared via the dispersion of 7% (w/w) of HPMC and 3% (w/w) of PEO in isopropyl alcohol (IPA). The total volume of the solvent system was then adjusted using purified water to obtain a final IPA/water ratio of 1:1 (w/w). The polymer solutions were subsequently stirred using a magnetic stirrer (Heidolph, Schwebach, Germany) at 300 RPM for 24 hours to attain complete dissolution. The solutions were then electrospun using a Nanospider® NS 1WS500U (Elmarco, Liberec, Czech Republic) needleless electrospinning machine. The parameters of the electrospinning process were set as follows: positive voltage on the spinning electrode, 40 kV; negative voltage on the collector, -10 kV; distance between the spinning electrode and collector, 140 mm. The temperature and relative humidity were maintained at (22 ± 3) °C and (18-22) %, respectively. A nonwoven (spunbond) polypropylene material was used as the substrate.

7.2.2 Solvent-casted ODFs

The procedure used for the preparation of the HPMC/PEO electrospinning solution was repeated for the preparation of the film-casting solutions. However, since the 10% (w/w) polymer solutions were not sufficiently viscous to cast a smooth film, a higher concentration of 15% (w/w) was required. Around 2 ml of the stock 15%-solution was then poured onto a glass plate (10 cm x 10 cm) and a stainless-steel micrometer adjustable film applicator (TQC Sheen, Leominster, UK) with a width

of 100 mm was used to obtain a smooth flat polymeric film. The casting gap was adjusted to 500 µm. The films were stored in a fume hood for 24 h at room temperature to allow for the solvents to completely evaporate.

7.3 Fabrication of PVA capsules (w/ and w/o GFP) by means of AC-electrospraying

7.3.1 Preparation of the PVA solution (with and without GFP)

The PVA solution was prepared by dissolving PVA powder (88% or 98% of hydrolysis) in a distilled water:EtOH solvent system (8:2, w/w) so as to ensure a final concentration of 10 wt%. The solution was stirred (IKA RCT standard magnetic stirrer, IKA-Werke GmbH & Co. KG, Staufen, GER) at an elevated temperature (heating to 80°C, water bath) for around 48 hours. Before adding the GFP suspension to the PVA, the suspension was thawed at 8°C for around 1 h. Subsequently, 20 μ g of GFP suspension was added to 3 g of 10% PVA solution (in a PS cuvette), shaken and then sonicated (GUC 02B, GETI, Opava, CZE) for 2 min so as to enhance the dispersion. The entire contents of the cuvette were transferred into a 5 ml PP syringe.

7.3.2 Experimental setup for the AC electrospraying

The schematic of the experimental set up used for the production of micro/nanoparticles by means of AC electrospraying is depicted in Figure 6.2. The configuration essentially consisted of three components - the polymer dispenser, the ultrasonic bath with the solvent containing the gradually dissolving polymer, and a high-voltage AC power source. The polymer dispenser consisted of an NE-300 syringe pump (New Era Pump Systems, Inc., Farmingdale, NY, USA) mounted on a laboratory lifting platform and a 5-mL polypropylene syringe connected via silicone tubing to a 21-gauge (40 x 0.8 mm) blunt needle. The needle was inserted into the cap of a Fisherbrand glass bottle (Fisher Scientific, Leicestershire, UK) perpendicular to the PCL solution so that the distance from the needle tip to the solution was approximately 5 cm. The glass bottle with the polymer solution was placed in a GUC 02B ultrasonic bath (GETI, Opava, Czech Republic). The sonification frequency was 40 kHz (60 W). The needle was connected to a 10/40A high-voltage amplifier (Trek Inc., Lockport, NY, USA) supplemented by a GW Instek MFG-2160MF function generator (Good Will Instrument Co., Ltd., New Taipei City, TWN) and a RIGOL DS1074Z-S plus digital oscilloscope (RIGOL Technologies EU GmbH, Gilching, GER). The alternating peak-to-peak voltage was set at 18.4 kV, and the frequency was set at 3 Hz. Spraying was performed for around 8 h. The dosage was 0.6 ml/hr. The bath temperature was maintained at (20°C ± 10) °C. The needle diameter was 1.2 mm.

7.4 Morphological analysis

7.4.1 Scanning electron microscopy

Morphological analysis was performed by scanning electron microscopy (Vega Tescan 3, Tescan, Brno, Czech Republic). All the samples were coated with gold (sputtering) prior to viewing so as to minimize the charging effects (14 nm for PCL+Alaptide/L-Arginine; 7 nm for PCL+LPPO). The fiber diameters were subsequently determined employing an ImageJ (National Institutes of Health, MD, USA) image analyzer (PCL+Alaptide/L-Arginine) or NIS Elements (Laboratory imaging s.r.o., Prague, Czech Republic) software (PCL+LPPO) via the measurement of randomly observed nanofibers (300 or 200) selected over different fields of view at an appropriate magnification (5000×). Concerning the particle analysis, the polymer solution was sprayed onto the surface of double-sided adhesive tape attached to a target and then sputtered with 2 nm of gold. Although the use of the fully automated analysis of the particle size applying different image analysis software is common, such automated approaches often fail in terms of the recognition of the individual particles, especially when the image features agglomerates of particles. Thus, this study measured the particle size distribution semi-automatically applying the classic stereological systematic uniform random sampling (SURS) approach. The SEM image of the particles (magnification of 5000x) was divided into 24 equivalent cells applying a grid, with a grid cell size of 8x8 μm. The fraction of the samples for measurement, f, was then $f = 1/p$. The periodicity, p, was chosen at 4, thus the total fraction for measurement was 1/4 and the total number of samples 6. In order to include randomness in the selection, a random number was generated from 1 to 4 prior to measurement to serve as the starting point. Finally, a stereological dissector was applied to the individual cells of the grid and the diameters of all the clearly seen and distinguishable particles were measured. Histograms were used to summarize data from fiber diameter/distribution measurement.

7.4.2 Polarized light microscopy

Polarized light microscopy was performed using an Olympus BX-60 (Olympus, Center Valley, Pennsylvania) microscope equipped with polarized filters and 10X, 20X, and 50X objectives. Macroscopic images of the ODF surfaces were captured using a Levenhuk DTX 90 (Levenhuk, Tampa, USA) USB microscope. The thicknesses of the nanofibrous layers were determined using a digital micrometer. The areal density (productivity), g/mm^2, of the nanofibrous layers was determined from the average weight of 5 samples with areas of 4.84 cm^2 (2.2 x 2.2 cm).

7.4.3 Epifluorescence microscopy

The presence and biological activity of the incorporated GFP were confirmed by observing the treated and untreated samples under an Axio Imager M2 epifluorescence microscope (Zeiss, Germany) equipped with an AxioCam MRm camera and

Axio-Vision SE64 Rel 4.9.1 software (Zeiss, Germany). Fluorescence images were obtained at an excitation wavelength range of 445-495 nm, and the observation filter had a long-pass filter wavelength of above 515 nm.

7.5 Mechanical properties of the electrospun nanofibrous layers

The mechanical properties of the electrospun nanofibrous layers were tested for tensile strength, Young's modulus, and elongation at break. The measurements were conducted using a LaborTech LabTest 2.010 (Opava, Czech Republic) tensile tester applying the following parameters: gauge length, 50 mm, and strain rate, 100 mm/min. The fibrous layers were cut with scissors into 10×50 mm rectangles (plus 10 mm on either end for the clamping of the samples). The thickness of the layers was determined using a digital micrometer (n=10). The tensile stress was defined as the ratio between the applied force and the sectional area of the sample (width of the sample multiplied by the thickness). The strain was defined as the ratio between the gauge displacement and the initial gauge distance. Eight samples were tested for each material to determine the average values and standard deviations.

7.6 Differential scanning calorimetry

A differential scanning calorimeter (Mettler Toledo Star 3, USA) was used for the investigation of the crystallization and melting behavior of the studied materials. The heating/cooling rate was set at 15°C/min within a temperature range of 25°C to 200°C. This temperature ramping was chosen to minimize the time delay between layer production and subsequent measurement. Each sample (around 10 mg) was first heated from 25°C to 200°C and subsequently cooled to 25°C; an empty sample pan was used as the reference. The area of the peak (normalized per sample unit weight) was determined in DSC thermograms. The crystallization temperature (T_{cc}) and the cold crystallization enthalpy (ΔH_{cc}) of the samples were determined from the cooling scan, while the melting temperature (T_m) and melting enthalpy (ΔH_m) were ascertained from the heating scan.

7.7 Spectroscopic methods

7.7.1 Raman spectroscopy

A DXR™ Raman microscope (Thermo Scientific, USA) with a 532 nm laser was used for the analysis of 2 HPMC powders. The instrument was calibrated automatically before each reading. The readings, which consisted of one scan, were taken at a power of 1.5-2.0 mW with a spectral region of 3500 cm^{-1} to 100 cm^{-1}. The Raman spectra were normalized using the standard normal variate (SNV) normalization

method by subtracting each spectrum by its own mean and dividing it by its own standard deviation.

7.7.2 Infrared-spectroscopy - FTIR

The materials were characterized using a Fourier transform spectrometer (Nicolet iZ10; Thermo Fisher, USA). A background reading was taken before each of the measurements. The samples were placed on the ATR diamond crystal for analysis, and the spectrum analysis was collected at 25°C using 16 scans in the infrared region in the range 400–4000 cm^{-1} and with a spectral resolution of 4 cm^{-1}.

7.8 High-performance liquid chromatography (HPLC) and *in vitro* drug release studies

7.8.1 Nanofibrous materials loaded with Alaptide and/or L-Arginine

First, small nanofibrous samples (n=3) with average weights of (50 ± 0.9) mg were cut from the nanofibrous layers of each material for the investigation of the release of the drug. The samples were then immersed in 20 mL of fresh PBS (pH 7.4) solution. The PCL + 0.1 wt% Alaptide sample was immersed in 5 mL of PBS so as to ensure that the concentration of the released drug was guaranteed to be in the high-performance liquid chromatography (HPLC) detection range, i.e., 5 mg/L. The samples were subsequently incubated in an incubator at (37 ± 1) °C (without stirring). Small aliquots of 1 ml were extracted from the tubes at predetermined time intervals and were replaced with the same volume of fresh PBS solution. The obtained aliquots were analyzed by means of HPLC. The HPLC system comprised a Dionex Ultimate 3000 with an LPG-3400SD quaternary gradient pump, an SR-3000 solvent rack, a WPS- 3000TSC autosampler, a TCC-3000SD column compartment and a DAD-3000 detector, with the use of a Phenomenex Kinetex Hilic core- shell column with a length of 150 mm and internal diameter of 4.6 mm. The aqueous component (A) of the mobile phase consisted of 5 % of acetonitrile in water. The organic component (B) of the mobile phase consisted of pure acetonitrile. A set linear gradient was applied. The initial proportion of B in the mobile phase was 90 %. At 1.5 min, a 1-min lasting gradient commenced from the initial conditions to 60 % of the B component. This mobile phase composition was maintained for 1 min and then returned to the initial conditions in 0.5 min. The chromato- gram was recorded for 6.6 min for each sample. The flow rate was 1.5 ml/min and the column temperature was maintained at 20 °C. An injection volume of 20 μL was applied. Chromatograms were recorded at wavelengths of 200, 205, 210 and 250 nm with a sampling rate of 2 Hz. The aliquot samples of released Alaptide were diluted with pure acetonitrile via the pipetting of 150 μL of the sample and 1500 μL of acetonitrile into a 2-mL vial, followed by vortexing. The samples were filtered through a 13-mm diameter nylon syringe filter with a pore size of 0.22 μL prior

to injection. The cumulative amount of the released drug was calculated using the following equation:

$$M(t) = C_n(t) \cdot V_R + V_s \cdot \sum_{i=1}^{n-1} C_i \qquad (7.1)$$

where $M(t)$ is the cumulative release weight of the substance at time t, C_i is the substance concentration within withdrawn aliquot at time t, V_R is the total volume of release medium, V_s is the volume of the withdrawn aliquot, and n is the sampling time.

In order to determine drug loading within the fibrous mats, the fiber samples with Alaptide were dissolved in 4 mL of chloroform/acetonitrile (1:1) solution and were then vortexed. The obtained solution with the dissolved fibers was mixed with pure methanol 1:1 and was vortexed. Finally, 850 μL of the methanol-containing solution was mixed with 150 μL of distilled water and 3 mL of pure acetonitrile and was vortexed. Similar procedure was followed in order to quantify an amount of Alaptide trapped in the fibrous mats at the end of the release experiment. The samples with L-arginine were dissolved in 2 ml of chloroform. The resulting solution was then mixed 1:1 with 2 ml of 0.25% heptafluorobutyric acid and 0.5% formic acid in water. This procedure resulted in the creation of a separate liquid phase with diluted L-arginine. One milliliter of this separated phase was used for the HPLC analysis. The L-arginine solution was filtered using a 0.22 μm nylon filter before proceeding with the HPLC analysis.

The solubility of Alaptide in the chloroform:ethanol (9:1, w/w) pure solvent system and the polymer solution at 22 °C, as well as the solubility in the release medium (PBS) at 37 °C, were determined using the shake-flask method. In order to determine the solubility in the PCL solution, an excess of Alaptide was added to the polymer solution and stirred overnight so as to attain equilibrium. The equilibrated samples were diluted with pure methanol and a mixture of ACN:CHCl$_3$ (1:1, v/v), following which water was added. The samples used for the determination of solubility in the PBS and in the pure solvents were simply diluted with ACN. Finally, the samples were filtered through a 13-mm- diameter nylon syringe filter with a pore size of 0.22 μm. All the diluted samples were quantified using HPLC (according to the method used for *in vitro* drug release studies describe above).

7.8.2 Nanofibrous materials loaded with LPPO

Samples ($n = 3$) were cut from prepared electrospun planar materials to final weight of (50 ± 0.9) mg. Individual samples were placed in 5 mL tubes with 5 mL of phosphate buffered saline (PBS) buffer (pH = 7.4), 0.02% sodium azide. The drug release study of the samples was performed at 37 °C, without shaking. Aliqouts (1 mL) of the solution were taken for subsequent HPLC analysis after predetermined intervals. The buffer solution was replaced with the same volume at the same time periods. Samples of solutions were analyzed for the LPPO content by HPLC.

The HPLC analyses were performed using Dionex Ultimate 3000 HPLC system equipped with a DAD 3000 UV–VIS diode array detector (Dionex, Sunnyvale, California, USA) controlled by Chromeleon 6.80 SR12 soft- ware on Phenomenex Kinetex Hilic column (particle size 2.6 μm, column dimensions 150 mm $\times$ 4.6 mm) at 40 °C, at a flow rate of 1.4 mL/min. Samples were diluted 1/4 with pure acetonitrile, vortexed for approximately 30 s, and consecutively filtered (nylon syringe filters, 0.22 μm, Chromservis, Prague, Czech Republic). The injection volume was 20 L. Wavelengths of 200, 207, 262 and 280 nm were used for the detection of LPPO. The gradient elution program is shown in Table S4. LPPO was quantified by comparison with external standards of LPPO DR-6180. The calibration levels used were 50, 100, 200, 500 and 1000 mg/L.

7.9 Determination of the apparent diffusion coefficient

In order to determine the diffusion coefficient of substances within the fibers, the experimentally obtained release kinetics data was fitted to the corresponding diffusion equation solution. Curve-fitting was conducted using Python language (version 3.8.5) and the "NonLinearModelFit" function in Wolfram Mathematica software (version 11.1). An equal weighting was used for the non-linear regression.

7.10 Statistical analysis (nanofiber diameters)

The normality of the fiber diameter data was verified primarily by means of the Shapiro-Wilk's test and the homoscedasticity was verified by means of the Levene's test (significance level of 0.05). The statistical significance of the differences between the nanofibrous layers were analyzed using non-parametric analysis since either the assumption of normality or homoscedasticity were violated. Subsequently, the Mann-Whitney test (or Kruskal-Wallis test) was performed for two (or the multiple-sample) sample comparisons considering a level of $p \leq 0.05$ as statistically significant. Numerical data were expressed as the mean $\pm$ standard deviation (SD). Fiber diameter data were as well expressed as median and inter-quartile range (IQR = Q3-Q1). Additionally, the coefficient of variation, CV, of the diameter distribution was used to characterize the homogeneity of the fiber distribution. The statistical data processing was conducted using Python language (version 3.8.5) and GraphPad Prism software (version 7.0).

Conclusion and outlook

This Ph.D. research aimed to explore novel approaches for designing and fabricating nanofibrous structures as drug delivery platforms, focusing on developing predictive tools to forecast their release behavior. The thesis covers a broad spectrum of experiments conducted to create an active wound dressing with incorporated bioactive substances. All fabricated materials underwent thorough characterization throughout the Ph.D. study using various techniques. Additionally, a mathematical model was developed to investigate the diffusion of substances from nanofibrous structures, which was later verified on real experimental data of drug release kinetics.

Based on qualitative and quantitative results obtained in this study, it can be concluded that the statistical and general mathematical treatment of electrospun nanofibrous-related data should be approached differently due to their unique, perhaps unapparent, complexity. The developed mathematical model based on the diffusion equation in cylindrical coordinates confirmed that even the electrospun systems produced from suspensions might be generally characterized in terms of a classical diffusion. On the other hand, the analysis of other model drugs revealed the complexity of the optimization process for non-stable or highly affinitive compounds. Despite this, it was demonstrated how the fiber diameter distribution affects the release of the substances from nanofibers.

While using a limited number of polymers as a drug carrier matrix limits the generalizability of the obtained results, the analytical approach provides new insights into the behavioral characteristics of nanofibrous structures during a drug release process. This research illustrates some hidden features behind the generalized variables in conventional mathematical models. On the other hand, it raises questions about the limits of the available experimental techniques.

To better understand the implications of these results, future studies could address the further verification and extension of the mathematical model. One of the most recommended directions for expanding the mathematical model is to consider the spherical beads (defects) common for electrospun nanofibers, which also might contain a significant amount of incorporated substance. For this, the combination of the solution of the diffusion equation in cylindrical and spherical coordinates is required. Experiments may be directed towards exploring the possible correlations between specific properties of molecules of the bioactive substances (e.g., topological polar surface area), which affects the diffusion and mass transfer coefficients. Both theoretical (computing) research should be conducted to investigate the mutual relationships and mathematical behavior of finite mass transfer coefficient at the fiber surface, particularly for small values of Sherwood number. The experimental ap-

proach might be derived from the experiment (mentioned in chapter 3.3.5), with the variation of the agitation speed of the release medium to estimate the thickness of the diffusional boundary layer at the fiber surface and how it is related to specific properties of a particular substance. Finally, the new study may be initiated toward investigation of the interaction between PCL and LPPO in order to describe and predict its release from nanofibers. To apply the developed model, the first experiments should be focused on estimation of the equilibrium concentration and solid-state solubility of LPPO and PCL.

This Ph.D. research contributes to the field from several perspectives. The results demonstrated successful strategies for incorporating various bioactive substances into biodegradable polymers. The extensive morphological analysis of the produced materials brings up the important discussion of whether the conventionally used statistical and kinetics-related approaches are appropriate for analyzing the nanofibrous structure. Indeed, as was demonstrated throughout the thesis, plenty of questions within the topic remain unanswered. It is believed that this thesis may serve as a solid outset for further deeper analysis and experimental work to fill the gaps in the general understanding of electrospun nanofiber-based drug delivery systems.

References

ACIKGOZ, Sabriye et al., 2016. Enhanced Radiative Decay Rate of Confined Green Fluorescent Protein in Polyvinylpyrrolidone-Based Nanofiber. *The Journal of Physical Chemistry C* [online]. Vol. 120, no. 31, pp. 17739–17744 [visited on 2023-02-08]. ISSN 1932-7447, ISSN 1932-7455. Available from DOI: 10.1021/acs.jpcc.6b04074. Number: 31.

AHMAD, Muhammad Shakeel; MUNAWAR, Rehana; BOKHARI, Syed Hamid Mehmood, 2021. Allama Muhammad Iqbal Critique of Western Democracy and his Vision of Spiritual Polity of Islam. *Al-Azhār*. Vol. 7, no. 02, pp. 8–17.

AKINOSHO, Hannah; HAWKINS, Samantha; WICKER, Louise, 2013. Hydroxypropyl methylcellulose substituent analysis and rheological properties. *Carbohydrate Polymers*. Vol. 98, no. 1, pp. 276–281. ISSN 01448617. Available from DOI: 10.1016/j.carbpol.2013.05.081.

ALEXANDER, J Wesley; SUPP, Dorothy M, 2014. Role of arginine and omega-3 fatty acids in wound healing and infection. *Advances in wound care*. Vol. 3, no. 11, pp. 682–690.

ALLUR SUBRAMANIYAN, Sivakumar et al., 2018. Fabrication of nanofiber coated with l-arginine via electrospinning technique: A novel nanomatrix to counter oxidative stress under crosstalk of co-cultured fibroblasts and satellite cells. *Cell Communication & Adhesion*. Vol. 24, no. 1, pp. 19–32.

ALOPAEUS, Julia F. et al., 2020. Mucoadhesive buccal films based on a graft co-polymer – A mucin-retentive hydrogel scaffold. *European Journal of Pharmaceutical Sciences*. Vol. 142, p. 105142. ISSN 18790720. Available from DOI: 10.1016/j.ejps.2019.105142.

ANDERSON, Philip W, 1972. More is different: broken symmetry and the nature of the hierarchical structure of science. *Science*. Vol. 177, no. 4047, pp. 393–396.

ARIFIN, Davis Yohanes; LEE, Lai Yeng; WANG, Chi-Hwa, 2006. Mathematical modeling and simulation of drug release from microspheres: Implications to drug delivery systems. *Advanced drug delivery reviews*. Vol. 58, no. 12-13, pp. 1274–1325.

ASATIANI, Nikifor; FILIPOVÁ, Barbora, et al., 2023. Electrospun HPMC/PEO-blend orodispersible films: how slight batch differences affect the crucial mechanical properties. *Cellulose*. Vol. 30, pp. 1–15.

ASATIANI, Nikifor; NOVOTNÝ, Vít, et al., 2021. A novel approach to studying the kinetics of release of alaptide from poly-ε-caprolactone nanofibers. *Journal of Drug Delivery Science and Technology*. Vol. 63, p. 102492.

AYDOGDU, Ayca; SUMNU, Gulum; SAHIN, Serpil, 2018. A novel electrospun hydroxypropyl methylcellulose/polyethylene oxide blend nanofibers: Morphology and physicochemical properties. *Carbohydrate Polymers*. Vol. 181, pp. 234–246. ISSN 01448617. Available from DOI: 10.1016/j.carbpol.2017.10.071.

BAHRAINIAN, Sara et al., 2017. A review on fast dissolving systems: From tablets to nanofibers. *Jundishapur Journal of Natural Pharmaceutical Products*. Vol. 12, no. 2, e34267. ISSN 22287876. Available from DOI: 10.5812/jjnpp.34267.

BAI, Yingfu et al., 2021. Testing of fast dissolution of ibuprofen from its electrospun hydrophilic polymer nanocomposites. *Polymer Testing*. Vol. 93. ISSN 01429418. Available from DOI: 10.1016/j.polymertesting.2020.106872.

BAKER, Maribel I. et al., 2012. A review of polyvinyl alcohol and its uses in cartilage and orthopedic applications. *Journal of Biomedical Materials Research Part B: Applied Biomaterials* [online]. Vol. 100B, no. 5, pp. 1451–1457 [visited on 2023-02-08]. ISSN 15524973. Available from DOI: 10.1002/jbm.b.32694. Number: 5.

BALA, Rajni et al., 2013. Orally dissolving strips: A new approach to oral drug delivery system. *International Journal of Pharmaceutical Investigation*. Vol. 3, no. 2, p. 67. ISSN 2230-973X. Available from DOI: 10.4103/2230-973x.114897.

BALOGH, Attila et al., 2016. AC and DC electrospinning of hydroxypropylmethylcellulose with polyethylene oxides as secondary polymer for improved drug dissolution. *International Journal of Pharmaceutics*. Vol. 505, no. 1-2, pp. 159–166. ISSN 18733476. Available from DOI: 10.1016/j.ijpharm.2016.03.024.

BAR-YAM, Yaneer, 2019. *Dynamics of complex systems*. CRC Press.

BIANCO, Alessandra; CALDERONE, Manuela; CACCIOTTI, Ilaria, 2013. Electrospun PHBV/PEO co-solution blends: Microstructure, thermal and mechanical properties. *Materials Science and Engineering C*. Vol. 33, no. 3, pp. 1067–1077. ISSN 09284931. Available from DOI: 10.1016/j.msec.2012.11.030.

BIRER, Mehmet; ACARTÜRK, Füsun, 2021. Electrospun orally disintegrating film formulation of telmisartan. *Pharmaceutical Development and Technology*. Vol. 26, no. 6, pp. 661–672. ISSN 10979867. Available from DOI: 10.1080/10837450.2021.1916031.

BOATENG, Joshua S et al., 2008. Wound healing dressings and drug delivery systems: a review. *Journal of pharmaceutical sciences*. Vol. 97, no. 8, pp. 2892–2923.

BOCK, N.; DARGAVILLE, T.R.; WOODRUFF, M.A., 2012. Electrospraying of polymers with therapeutic molecules: State of the art. *Progress in Polymer Science* [online]. Vol. 37, no. 11, pp. 1510–1551 [visited on 2023-02-08]. ISSN 00796700. Available from DOI: 10.1016/j.progpolymsci.2012.03.002. Number: 11.

BORGES, Ana Filipa et al., 2015. Oral films: Current status and future perspectives II-Intellectual property, technologies and market needs. *Journal of Controlled Release*. Vol. 206, pp. 108–121. ISSN 18734995. Available from DOI: 10.1016/j.jconrel.2015.03.012.

BOWDEN, Nathan A; SANDERS, Johan PM; BRUINS, Marieke E, 2018. Solubility of the proteinogenic α-amino acids in water, ethanol, and ethanol–water mixtures. *Journal of Chemical & Engineering Data*. Vol. 63, no. 3, pp. 488–497.

BROUGH, Chris et al., 2016. Use of Polyvinyl Alcohol as a Solubility-Enhancing Polymer for Poorly Water Soluble Drug Delivery (Part 1). *AAPS PharmSciTech* [online]. Vol. 17, no. 1, pp. 167–179 [visited on 2023-02-08]. ISSN 1530-9932. Available from DOI: 10.1208/s12249-015-0458-y. Number: 1.

BROWN, Eric D; WRIGHT, Gerard D, 2016. Antibacterial drug discovery in the resistance era. *Nature*. Vol. 529, no. 7586, pp. 336–343.

BRUNNER, Erich, 1904. *Zeitschrift für Physikalische Chemie*. Vol. 47U, no. 1, pp. 56–102. Available from DOI: doi:10.1515/zpch-1904-4705.

CABRERA, María I.; LUNA, Julio A.; GRAU, Ricardo J.A., 2006. Modeling of dissolution-diffusion controlled drug release from planar polymeric systems with finite dissolution rate and arbitrary drug loading. *Journal of Membrane Science*. Vol. 280, no. 1-2, pp. 693–704. ISSN 03767388. Available from DOI: 10.1016/j.memsci.2006.02.025.

CARTOTTO, Robert, 2017. Topical antimicrobial agents for pediatric burns. *Burns & trauma*. Vol. 5. Available from DOI: 10.1186/s41038-017-0096-6.

CERNIKOVA, Aneta et al., 2014. Rapid screening of permeation of rutin through skin using alaptide enantiomers. *ADMET and DMPK*. Vol. 2, no. 4, pp. 248–253. ISSN 18487718. Available from DOI: 10.5599/admet.2.4.155.

CHANG, Shuyue et al., 2020. Sheath-separate-core nanocomposites fabricated using a trifluid electrospinning. *Materials and Design*. Vol. 192. ISSN 18734197. Available from DOI: 10.1016/j.matdes.2020.108782.

CHIEN, Yie W et al., 1975. Controlled drug release from polymeric delivery devices III: In vitro-in vivo correlation for intravaginal release of ethynodiol diacetate from silicone devices in rabbits. *Journal of pharmaceutical sciences*. Vol. 64, no. 11, pp. 1776–1781.

CHILDRESS, Beverly; STECHMILLER, Joyce K; SCHULTZ, Gregory S, 2008. Arginine metabolites in wound fluids from pressure ulcers: a pilot study. *Biological Research For Nursing*. Vol. 10, no. 2, pp. 87–92.

CHOMCZYNSKI, Piotr; SACCHI, Nicoletta, 2006. The single-step method of RNA isolation by acid guanidinium thiocyanate–phenol–chloroform extraction: twenty-something years on. *Nature Protocols* [online]. Vol. 1, no. 2, pp. 581–585 [visited on 2023-02-08]. ISSN 1754-2189, ISSN 1750-2799. Available from DOI: 10.1038/nprot.2006.83. Number: 2.

CHOU, Shih-Feng; CARSON, Daniel; WOODROW, Kim A, 2015. Current strategies for sustaining drug release from electrospun nanofibers. *Journal of Controlled Release*. Vol. 220, pp. 584–591.

CHUNG, Junho; KWAK, Seung Yeop, 2019. Effect of nanoscale confinement on molecular mobility and drug release properties of cellulose acetate/sulindac nanofibers. *Journal of Applied Polymer Science*. Vol. 136, no. 33. ISSN 10974628. Available from DOI: 10.1002/app.47863.

COLMENARES-ROLDÁN, Gabriel Jaime et al., 2017. Influence of the molecular weight of polymer, solvents and operational condition in the electrospinning of polycaprolactone. *Revista Facultad de Ingenieria*. Vol. 2017, no. 84, pp. 35–45. ISSN 24222844. Available from DOI: 10.17533/udea.redin.n84a05.

CRANK, John, 1979. *The mathematics of diffusion*. Oxford university press.

DHIVYA, Selvaraj; PADMA, Viswanadha Vijaya; SANTHINI, Elango, 2015. Wound dressings–a review. *BioMedicine*. Vol. 5, no. 4, p. 22.

DHONT, Jan K. G., 1996. *An introduction to dynamics of colloids*. Vol. 2. Amsterdam, Netherlands ; New York: Elsevier. Studies in interface science. ISBN 978-0-444-82009-9.

DING, Yanfei et al., 2020. Core-shell eudragit S100 nanofibers preparedvia triaxial electrospinning to providea colon-targeted extended drug release. *Polymers*. Vol. 12, no. 9. ISSN 20734360. Available from DOI: 10.3390/POLYM12092034.

DO PHAM, Duy Dinh et al., 2021. Novel lipophosphonoxin-loaded polycaprolactone electrospun nanofiber dressing reduces Staphylococcus aureus induced wound infection in mice. *Scientific reports*. Vol. 11, no. 1, p. 17688.

DUBY, Marie-Hélène et al., 2006. Stabilization of monodisperse electrosprays in the multi-jet mode via electric field enhancement. *Journal of Aerosol Science* [online]. Vol. 37, no. 3, pp. 306–322 [visited on 2023-02-08]. ISSN 00218502. Available from DOI: 10.1016/j.jaerosci.2005.05.013. Number: 3.

EFFIONG DANIEL EKPA et al., 2020. The oral film delivery- Application of nanotechnology and potential in medication adherence. *GSC Biological and Pharmaceutical Sciences*. Vol. 11, no. 3, pp. 034–051. Available from DOI: 10.30574/gscbps.2020.11.3.0154.

EKRAM, Basma et al., 2017. Optimum parameters for the production of nano-scale electrospun polycaprolactone to be used as a biomedical material. *Advances in Natural Sciences: Nanoscience and Nanotechnology*. Vol. 8, no. 045018. Available from DOI: 10.1088/2043-6254/aa92b4.

ETTERS, JN, 1995. Kinetics of dye sorption: Effect of Dyebath flow on dyeing uniformity. *American Dyestuff Reporter*. Vol. 84, no. 1, pp. 38–43.

FAN, L; SINGH, S K, 1989. *Controlled Release: A Quantitative Treatment*. Springer-Verlag. Polymers, properties and applications. ISBN 9780387508238. Available also from: https://books.google.cz/books?id=ueGgQgAACAAJ.

FAN, Q., 2008. Fabric chemical testing. In: *Fabric Testing* [online]. Elsevier, pp. 125–147 [visited on 2023-02-08]. ISBN 978-1-84569-297-1. Available from DOI: 10.1533/9781845695064.125.

FEIZABADI, Farideh; MINAIYAN, Mohsen; TAHERI, Azade, 2018. Arginine functionalized bacterial cellulose nanofibers containing gel as an effective wound dressing: in vitro and in vivo evaluation. *Current Drug Delivery*. Vol. 15, no. 6, pp. 840–849.

FICK, Adolf Eugen, 1855. Ueber die Diffusion. *Annalen der Physik*. Vol. 94, no. 1, pp. 59–86.

GANDHI, M. et al., 2009. Mechanistic examination of protein release from polymer nanofibers. *Molecular Pharmaceutics*. Vol. 6, no. 2, pp. 641–647. ISSN 15438392. Available from DOI: 10.1021/mp800160p.

GARDNER, Kevin H.; THEIS, Thomas L., 1996. A Unified Kinetic Model for Particle Aggregation. *Journal of Colloid and Interface Science* [online]. Vol. 180, no. 1, pp. 162–173 [visited on 2023-02-08]. ISSN 00219797. Available from DOI: 10.1006/jcis.1996.0286. Number: 1.

GEORGE BROUGHTON, II; JANIS, Jeffrey E; ATTINGER, Christopher E, 2006. Wound healing: an overview. *Plastic and reconstructive surgery*. Vol. 117, no. 7S, 1e–S.

GESSER, B et al., 2011. Dimethylfumarate inhibits MIF-induced proliferation of keratinocytes by inhibiting MSK1 and RSK1 activation and by inducing nuclear pc-Jun (S63) and p-p53 (S15) expression. *Inflammation Research*. Vol. 60, pp. 643–653.

GHAFOOR, Bakhtawar et al., 2018. Review of the fabrication techniques and applications of polymeric electrospun nanofibers for drug delivery systems. Vol. 48, pp. 82–87. ISSN 17732247. Available from DOI: 10.1016/j.jddst.2018.09.005.

GILLIVER, Stephen C et al., 2011. MIF: a key player in cutaneous biology and wound healing. *Experimental dermatology*. Vol. 20, no. 1, pp. 1–6.

GNEIST, G.; BART, H.-J., 2002. Droplet Formation in Liquid/Liquid Systems Using High Frequency AC Fields. *Chemical Engineering & Technology* [online]. Vol. 25, no. 2, p. 129 [visited on 2023-02-08]. ISSN 09307516, ISSN 15214125. Available from DOI: 10.1002/1521-4125(200202)25:2<129::AID-CEAT129>3.0.CO;2-8. Number: 2.

GOMES, Ana et al., 2017. Wound-healing peptides for treatment of chronic diabetic foot ulcers and other infected skin injuries. *Molecules*. Vol. 22, no. 10, p. 1743.

GONZALEZ, Ana Cristina de Oliveira et al., 2016. Wound healing-A literature review. *Anais brasileiros de dermatologia*. Vol. 91, pp. 614–620.

GRASSI, Mario; GRASSI, Gabriele, 2005. Mathematical Modelling and Controlled Drug Delivery: Matrix Systems. *Current Drug Delivery*. Vol. 2, no. 1, pp. 97–116. ISSN 15672018. Available from DOI: 10.2174/1567201052772906.

GRIGOR'EV, A. I., 2000. Electric dispersion of fluid under the oscillatory instability of its free surface. *Technical Physics* [online]. Vol. 45, no. 5, pp. 543–548 [visited on 2023-02-08]. ISSN 1063-7842, ISSN 1090-6525. Available from DOI: 10.1134/1.1259674. Number: 5.

GUPTA, Archana; PANIGRAHI, P. K., 2020. Alternating current coaxial electrospray for micro-encapsulation. *Experiments in Fluids* [online]. Vol. 61, no. 2, p. 29 [visited on 2023-02-08]. ISSN 0723-4864, ISSN 1432-1114. Available from DOI: 10.1007/s00348-019-2851-x. Number: 2.

GUPTA, Maram Suresh; KUMAR, Tegginamath Pramod, 2020. Characterization of Orodispersible Films: An Overview of Methods and Introduction to a New Disintegration Test Apparatus Using LDR - LED Sensors. *Journal of Pharmaceutical Sciences*. Vol. 109, no. 10, pp. 2925–2942. ISSN 15206017. Available from DOI: 10.1016/j.xphs.2020.06.012.

HALWES, Michael E. et al., 2018. Computational Modeling of Antiviral Drug Diffusion from Poly(lactic- co -glycolic-acid) Fibers and Multicompartment Pharmacokinetics for Application to the Female Reproductive Tract. *Molecular Pharmaceutics*. Vol. 15, no. 4, pp. 1534–1547. ISSN 15438392. Available from DOI: 10.1021/acs.molpharmaceut.7b01089.

HASSIBA, Alaa J et al., 2016. Review of recent research on biomedical applications of electrospun polymer nanofibers for improved wound healing. *Nanomedicine*. Vol. 11, no. 6, pp. 715–737.

HERSKOVITS, Theodore T. et al., 1977. Solvent denaturation of globular proteins Unfolding by the monoalkyl- and dialkyl-substituted formamides and ureas. *Biochimica et Biophysica Acta (BBA) - Protein Structure* [online]. Vol. 490, no. 1, pp. 192–199 [visited on 2023-02-08]. ISSN 00052795. Available from DOI: 10.1016/0005-2795(77)90119-2. Number: 1.

HIGUCHI, T., 1963. Mechanism of sustained-action medication. Theoretical analysis of rate of release of solid drugs dispersed in solid matrices. *Journal of Pharmaceutical Sciences*. Vol. 52, no. 12, pp. 1145–1149. ISBN 0022-3549. ISSN 15206017. Available from DOI: 10.1002/jps.2600521210.

HIGUCHI, Takeru, 1961. Rate of release of medicaments from ointment bases containing drugs in suspension. *Journal of Pharmaceutical Sciences*. Vol. 50, no. 10, pp. 874–875. ISSN 15206017. Available from DOI: 10.1002/jps.2600501018.

HLINAK, Z; KREJCI, I, 1992. Prolonged social recognition in male rats treated with alaptide or oxiracetam. *Behavioural Pharmacology*. Vol. 3, no. 2, pp. 129–132.

HLIŇÁK, Zdeněk; KREJČÍ, Ivan, 2005. Oxiracetam pre-but not post-treatment prevented social recognition deficits produced with trimethyltin in rats. *Behavioural brain research*. Vol. 161, no. 2, pp. 213–219.

HOFFMANN, Eva Maria; BREITENBACH, Armin; BREITKREUTZ, Jörg, 2011. Advances in orodispersible films for drug delivery. *Expert Opinion on Drug Delivery*. Vol. 8, no. 3, pp. 299–316. ISSN 17425247. Available from DOI: [10.1517/17425247.2011.553217](10.1517/17425247.2011.553217).

HORAKOVA, Jana et al., 2020. The assessment of electrospun scaffolds fabricated from polycaprolactone with the addition of L-arginine. *Biomedical physics & engineering express*. Vol. 6, no. 2, p. 025012.

HUANG, Shiyang et al., 2022. A comprehensive review of electrospray technique for membrane development: Current status, challenges, and opportunities. *Journal of Membrane Science* [online]. Vol. 646, p. 120248 [visited on 2023-02-08]. ISSN 03767388. Available from DOI: 10.1016/j.memsci.2021.120248.

IRFAN, Muhammad et al., 2016. Orally disintegrating films: A modern expansion in drug delivery system. *Saudi Pharmaceutical Journal*. Vol. 24, no. 5, pp. 537–546. ISSN 13190164. Available from DOI: 10.1016/j.jsps.2015.02.024.

JOHNSON, Noah Ray; WANG, Yadong, 2013. Controlled delivery of heparin-binding EGF-like growth factor yields fast and comprehensive wound healing. *Journal of Controlled Release*. Vol. 166, no. 2, pp. 124–129.

JULÍNEK, Ondřej et al., 2010. Product of alaptide synthesis: determination of the absolute configuration. *Journal of pharmaceutical and biomedical analysis*. Vol. 53, no. 4, pp. 958–961.

KACHANOSKI, R. G.; VORONEY, R. P.; GREGORICH, E. G., 1988. ULTRASONIC DISPERSION OF AGGREGATES: DISTRIBUTION OF ORGANIC MATTER IN SIZE FRACTIONS. *Canadian Journal of Soil Science* [online]. Vol. 68, no. 2, pp. 395–403 [visited on 2023-02-08]. ISSN 0008-4271, ISSN 1918-1841. Available from DOI: 10.4141/cjss88-036. Number: 2.

KASAFIREK, E et al., 1984. SPOFA–United Pharmaceutical Works & Research Institute for Pharmacy and Biochemistry (assignees). 2, 5-Piperazinedione derivs. *Belg. P*. Vol. 897843.

KASAFÍREK, Evžen et al., 1992. Two-step generation of spirocyclic dipeptides from linear peptide ethyl ester precursors. *Life sciences*. Vol. 50, no. 3, pp. 187–193.

KATARIA, K et al., 2014. In vivo wound healing performance of drug loaded electrospun composite nanofibers transdermal patch. *International journal of pharmaceutics*. Vol. 469, no. 1, pp. 102–110.

KENAWY, El Refaie et al., 2002. Release of tetracycline hydrochloride from electrospun poly(ethylene-co-vinylacetate), poly(lactic acid), and a blend. *Journal of Controlled Release*. Vol. 81, no. 1-2, pp. 57–64. ISSN 01683659. Available from DOI: [10.1016/S0168-3659(02)00041-X](10.1016/S0168-3659(02)00041-X).

KESSICK, Royal; FENN, John; TEPPER, Gary, 2004. The use of AC potentials in electrospraying and electrospinning processes. *Polymer* [online]. Vol. 45, no. 9, pp. 2981–2984 [visited on 2023-02-08]. ISSN 00323861. Available from DOI: 10.1016/j.polymer.2004.02.056. Number: 9.

KHANSARI, S. et al., 2013. Two-stage desorption-controlled release of fluorescent dye and vitamin from solution-blown and electrospun nanofiber mats containing porogens. *Molecular Pharmaceutics*. Vol. 10, no. 12, pp. 4509–4526. ISSN 15438384. Available from DOI: 10.1021/mp4003442.

KOEDA, Shuhei et al., 2016. Construction and Characterization of Protein-Encapsulated Electrospun Fibermats Prepared from a Silica/Poly(-glutamate) Hybrid. *Langmuir* [online]. Vol. 32, no. 1, pp. 221–229 [visited on 2023-02-08]. ISSN 0743-7463, ISSN 1520-5827. Available from DOI: 10.1021/acs.langmuir. 5b02862. Number: 1.

KOJIC, M. et al., 2017. A radial 1D finite element for drug release from drug loaded nanofibers. *Journal of the Serbian Society for Computational Mechanics*. Vol. 11, no. 1, pp. 82–93. ISSN 18206530. Available from DOI: 10.24874/jsscm.2017.11.01. 08.

KUANG, Gaizhen et al., 2018. Biphasic drug release from electrospun polyblend nanofibers for optimized local cancer treatment. *Biomaterials Science*. Vol. 6, no. 2, pp. 324–331. ISSN 20474849. Available from DOI: 10.1039/c7bm01018d.

LI, Ke et al., 2015. Effect of ultrasound treatment on functional properties of reduced-salt chicken breast meat batter. *Journal of Food Science and Technology* [online]. Vol. 52, no. 5, pp. 2622–2633 [visited on 2023-02-08]. ISSN 0022-1155, ISSN 0975-8402. Available from DOI: 10.1007/s13197-014-1356-0. Number: 5.

LI, Yonghui et al., 2012. Isothermal crystallization and melting behaviors of bio-nanocomposites from poly(lactic acid) and TiO 2 nanowires. *Journal of Applied Polymer Science*. Vol. 124, no. 4, pp. 2968–2977. ISSN 00218995. Available from DOI: 10.1002/app.35326.

LI, Zhuang et al., 2014. Effects of electrode reversal on the distribution of naproxen in the electrospun cellulose acetate nanofibers. *Journal of Nanomaterials*. Vol. 2014, pp. 2–2.

LI, Zibiao; TAN, Beng Hoon, 2014. Towards the development of polycaprolactone based amphiphilic block copolymers: molecular design, self-assembly and biomedical applications. *Materials Science and Engineering: C*. Vol. 45, pp. 620–634.

LIEW, Kai Bin; TAN, Yvonne Tze Fung; PEH, Kok Khiang, 2014. Effect of polymer, plasticizer and filler on orally disintegrating film. *Drug Development and Industrial Pharmacy*. Vol. 40, no. 1, pp. 110–119. ISSN 03639045. Available from DOI: 10.3109/03639045.2012.749889.

LOVINGER, Andrew J.; GRYTE, Carl C., 1976. The Morphology of Directionally Solidified Poly(ethylene oxide) Spherulites. *Macromolecules*. Vol. 9, no. 2, pp. 247–253. ISSN 15205835. Available from DOI: 10.1021/ma60050a014.

LOWERY, Joseph L.; DATTA, Néha; RUTLEDGE, Gregory C., 2010. Effect of fiber diameter, pore size and seeding method on growth of human dermal fibroblasts in electrospun poly(ϵ-caprolactone) fibrous mats. *Biomaterials*. Vol. 31, no. 3, pp. 491–504. ISSN 01429612. Available from DOI: 10.1016/j.biomaterials.2009.09.072.

LUO, CJ; STRIDE, E; EDIRISINGHE, M, 2012. Mapping the influence of solubility and dielectric constant on electrospinning polycaprolactone solutions. *Macromolecules*. Vol. 45, no. 11, pp. 4669–4680.

LUO, Jian-dong; CHEN, Alex F, 2005. Nitric oxide: a newly discovered function on wound healing. *Acta Pharmacologica Sinica*. Vol. 26, no. 3, pp. 259–264.

MAHBOOB, Muhammad Bilal Hassan et al., 2016. Oral Films: A Comprehensive Review. *International Current Pharmaceutical Journal*. Vol. 5, no. 12, pp. 111–117. ISSN 2224-9486. Available from DOI: 10.3329/icpj.v5i12.30413.

MAHESHWARI, Siddharth; CHETWANI, Nishant; CHANG, Hsueh-Chia, 2009. Alternating Current Electrospraying. *Industrial & Engineering Chemistry Research* [online]. Vol. 48, no. 21, pp. 9358–9368 [visited on 2023-02-08]. ISSN 0888-5885, ISSN 1520-5045. Available from DOI: 10.1021/ie801841r. Number: 21.

MERUVA, Saikishore; DONOVAN, Maureen D., 2020. Polyethylene Oxide (PEO) Molecular Weight Effects on Abuse-Deterrent Properties of Matrix Tablets. *AAPS PharmSciTech*. Vol. 21, no. 1, p. 28. ISSN 15309932. Available from DOI: 10.1208/s12249-019-1565-y.

MIKES, Petr et al., 2021. Comparison and characterization of different polyester nano/micro fibres for use in tissue engineering applications. *Journal of Industrial Textiles*. Vol. 50, no. 6, pp. 870–890.

MIKEŠ, Petr et al., 2020. In vitro and in vivo testing of nanofibrous membranes doped with alaptide and L-arginine for wound treatment. *Biomedical Materials*. Vol. 15, no. 6, p. 065023.

MILOSEVIC, Miljan; STOJANOVIC, Dusica, et al., 2018. A computational model for drug release from PLGA implant. *Materials*. Vol. 11, no. 12. ISSN 19961944. Available from DOI: 10.3390/ma11122416.

MILOSEVIC, Miljan; STOJANOVIC, Dusica B., et al., 2020. Preparation and modeling of three-layered PCL/PLGA/PCL fibrous scaffolds for prolonged drug release. *Scientific Reports*. Vol. 10, no. 1. ISSN 20452322. Available from DOI: 10.1038/s41598-020-68117-9.

MONDAL, Debasish; GRIFFITH, May; VENKATRAMAN, Subbu S., 2016. Polycaprolactone-based biomaterials for tissue engineering and drug delivery: Current scenario and challenges. *International Journal of Polymeric Materials and Polymeric Biomaterials* [online]. Vol. 65, no. 5, pp. 255–265 [visited on 2023-02-08]. ISSN 0091-4037, ISSN 1563-535X. Available from DOI: 10.1080/00914037.2015.1103241. Number: 5.

MONEY, Benson K.; SWENSON, Jan, 2013. Dynamics of poly(ethylene oxide) around its melting temperature. *Macromolecules.* Vol. 46, no. 17, pp. 6949–6954. ISSN 00249297. Available from DOI: 10.1021/ma4003598.

MUSCHERT, S. et al., 2009. Prediction of drug release from ethylcellulose coated pellets. *Journal of Controlled Release.* Vol. 135, no. 1, pp. 71–79. ISSN 01683659. Available from DOI: 10.1016/j.jconrel.2008.12.003.

NAKIELSKI, Paweł et al., 2015. Experimental and numerical evaluation of drug release from nanofiber mats to brain tissue. *Journal of Biomedical Materials Research - Part B Applied Biomaterials.* Vol. 103, no. 2, pp. 282–291. ISSN 15524981. Available from DOI: 10.1002/jbm.b.33197.

NIJENHUIS, A. J. et al., 1996. High molecular weight poly(L-lactide) and poly(ethylene oxide) blends: Thermal characterization and physical properties. *Polymer.* Vol. 37, no. 26, pp. 5849–5857. ISSN 00323861. Available from DOI: 10.1016/S0032-3861(96)00455-7.

NUTTELMAN, Charles R; HENRY, Scott M; ANSETH, Kristi S, 2002. Synthesis and characterization of photocrosslinkable, degradable poly(vinyl alcohol)-based tissue engineering scaffolds. *Biomaterials* [online]. Vol. 23, no. 17, pp. 3617–3626 [visited on 2023-02-08]. ISSN 01429612. Available from DOI: 10.1016/S0142-9612(02)00093-5. Number: 17.

NYAMWEYA, Nasser; HOAG, Stephen W., 2000. Assessment of polymer-polymer interactions in blends of HPMC and film forming polymers by modulated temperature differential scanning calorimetry. *Pharmaceutical Research.* Vol. 17, no. 5, pp. 625–631. ISSN 07248741. Available from DOI: 10.1023/A:1007585403781.

NYFLÖTT, Åsa et al., 2017. The influence of moisture content on the polymer structure of polyvinyl alcohol in dispersion barrier coatings and its effect on the mass transport of oxygen. *Journal of Coatings Technology and Research* [online]. Vol. 14, no. 6, pp. 1345–1355 [visited on 2023-02-08]. ISSN 1547-0091, ISSN 1935-3804. Available from DOI: 10.1007/s11998-017-9937-2. Number: 6.

O'MALLEY, Brian, 1971. *British Medical Journal.* Vol. 4, European Pharmacopoeia. 10th. ed. Strasbourg: Council of Europe. No. 5790. ISBN 9789287189127 9287189129. ISSN 00071447. Available from DOI: 10.1136/bmj.4.5790.815-b.

OPATRILOVA, Radka et al., 2013. In vitro permeation of micronized and nanonized alaptide from semisolid formulations. *The Scientific World Journal.* Vol. 2013.

ORLU, Mine et al., 2017. Acceptability of orodispersible films for delivery of medicines to infants and preschool children. *Drug Delivery.* Vol. 24, no. 1, pp. 1243–1248. ISSN 15210464. Available from DOI: 10.1080/10717544.2017.1370512.

PAAVER, Urve et al., 2015. Electrospun nanofibers as a potential controlled-release solid dispersion system for poorly water-soluble drugs. *International Journal of Pharmaceutics.* Vol. 479, no. 1, pp. 252–260. ISSN 18733476. Available from DOI: 10.1016/j.ijpharm.2014.12.024.

PANOVA, Natalya et al., 2015. Insights into the mechanism of action of bactericidal lipophosphonoxins. *PLoS One.* Vol. 10, no. 12, e0145918.

PARK, Jae Woo; RHEE, Young Min, 2016. Electric Field Keeps Chromophore Planar and Produces High Yield Fluorescence in Green Fluorescent Protein. *Journal of the American Chemical Society* [online]. Vol. 138, no. 41, pp. 13619–13629 [visited on 2023-02-08]. ISSN 0002-7863, ISSN 1520-5126. Available from DOI: 10.1021/jacs.6b06833. Number: 41.

PENNA, Thereza Christina Vessoni et al., 2005. Stability of Recombinant Green Fluorescent Protein (GFPuv) in Glucose Solutions at Different Concentrations and pH Values. *Applied Biochemistry and Biotechnology* [online]. Vol. 122, no. 1-3, pp. 0501–0528 [visited on 2023-02-08]. ISSN 0273-2289. Available from DOI: 10.1385/ABAB:122:1-3:0501. Number: 1-3.

PEPPAS, N. A., 1985. Analysis of Fickian and non-Fickian drug release from polymers. *Pharmaceutica Acta Helvetiae.* Vol. 60, no. 4, pp. 110–111. ISSN 00316865.

PETERNEL, Špela; KOMEL, Radovan, 2010. Isolation of biologically active nanomaterial (inclusion bodies) from bacterial cells. *Microbial Cell Factories* [online]. Vol. 9, no. 1, p. 66 [visited on 2023-02-08]. ISSN 1475-2859. Available from DOI: 10.1186/1475-2859-9-66. Number: 1.

PETLIN, D. G. et al., 2017. A fiber distribution model for predicting drug release rates. *Journal of Controlled Release.* Vol. 258, pp. 218–225. ISSN 18734995. Available from DOI: 10.1016/j.jconrel.2017.05.021.

PISANI, Silvia et al., 2019. Release profile of gentamicin sulfate from polylactide-co-polycaprolactone electrospun nanofiber matrices. *Pharmaceutics.* Vol. 11, no. 4. ISSN 19994923. Available from DOI: 10.3390/pharmaceutics11040161.

POKORNY, P. et al., 2014. Effective AC needleless and collectorless electrospinning for yarn production. *Phys. Chem. Chem. Phys.* [online]. Vol. 16, no. 48, pp. 26816–26822 [visited on 2023-02-08]. ISSN 1463-9076, ISSN 1463-9084. Available from DOI: 10.1039/C4CP04346D. Number: 48.

PREEM, Liis et al., 2017. Interactions between Chloramphenicol, Carrier Polymers, and Bacteria-Implications for Designing Electrospun Drug Delivery Systems Countering Wound Infection. *Molecular Pharmaceutics.* Vol. 14, no. 12, pp. 4417–4430. ISSN 15438392. Available from DOI: 10.1021/acs.molpharmaceut.7b00524.

PREIS, Maren, 2015. Orally Disintegrating Films and Mini-Tablets—Innovative Dosage Forms of Choice for Pediatric Use. *AAPS PharmSciTech.* Vol. 16, no. 2, pp. 234–241. ISSN 15309932. Available from DOI: 10.1208/s12249-015-0313-1.

PUPPI, Dario et al., 2010. Poly (lactic-co-glycolic acid) electrospun fibrous meshes for the controlled release of retinoic acid. *Acta biomaterialia.* Vol. 6, no. 4, pp. 1258–1268.

PUTTHANARAT, S. et al., 2006. Electrospun Bombyx mori gland silk. *Polymer* [online]. Vol. 47, no. 15, pp. 5630–5632 [visited on 2023-02-08]. ISSN 00323861. Available from DOI: 10.1016/j.polymer.2005.06.130. Number: 15.

RADL, S; KASAFIREK, E; KREJCI, I, 1990. Alaptide. *Drugs of the Future*. Vol. 15, pp. 445–447.

RATHNA, Gundloori Venkata Naga; JOG, Jyoti Prakash; GAIKWAD, Anil Bhikaji, 2011. Development of non-woven nanofibers of egg albumen-poly (vinyl alcohol) blends: Influence of solution properties on morphology of nanofibers. *Polymer Journal*. Vol. 43, no. 7, pp. 654–661. ISSN 00323896. Available from DOI: [10.1038/pj.2011.34](10.1038/pj.2011.34).

REESI, Fatemeh; MINAIYAN, Mohsen; TAHERI, Azade, 2018. A novel lignin-based nanofibrous dressing containing arginine for wound-healing applications. *Drug Delivery and Translational Research*. Vol. 8, pp. 111–122.

RENKLER, Nergis Zeynep et al., 2021. Facile modification of polycaprolactone nanofibers with egg white protein. *Journal of Materials Science: Materials in Medicine*. Vol. 32, no. 4, p. 34. ISSN 1573-4838. Available from DOI: [10.1007/s10856-021-06505-x](10.1007/s10856-021-06505-x).

RIEGER, Katrina A.; BIRCH, Nathan P.; SCHIFFMAN, Jessica D., 2013. Designing electrospun nanofiber mats to promote wound healing – a review. *J. Mater. Chem. B*. Vol. 1, pp. 4531–4541. Available from DOI: [10.1039/C3TB20795A](10.1039/C3TB20795A).

ROBSON, Martin C, 1997. Wound infection: a failure of wound healing caused by an imbalance of bacteria. *Surgical Clinics of North America*. Vol. 77, no. 3, pp. 637–650.

ROSEMAN, TJ; YALKOWSKY, SH, 1976. Importance of solute partitioning on the kinetics of drug release from matrix systems, pp. 33–52. Available from DOI: [doi:10.1021/bk-1976-0033.ch004](doi:10.1021/bk-1976-0033.ch004).

ROSENBERG, R. et al., 2007. Anomalous release of hydrophilic drugs from poly(ϵ-caprolactone) matrices. *Molecular Pharmaceutics*. Vol. 4, no. 6, pp. 943–948. ISSN 15438384. Available from DOI: [10.1021/mp700097x](10.1021/mp700097x).

SAMPLE, Steven B; BOLLINI, Raghupathy, 1972. Production of liquid aerosols by harmonic electrical spraying. *Journal of Colloid and Interface Science* [online]. Vol. 41, no. 2, pp. 185–193 [visited on 2023-02-08]. ISSN 00219797. Available from DOI: [10.1016/0021-9797(72)90107-5](10.1016/0021-9797(72)90107-5). Number: 2.

SAMPRASIT, Wipada et al., 2015. Fast releasing oral electrospun PVP/CD nanofiber mats of taste-masked meloxicam. *International Journal of Pharmaceutics*. Vol. 487, no. 1-2, pp. 213–222. ISSN 18733476. Available from DOI: 10.1016/j.ijpharm.2015.04.044.

SATO, Masayuki, 1984. The production of essentially uniform-sized liquid droplets in gaseous or immiscible liquid media under applied a.c. potential. *Journal of Electrostatics* [online]. Vol. 15, no. 2, pp. 237–247 [visited on 2023-02-08]. ISSN 03043886. Available from DOI: [10.1016/0304-3886(84)90009-3](10.1016/0304-3886(84)90009-3). Number: 2.

SETHURAM, Lakshimipriya; THOMAS, John, 2023. Therapeutic applications of electrospun nanofibers impregnated with various biological macromolecules for effective wound healing strategy – A review. *Biomedicine Pharmacotherapy*. Vol. 157, p. 113996. ISSN 0753-3322. Available from DOI: https://doi.org/10.1016/j.biopha.2022.113996.

SEYDLOVÁ, Gabriela et al., 2017. Lipophosphonoxins II: design, synthesis, and properties of novel broad spectrum antibacterial agents. *Journal of Medicinal Chemistry*. Vol. 60, no. 14, pp. 6098–6118.

SHI, Shih Chen; CHEN, Tao Hsing; MANDAL, Pramod Kumar, 2020. Enhancing the mechanical and tribological properties of cellulose nanocomposites with aluminum nanoadditives. *Polymers*. Vol. 12, no. 6, p. 1246. ISSN 20734360. Available from DOI: 10.3390/POLYM12061246.

SHIN, Yongdae et al., 2009. Single-molecule denaturation and degradation of proteins by the AAA+ ClpXP protease. *Proceedings of the National Academy of Sciences* [online]. Vol. 106, no. 46, pp. 19340–19345 [visited on 2023-02-08]. ISSN 0027-8424, ISSN 1091-6490. Available from DOI: 10.1073/pnas.0910484106. Number: 46.

SIEPMANN, J.; LECOMTE, F.; BODMEIER, R., 1999. Diffusion-controlled drug delivery systems: Calculation of the required composition to achieve desired release profiles. *Journal of Controlled Release*. Vol. 60, no. 2-3, pp. 379–389. ISSN 01683659. Available from DOI: 10.1016/S0168-3659(99)00093-0.

SIEPMANN, J.; SIEPMANN, F., 2008. *International Journal of Pharmaceutics*. Vol. 364, Mathematical modeling of drug delivery. No. 2. ISSN 03785173. Available from DOI: 10.1016/j.ijpharm.2008.09.004.

SIEPMANN, J.; SIEPMANN, F., 2013. Mathematical modeling of drug dissolution. *International Journal of Pharmaceutics*. Vol. 453, no. 1, pp. 12–24. ISSN 0378-5173. Available from DOI: https://doi.org/10.1016/j.ijpharm.2013.04.044. Poorly Soluble Drugs.

SIEPMANN, Juergen; SIEPMANN, Florence, 2012. Modeling of diffusion controlled drug delivery. *Journal of Controlled Release*. Vol. 161, no. 2, pp. 351–362. ISBN 1873-4995 (Electronic)0168-3659 (Linking). ISSN 01683659. Available from DOI: 10.1016/j.jconrel.2011.10.006.

SKLENÁŘ, Zbyněk et al., 2013. Formulation and release of alaptide from cellulose-based hydrogels. *Acta Veterinaria Brno*. Vol. 81, no. 3, pp. 301–306.

SLAVKOVA, Marta; BREITKREUTZ, Jörg, 2015. Orodispersible drug formulations for children and elderly. *European Journal of Pharmaceutical Sciences*. Vol. 75, pp. 2–9. ISSN 18790720. Available from DOI: 10.1016/j.ejps.2015.02.015.

SOCRATES, G., 2004. *Infrared and Raman Characteristic Group Frequencies: Tables and Charts*. Wiley. ISBN 9780470093078. Available also from: https://books.google.cz/books?id=LDoAAjMnwEIC.

SPIRIDONOVA, Tatiana I.; TVERDOKHLEBOV, Sergei I.; ANISSIMOV, Yuri G., 2019. Investigation of the Size Distribution for Diffusion-Controlled Drug Release From Drug Delivery Systems of Various Geometries. *Journal of Pharmaceutical Sciences*. Vol. 108, no. 8, pp. 2690–2697. ISSN 15206017. Available from DOI: 10.1016/j.xphs.2019.03.036.

SRIKAR, R. et al., 2009. Desorption-limited mechanism of release from polymer nanofibers. In: *Proceedings of the ASME International Manufacturing Science and Engineering Conference, MSEC2008*. Vol. 2, pp. 465–474. ISBN 9780791848517. ISSN 07437463. Available from DOI: 10.1115/MSEC_ICMP2008-72054.

STACK, Mary et al., 2018. Electrospun nanofibers for drug delivery. In: *Electrospinning: Nanofabrication and Applications*, pp. 735–764. ISBN 9780323512701. Available from DOI: 10.1016/B978-0-323-51270-1.00025-X.

STECHMILLER, Joyce K; CHILDRESS, Beverly; COWAN, Linda, 2005. Arginine supplementation and wound healing. *Nutrition in Clinical Practice*. Vol. 20, no. 1, pp. 52–61.

ŠVÁRA, Dominik et al., 2022. The impact of the lamination pressure on the properties of electrospinned nanofibrous films. *European Journal of Pharmaceutical Sciences*. Vol. 173, p. 106170. ISSN 18790720. Available from DOI: 10.1016/j.ejps.2022.106170.

THAKKAR, Shreya; MISRA, Manju, 2017. *European Journal of Pharmaceutical Sciences*. Vol. 107, Electrospun polymeric nanofibers: New horizons in drug delivery. ISSN 18790720. Available from DOI: 10.1016/j.ejps.2017.07.001.

TORT, Serdar; ACARTÜRK, Füsun, 2016. Preparation and characterization of electrospun nanofibers containing glutamine. *Carbohydrate Polymers*. Vol. 152, pp. 802–814. ISSN 01448617. Available from DOI: 10.1016/j.carbpol.2016.07.028.

TSUBOYAMA, Kotaro et al., 2020. A widespread family of heat-resistant obscure (Hero) proteins protect against protein instability and aggregation. *PLOS Biology* [online]. Vol. 18, no. 3, e3000632 [visited on 2023-02-08]. ISSN 1545-7885. Available from DOI: 10.1371/journal.pbio.3000632. Number: 3.

VERGNAUD, J.M., 1993. *Controlled Drug Release Of Oral Dosage Forms*. Taylor & Francis. ELLIS HORWOOD BOOKS IN THE BIOLOGICAL SCIENCES. ISBN 9780131749542. Available also from: https://books.google.cz/books?id=s1qcwSfuELMC.

VISSER, J. Carolina et al., 2017. Development of orodispersible films with selected Indonesian medicinal plant extracts. *Journal of Herbal Medicine*. Vol. 7, pp. 37–46. ISSN 22108041. Available from DOI: 10.1016/j.hermed.2016.10.002.

WANG, Chenggui et al., 2018. Highly efficient local delivery of endothelial progenitor cells significantly potentiates angiogenesis and full-thickness wound healing. *Acta Biomaterialia*. Vol. 69, pp. 156–169.

WANG, Ping; MAHESHWARI, Siddharth; CHANG, Hsueh-Chia, 2006. Polyhedra Formation and Transient Cone Ejection of a Resonant Microdrop Forced by an ac Electric Field. *Physical Review Letters* [online]. Vol. 96, no. 25, p. 254502 [visited on 2023-02-08]. ISSN 0031-9007, ISSN 1079-7114. Available from DOI: 10.1103/PhysRevLett.96.254502. Number: 25.

XIONG, Erhui et al., 2014. Chloroform-Assisted Phenol Extraction Improving Proteome Profiling of Maize Embryos through Selective Depletion of High-Abundance Storage Proteins. *PLoS ONE* [online]. Vol. 9, no. 11, e112724 [visited on 2023-02-08]. ISSN 1932-6203. Available from DOI: 10.1371/journal.pone.0112724. Number: 11.

XU, Qian et al., 2018. A hybrid injectable hydrogel from hyperbranched PEG macromer as a stem cell delivery and retention platform for diabetic wound healing. *Acta biomaterialia.* Vol. 75, pp. 63–74.

YAQOOB, Muhammad; JALIL, Aamir; BERNKOP-SCHNÜRCH, Andreas, 2021. Mucoadhesive Polymers: Gateway to Innovative Drug Delivery. In: *Modeling and Control of Drug Delivery Systems* [online]. Elsevier, pp. 351–383 [visited on 2023-02-08]. ISBN 978-0-12-821185-4. Available from DOI: [10.1016/B978-0-12-821185-4.00020-8](10.1016/B978-0-12-821185-4.00020-8).

YEO, Leslie Y. et al., 2004. A New ac Electrospray Mechanism by Maxwell-Wagner Polarization and Capillary Resonance. *Physical Review Letters* [online]. Vol. 92, no. 13, p. 133902 [visited on 2023-02-08]. ISSN 0031-9007, ISSN 1079-7114. Available from DOI: 10.1103/PhysRevLett.92.133902. Number: 13.

YOO, Hyuk Sang; KIM, Taek Gyoung; PARK, Tae Gwan, 2009. Surface-functionalized electrospun nanofibers for tissue engineering and drug delivery. *Advanced drug delivery reviews.* Vol. 61, no. 12, pp. 1033–1042.

ZAHEDI, Payam et al., 2013. Preparation and release properties of electrospun poly(vinyl alcohol)/poly(-caprolactone) hybrid nanofibers: Optimization of process parameters via D-optimal design method. *Macromolecular Research.* Vol. 21, no. 6, pp. 649–659. ISSN 2092-7673. Available from DOI: [10.1007/s13233-013-1064-z](10.1007/s13233-013-1064-z).

ZAJICEK, Robert et al., 2021. *Nanofibrous material particularly for topical use in therapies.* Inventor: Robert ZAJICEK et al. Publ.: 2021-12. WO2021244684A1. Available also from: https://patents.google.com/patent/WO2021244684A1.

ZBORNIKOVA, Eva et al., 2020. Evaluation of second-generation lipophosphonoxins as antimicrobial additives in bone cement. *ACS omega.* Vol. 5, no. 7, pp. 3165–3171.

ZHANG, Qiang et al., 2017. Electrospun polymeric micro/nanofibrous scaffolds for long-term drug release and their biomedical applications. *Drug Discovery Today.* Vol. 22, no. 9, pp. 1351–1366.